

SYNTHESIS OF THIAZOLOTHIAZOLE FUNCTIONALIZED PORPHYRINS FOR  
ORGANIC SOLAR CELL APPLICATIONS

by

Nicholas George Grubich

A thesis submitted to the faculty of  
The University of North Carolina at Charlotte  
in partial fulfillment of the requirements  
for the degree of Master of Science in  
Chemistry

Charlotte

2014

Approved by:

---

Dr. Michael G. Walter

---

Dr. Thomas A. Schmedake

---

Dr. Juan L. Vivero-Escoto

---

Dr. Mona Azarbayjani

© 2014  
Nicholas G. Grubich  
ALL RIGHTS RESERVED

## ABSTRACT

NICHOLAS GEORGE GRUBICH. Synthesis of thiazolothiazole functionalized porphyrins for organic solar cell applications. (Under the direction of DR. MICHAEL GEORGE WALTER)

Porphyrin light-harvesting systems have recently shown promising solar energy conversion properties in organic photovoltaic devices. Porphyrins, which absorb a broad portion of the solar spectrum and can be easily tuned with peripheral substituents, make them ideal candidates for solar energy conversion research. However, polymers and small molecule systems using porphyrins have been plagued by low hole mobilities. Thiazolothiazole is a fused bicyclic aromatic ring system that has been shown to produce materials with high hole mobilities. In efforts to synthesize porphyrin materials for organic solar cell applications with increased red light sensitivity and hole mobilities, a series of thiazolothiazole-functionalized porphyrins have been modeled computationally and pursued synthetically. Several porphyrin and thiazolothiazole precursors have been synthesized and characterized spectroscopically. Sonogashira cross-coupling of porphyrins and ethynyl containing symmetric thiazolothiazoles for small-molecule and polymer systems have been pursued. Preliminary data of a porphyrin-thiazolothiazole polymer system suggests increased red light sensitivity, characterized by a red-shifted Soret absorption peak relative to the porphyrin starting material, along with an enhanced Q band region.

## ACKNOWLEDGMENTS

I've been in the UNC Charlotte community for over 10 years now (my sister, Lisa, attended from '04 – '08) and it will be difficult to leave this University once it's all said and done. I've seen the astounding expansion of the University's facilities over the past 10 years and am still in awe when I remember what the University looked like in 2004. As apprehensive as I am by leaving the University, I look forward to the challenges ahead.

I would like to first thank Dr. Michael Walter for being such a great mentor in the development of my education and skills as a chemist. Whether it be carrying a positive attitude even if one of the other students or I broke something or always being able to share a laugh, I believe that working under your direction was one of the best overall educational experiences I have had during my time at UNC Charlotte.

Special thanks must be expressed to the members of my thesis committee Dr. Mona Azarbayjani, Dr. Thomas Schmedake, and Dr. Juan Vivero-Escoto for keeping me engaged in my research and for maintaining an interest in my development as a scientist. I am grateful for the feedback and words of encouragement you have provided over the past two years.

I want to acknowledge the support from the other members of the Walter Research Group: Reynolds Ivins, Li Nguyen, Angy Ortiz, Dawn Marin, and Nik Hall. Thanks for the feedback and aiding in my growth as a scientist. I also want to recognize the feedback I received from my students the past couple years, as it has proven to be a vital component of my growth as a professional and instructor.

I would also like to acknowledge the support of my roommates, Marcos Castro and Sean Burke. Thanks for listening to me complain about my research problems and for always being ready for a getaway yourselves, whether it be going out of town for the day on weekends to avoid your own Engineering coursework, or for being up for late-night rounds of Super Smash Brothers.

I must also thank my other friends and family (Mom, Dad, Lisa, and Matt) for the words of encouragement over the years. Always mentioning how proud you were of me has kept me going through the rough patches of college. Not to mention the understood, unspoken sibling rivalry between Lisa and myself to become the most successful child.

To the departmental mother figures, Robin Burns and Caroline Kennedy, thanks for always lending an ear. Robin, you've always got something funny to say to help clear my mind. I also enjoyed coming into the office just to bug you for a little while. Caroline, the Chemistry Department misses you! Since you moved over to Woodward, it just isn't the same.

Last but not least, I dedicate a portion of this thesis work to the late Steven Archer. Although the group from the "Ho House Penthouse" (Holshouser, 11<sup>th</sup> floor; Rob Moore, Sean Burke, Marcos Castro, Kevin Brickhouse, Corey Grady, Brian Mister, Dane Wilhelm, Chris Ellis, Andy May, John Dew, and myself) was only able to spend time with you for a few short months, we all agree that you were one of the few genuinely nice people in the world. Your soft-spoken, always-positive approach to everything changed all of our outlooks on life.

## TABLE OF CONTENTS

LIST OF ABBREVIATIONS	viii
CHAPTER 1: INTRODUCTION	1
1.1 Photovoltaics	1
1.2 Organic Photovoltaics	4
1.3 Bulk Heterojunction Solar Cells	7
1.4 Porphyrins	10
1.5 Porphyrins in Nature	13
1.6 Porphyrins in Organic Photovoltaics	14
1.7 Thiazolothiazoles	17
1.8 Thiazolothiazoles in Organic Photovoltaics	19
1.9 Design of New Porphyrin Dyes for OPVs	21
CHAPTER 2: EXPERIMENTAL	24
2.1 Synthesis of Thiazolothiazole Functionalized Porphyrins	24
2.1.1 Thiazolothiazole Syntheses	24
2.1.1.a Synthesis of Di-TMS TTz	26
2.1.1.b Synthesis of Di-Ethynyl TTz	26
2.1.1.c Synthesis of Asymmetric TTz	27
2.1.2 Synthesis of Porphyrin Precursors	27
2.1.2.a Synthesis of 1,3-Dioctoxybenzene	29
2.1.2.b Synthesis of 2,6-Dioctoxybenzaldehyde	29
2.1.2.c Synthesis of <i>trans</i> -(Dioctoxyphenyl)porphyrin	30
2.1.2.d Synthesis of Bromo-(Dioctoxyphenyl)porphyrin	31

2.1.2.e Synthesis of Bromo-(Diocetoxyphenyl)porphyrin [Zn]	31
2.1.2.f Synthesis of Dibromo-(Diocetoxyphenyl)porphyrin	32
2.1.2.g Synthesis of Dibromo-(Diocetoxyphenyl)porphyrin [Zn]	32
2.1.3 Sonogashira Coupling of Thiazolothiazoles and Porphyrins	33
2.1.3.a D-A-D P-TTz-P Dyad Synthesis	34
2.1.3.b D-A P-TTz Polymer Synthesis	34
2.2 Molecular Modeling	35
2.3 Dibromo-(Diocetoxyphenyl)porphyrin Crystal Structure	35
2.4 UV-Vis Spectroscopy	36
CHAPTER 3: RESULTS AND DISCUSSION	37
3.1 Computational Models for Porphyrin Dyes	37
3.1.1 <i>trans</i> -(Diocetoxyphenyl)porphyrin [Zn]	37
3.1.2 D-A P-TTz	38
3.1.3 A-D-A TTz-P-TTz	39
3.1.3.a Alkoxy TTz Functional Groups	39
3.1.3.b Ethynyl TTz Functional Groups	40
3.1.4 D-A-D P-TTz-P	41
3.2 UV-Vis Spectroscopy	42
3.2.1 Porphyrin Compounds	42
3.2.1.a <i>trans</i> -(Diocetoxyphenyl)porphyrin	42
3.2.1.b Bromo-(Diocetoxyphenyl)porphyrin	43
3.2.1.c Bromo-(Diocetoxyphenyl)porphyrin [Zn]	44
3.2.1.d Dibromo-(Diocetoxyphenyl)porphyrin	45

3.2.1.e Dibromo-(Diocetoxyphenyl)porphyrin [Zn]	45
3.2.2 Thiazolothiazole Compounds	46
3.2.2.a Di-TMS TTz	46
3.2.2.b Di-Ethynyl TTz	47
3.2.3 Palladium Coupling	48
3.2.3.a P-TTz Polymer	48
3.2.3.b P-TTz-P Dyad	49
3.3 Dibromo-(Diocetoxyphenyl)porphyrin Crystal Structure	50
CHAPTER 4: CONCLUSION	52
REFERENCES	54
APPENDIX A: UV-IVS CALIBRATION CURVES	60
APPENDIX B: <sup>1</sup> H NMR SPECTRA	70
APPENDIX C: MALDI – TOF SPECTRA	80

## LIST OF ABBREVIATIONS

BHJ	bulk heterojunction
OPV	organic photovoltaic
OSC	organic solar cell
PV	photovoltaic
eV	electron volt
HOMO	highest occupied molecular orbital
LUMO	lowest unoccupied molecular orbital
OFET	organic field-effect transistor
OLED	organic light-emitting diode
D-A	Donor-Acceptor
D-A-D	Donor-Acceptor-Donor
A-D-A	Acceptor-Donor-Acceptor
DSSC	dye-sensitized solar cell
TPP	tetraphenylporphyrin
TTz	thiazolothiazole
TMS TTz	2,5-bis-(4-trimethylsilanylethynyl-phenyl)-thiazolo[5,4- <i>d</i> ]thiazole
UV-Vis	ultraviolet-visible spectroscopy
NMR	nuclear magnetic resonance
di-ethynyl TTz	2,5-bis-(4-ethynylphenyl)-thiazolo[5,4- <i>d</i> ]thiazole
asymmetric TTz	2-(4-octoxyphenyl)-5-(4-trimethylsilanylethynyl-phenyl)- thiazolo[5,4- <i>d</i> ]thiazole
TMS	trimethylsilyl protecting group

HPFC	High-Performance Flash Chromatography
R <sub>f</sub>	retention factor
TLC	thin-layer chromatography
RTzR	2,5-bis(5-(5-(5-hexylthiophen-2-yl)thiophen-2-yl) thiophen-2-yl)thiazolo[5,4, <i>d</i> ]thiazole
M2	2,5-bis(2-triphenylamino-3-decylthiophen-2-yl)thiazolo[5,4, <i>d</i> ]thiazole
TT-TTPA	2,5-bis(5-triphenylamino-3-dodecylthiophen-2-yl)thiazolo[5,4, <i>d</i> ]thiazole

## CHAPTER 1. INTRODUCTION

### 1.1 Photovoltaics

As the world's population is expected to exceed 9 billion by 2050, an ever-increasing strain is placed on the world's finite fuel reserves.<sup>1</sup> Current data of fossil fuel reserve depletion rates reveals a stark reality of the world's energy crisis. This data, along with the most recent formula adapted from the Klass model determines depletion times of approximately 35, 107, and 37 years for oil, coal, and natural gas, respectively.<sup>2</sup>

As a result, alternative energy sources have garnered interest in recent decades as potential replacements for the world's demand on non-renewable fuel sources. In particular, solar energy is lending itself as a viable alternative to our dependence on non-renewable fuel sources. The major draw towards solar energy is due to its sheer abundance and essentially endless supply. The amount of energy striking the earth in the form of solar irradiation in just one hour is enough to provide for the world's energy needs for an entire year; in one year, it would amass to nearly twice the amount of energy that could ever to be collected from non-renewable resources.<sup>3,4</sup>

Photovoltaic (PV) systems are designed to absorb a portion of the solar spectrum and convert it to usable energy in the form of electricity for everyday uses. Since PV systems only work when exposed to a light source, research is focusing on storing the energy harvested during the day in the form of batteries or chemical bonds like hydrogen.<sup>5-8</sup>

The most comprehensive method for determining a PV cell's efficiency is to measure its photoconversion efficiency (PCE), which is a comparison of the total energy of the

solar irradiance to the total electrical energy produced by the device.<sup>9</sup> Equation (1) is used to determine this overall PCE, ( $\eta$ ).

$$\eta (\%) = \frac{V_{oc} J_{sc} ff}{P_{in}} \times 100 \% \quad (1)$$

In equation (1), the overall PCE is reported as a percent. Open-circuit voltage,  $V_{oc}$ , is the voltage measured between the device's terminals with no electrical current flow. Fill factor,  $ff$ , is reported as a ratio of the maximum power to the ideal power.<sup>9</sup> Short-circuit current density,  $J_{sc}$ , is the current measured when the device's terminals are in contact with each other and no applied voltage.  $P_{in}$  is the intensity of the light source under standard 1 sun illumination (AM 1.5); this is a constant for device testing with a value of  $100 \text{ mW cm}^{-2}$ . Using Eq. 1, it is apparent that increasing the open-circuit voltage or short-circuit current can lead to increased device efficiencies.

Although roughly half of the total energy from sunlight appears below 700 nm, Figure 1 suggests that by absorbing more light at longer wavelengths, a larger short-circuit current can theoretically be obtained, thus increasing a device's efficiency. By pushing absorption into longer wavelengths, the optical band gap is lowered (see Section 1.2) but there is a negative effect of the short-wave photons on the lowered band gap.

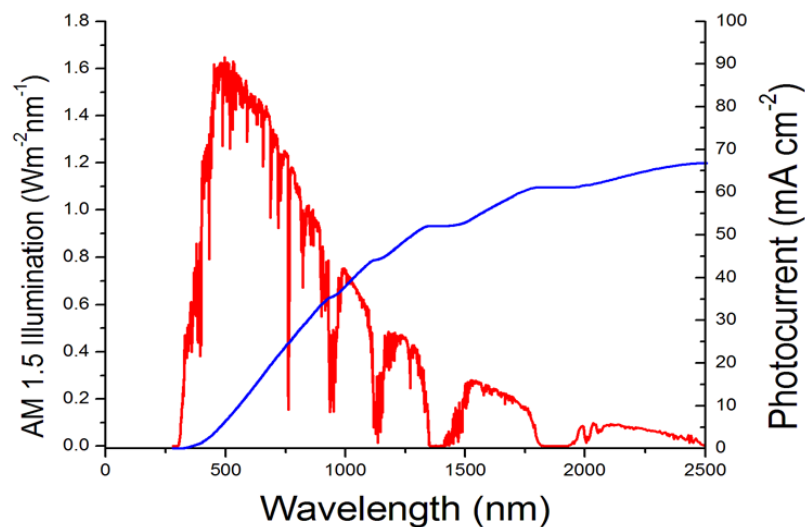


Figure 1: Solar irradiance spectrum, for single band gap containing material at AM 1.5 illumination (red) vs. maximum theoretical photocurrent at a given wavelength (blue).

Solar PV technology has been dominated largely by silicon-based devices over the last 50 years.<sup>10</sup> While commercial single-junction silicon-based solar cells are reaching efficiencies of 20 %, they are still plagued by high costs due to scalability issues: the manufacturing of PV devices is an energy-intensive process that also requires the use of non-earth abundant elements like indium and tellurium.<sup>10-12</sup>

This dilemma has led researchers to investigate low-cost alternatives to the traditional silicon-based PV systems that also allow for large-scale production. Conjugated organic photovoltaic (OPV) systems have garnered interest in recent years as a potential low-cost alternative to the silicon-based PV systems because they can be constructed on large areas of lightweight flexible substrates by scalable processes.<sup>13,14</sup> In order to design a functional photovoltaic cell, a set of general optoelectronic requirements must be met: 1) an excited state is formed when a photoactive material absorbs light; 2) that excited state migrates to an interface where an electron transfer event takes place; 3)

the oxidized (hole) and reduced (electron) species must migrate to their respective electrodes so they can be collected as electrical energy.<sup>9</sup>

## 1.2 Organic Photovoltaics

Organic photovoltaic studies began in 1959 when Kallman and Pope observed a photovoltaic effect in a single crystal of anthracene when it was sandwiched between two identical electrodes and illuminated from one side.<sup>15</sup> Just a few years later, they also observed the same effect in a tetracene / water system.<sup>16</sup>

Just twenty years after the Kallman group reported their findings on the tetracene / water system, C. W. Tang reported findings of a single junction bilayer device utilizing a donor / acceptor construct, yielding a PCE of about 1 %.<sup>17</sup> Figure 2 illustrates the two materials used in the device: the electron donor material, a copper phthalocyanine, was vapor deposited onto a substrate, followed by the perylene tetracarboxylic derivative electron acceptor material.

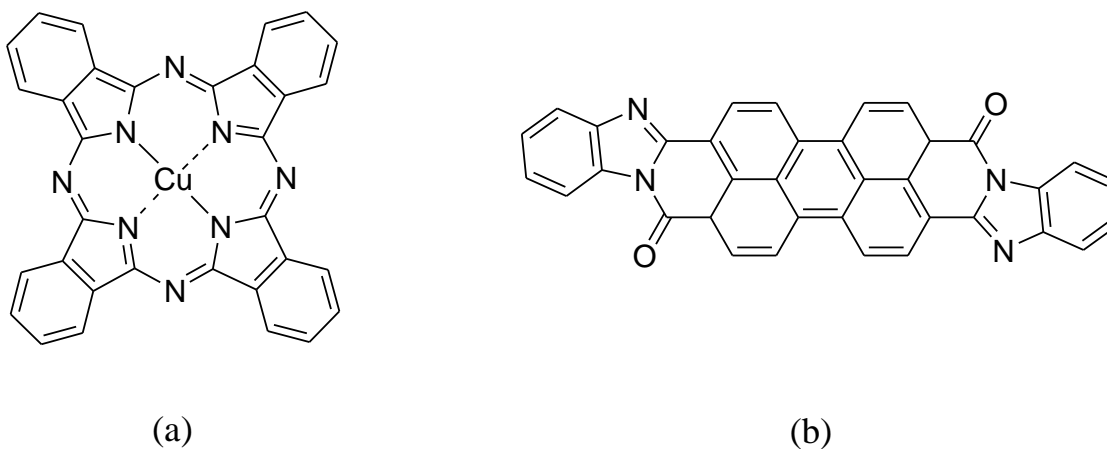


Figure 2: Compounds found in the active layer of the PV device constructed by C. W. Tang, (a) copper phthalocyanine (CuPc) and (b) perylene tetracarboxylic derivative acceptor.

While using vapor deposition techniques allows for a finer control of photoactive layer thickness and continuity, the main drawback to using vapor deposition techniques

in the construction of OPV devices is the cost. Vapor deposition typically requires special equipment and high temperatures to process a device, driving up cost. In an effort to lower the cost of OPV devices, solution processing has attracted attention in recent years.<sup>14,18</sup>

Solution processing with small molecule and polymer photoactive materials allows for large scale manufacturing on lightweight, flexible substrates and frequently in large batches. One of the most studied photoactive layers in OPV research is the bulk heterojunction (BHJ) solar cell.<sup>19,20</sup> With photoconversion efficiencies of small molecule systems and polymer systems recently breaking 10 % and 9 %, respectively, BHJ systems, they are emerging as direct competition with the slightly more efficient (and more expensive) silicon based devices currently on the market.<sup>21,22</sup> Figure 3 illustrates the PCE records of research PV devices certified by the National Renewable Energy Laboratory (NREL), including single- and multi-junction PV cells. As shown in the chart, organic devices have seen a significant increase in efficiency improvements over the past 14 years, while the traditional silicon-based PV devices have remained relatively constant since the early 1990s.

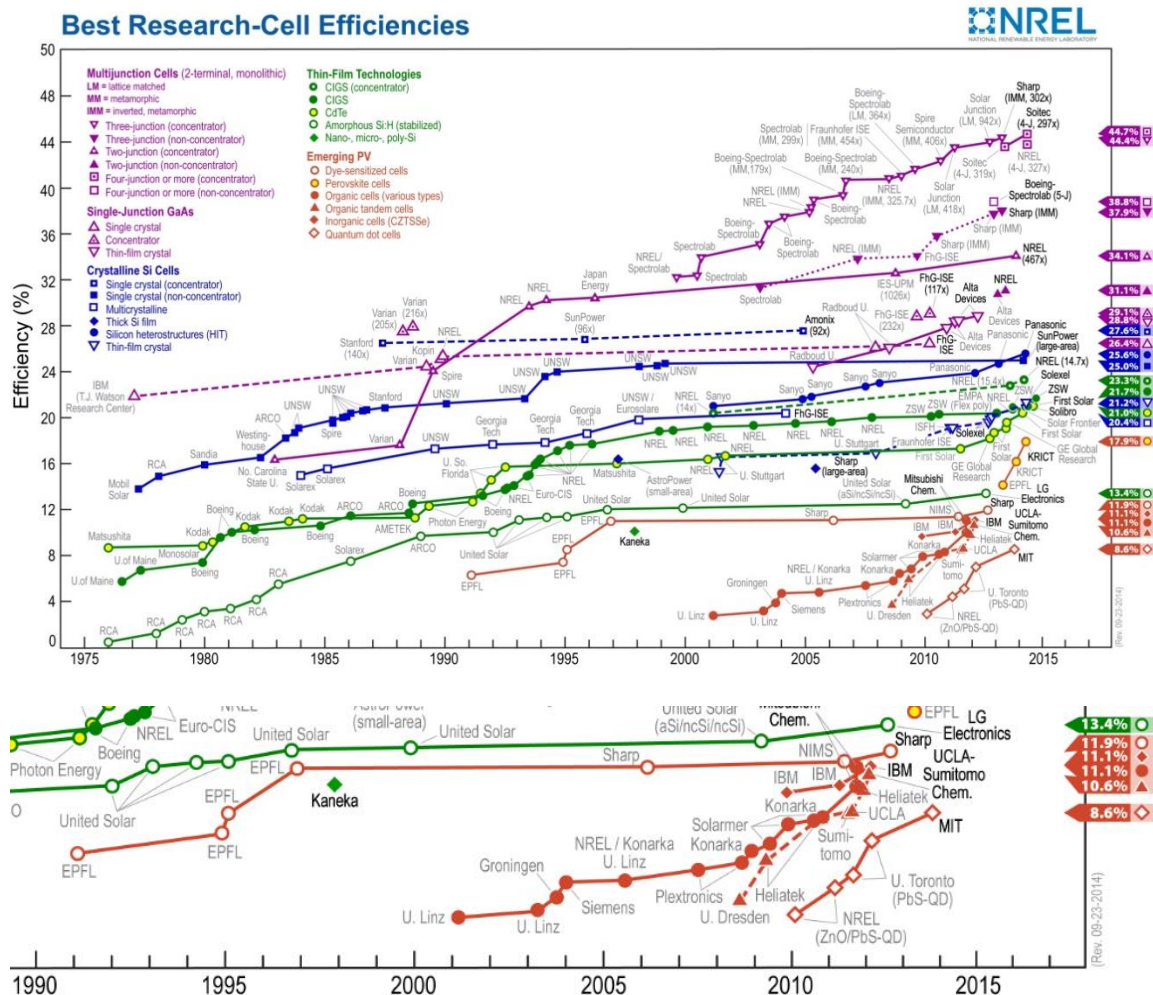


Figure 3: National Renewable Energy Laboratory (NREL) ranking of various PV device efficiencies (top) and an enlarged view of emerging device efficiencies (bottom).<sup>23</sup>

Although device efficiencies continue to improve, thin-film OPV devices are not without their disadvantages. Research cells (Fig. 3) are not optimized for environmental stability, and as a result, suffer from short-lived device lifetimes due to decomposition or degradation of the photoactive material.<sup>24–26</sup> Reproducibly generating the same morphology in the photoactive layer via solution processable techniques also raises concerns for OPV devices. In BHJ devices, the donor and acceptor material are mixed together and either drop-casted or doctor-bladed onto the substrate, generating a random blend of donor / acceptor materials due to phase segregation.<sup>27–29</sup>

In order to increase the device efficiencies of organic PV devices, new photoactive materials must be better designed to improve the photophysical properties that allow for efficient solar energy conversion, while protecting against environmental factors and dictating the ideal morphology of the film.

### 1.3 Bulk Heterojunction Solar Cells

Bulk heterojunction solar cells function to increase the surface area between two materials, in efforts to separate charge more efficiently. The two materials are composed of a donor material, the principle light absorber and electron transporter, and an acceptor material, the principle electron acceptor and transporter. Figure 4 shows the typical morphology of a BHJ cell, with a phase segregated blend of donor and acceptor materials laced throughout the device.

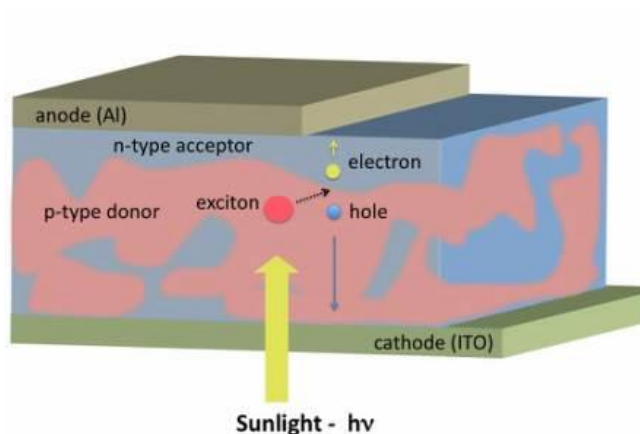


Figure 4: Design and morphology of a typical BHJ solar cell, with the donor material (red) blended with the acceptor material (blue) in the active layer.<sup>9</sup>

The fundamental photoconversion process for a BHJ solar cell is outlined in Figure 5. In this process, a series of steps must occur in order to generate an electrical current. First, a photon must be able to excite an electron ( $e^-$ ) from the highest occupied molecular orbital (HOMO) to the lowest unoccupied molecular orbital (LUMO) in the donor material, leaving a vacant spot where the electron was located, known as a hole

( $h^+$ ). This energy absorption generates a coulomb-correlated electron-hole pair (exciton), which has a binding energy that can vary from 0.1 – 0.5 eV.<sup>30</sup> The exciton then moves through the donor material, with a diffusion length (how far the exciton can move before the electron and hole recombine and the energy is lost) ranging from 10 – 80 nm.<sup>31,32</sup> Once the exciton reaches an interface, the electron is transferred from the LUMO of the donor material to the LUMO of the acceptor material, after which the electron and hole migrate to their respective electrodes. An external wire completes the circuit.

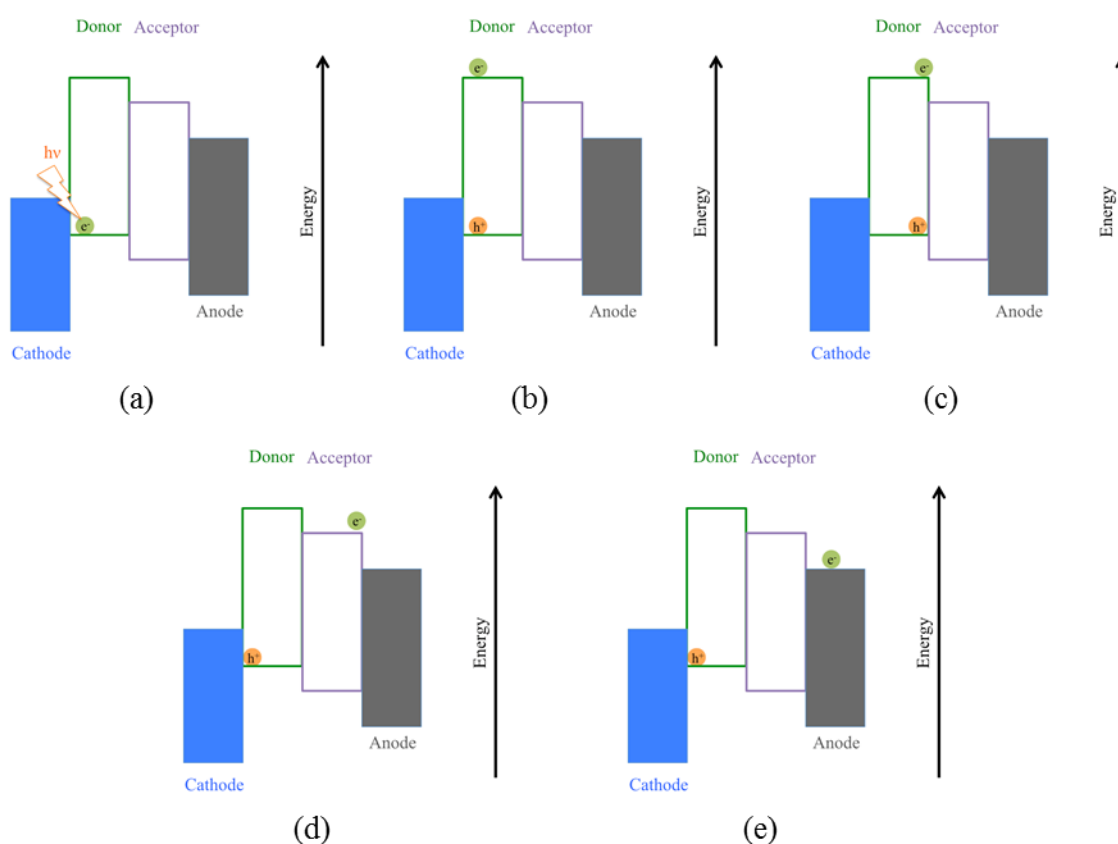


Figure 5: Schematic of charge generation and separation in a BHJ device. (a) a photon striking the donor material, generating an exciton(b); (c) excitation diffusion through the donor material until it reaches a donor / acceptor interface; (d) transfer of electron to the acceptor material; (e) electron and hole migration to opposite electrodes, due to electrode work function offset.

In order to have an effective photoconversion process occur in the BHJ active layer, the band gaps between the donor and acceptor materials must be aligned accordingly (Fig. 5). The electron transfer process must follow a “downhill” path in order to favor the electron transfer rather than the recombination of the electron-hole pair. This electron flow dictates that the LUMO of the donor material must be higher than the LUMO of the acceptor material by an energy difference greater than the exciton binding energy (0.1 – 1 eV).

The alignment of the energy levels of the donor and acceptor materials also gives insight to a device’s potential performance. Figure 6 shows that the difference between the HOMO of the donor material and the LUMO of the acceptor material provides the maximum theoretical  $V_{oc}$  that could be produced by the active layer.<sup>33</sup>

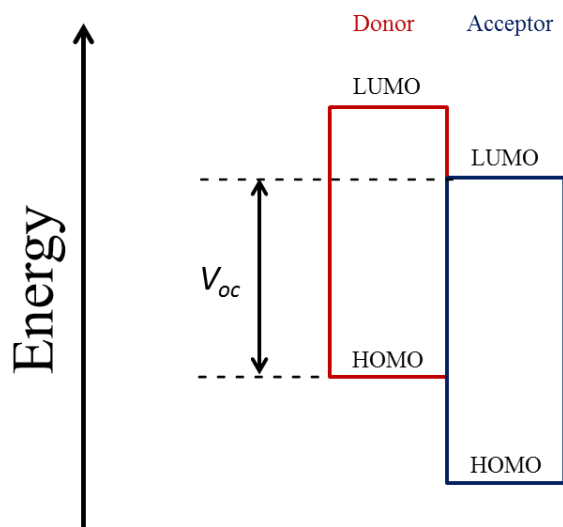


Figure 6: Energy level diagram of a typical BHJ active layer, showing that the energy difference between the HOMO of the donor material and the LUMO material indicates the maximum theoretical  $V_{oc}$ .

Motivated by the desire to create reproducible active layers in a BHJ device, research has refocused from the traditional blended bilayer to creating an intramolecular donor / acceptor system in polymers as well as small molecule systems.<sup>13,34–37</sup> Estimating

HOMO / LUMO levels of this intramolecular donor / acceptor system is straightforward. The HOMO of the donor component is taken as the HOMO of the resultant system, while the LUMO of the acceptor is taken as the LUMO of the resultant system (Figure 7). This method allows for simple manipulation of the components to lower the band gap of the system, therefore increasing light absorption at lower energy (longer wavelengths).<sup>38</sup>

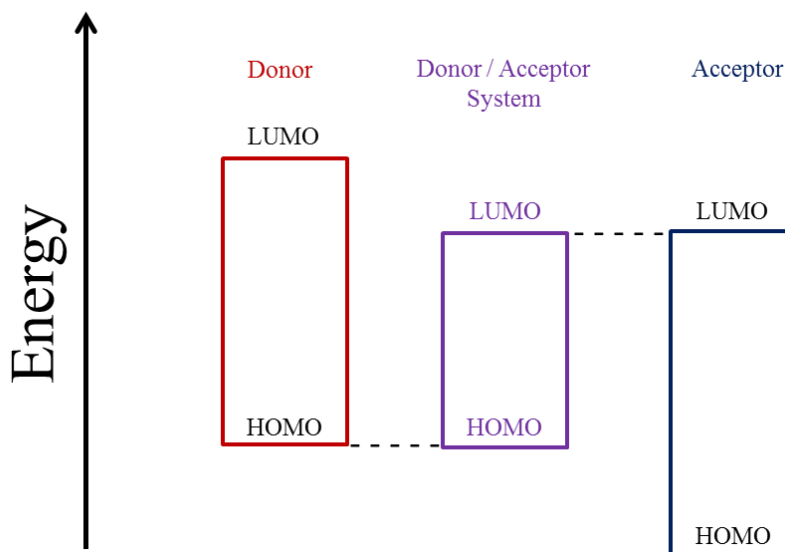


Figure 7: Energy level diagram of a donor and acceptor material, where the HOMO of the donor material and the LUMO of the acceptor material are used to estimate the HOMO / LUMO levels of the donor / acceptor system.

#### 1.4 Porphyrins

Porphyrins are conjugated, aromatic macrocycles composed of four pyrrolic rings linked together by methine carbons, as shown in Figure 8. There are 22  $\pi$  electrons present in the macrocycle, of which 18 are active in the conjugated system, thus obeying Hückel's Rules for aromaticity ( $n = 4$ ). This aromaticity is typically associated with the presence of a diaza[18]annulene substructure.<sup>39-41</sup> This aromaticity lowers the HOMO / LUMO band gap and allows for porphyrins to absorb light across the visible spectrum.

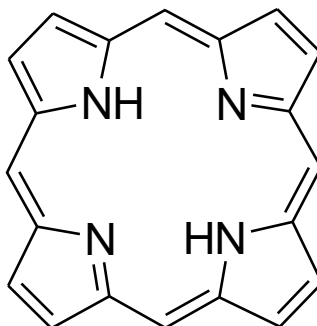


Figure 8: Structure of the most basic porphyrin, porphine.

Porphyrins are easily modified to allow for light absorption at different wavelengths by altering the types of substituents present on the macrocycle and also by coordinating different divalent metals inside the core of the macrocycle. By extending the  $\pi$ -conjugation out and away from the macrocycle to the periphery, red-shifted absorbances ( $\pi - \pi^*$  transitions) are observed. Porphyrins that have no metal coordinated in its core (free base) are characterized by a strong absorption maximum around 400 nm ( $\epsilon = 10^5 \text{ M}^{-1} \cdot \text{cm}^{-1}$ ) and four Q bands ranging from 480 – 700 nm in their absorption spectra, as seen in Figure 9.<sup>42</sup> The Q bands are a result of vibrations of the inner two hydrogens within the macrocycle's core, located on the pyrrolic nitrogens. When a divalent metal ion is coordinated in the core of the porphyrin macrocycle, the saddle-shaped core is flattened resulting in a slight increase in aromaticity and symmetry (Figure 9), shifting the Soret peak absorbance to longer wavelengths. The replacement of the two pyrrolic hydrogens with a divalent metal ion also results in the loss of two of the Q bands.

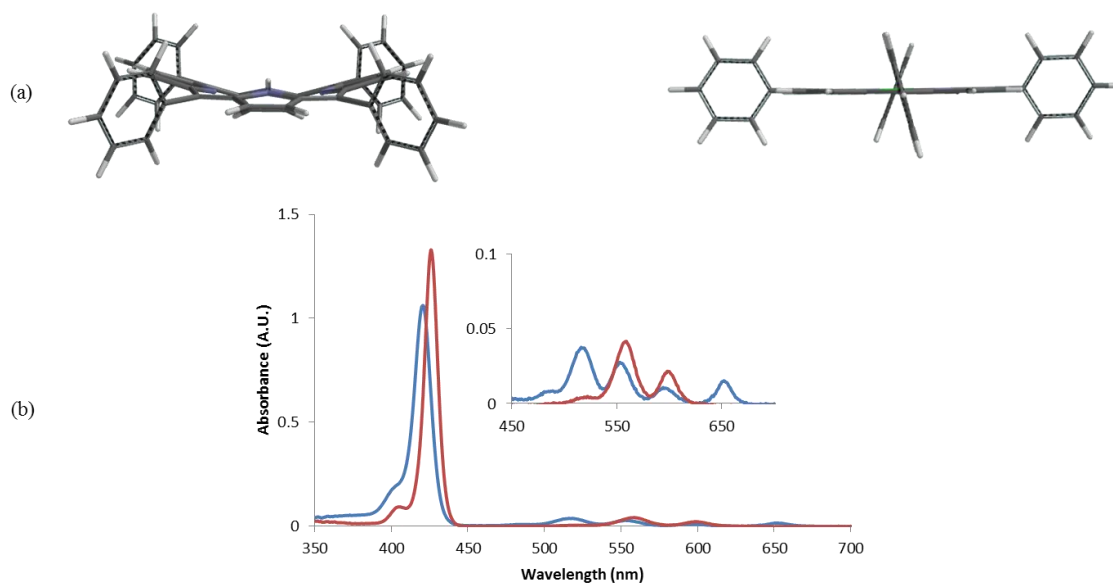


Figure 9: (a) Computational models of tetraphenylporphyrin (TPP), left, and zinc-metallated tetraphenylporphyrin (Zn-TPP), right, illustrating the increase in planarity of the porphyrin macrocycle upon coordination of a divalent metal ion. (b) Absorption spectra of TPP (blue) and Zn-TPP (red) showing the relative locations of the Soret peaks and Q bands between the two porphyrins.

The porphyrin macrocycle with its easily-tuned band gaps has received attention in a wide range of research applications from OSCs,<sup>20,37,43,44</sup> to organic field effect transistors (OFETs),<sup>34,45</sup> and even pharmacological applications in photodynamic therapy.<sup>46,47</sup>

Direct synthesis of *meso*-substituted porphyrins has seen several improvements over the years, in terms of reaction conditions and overall product yields. TPP was first synthesized by Rothmund in 1936 by reacting benzaldehyde and pyrrole in pyridine in a sealed bomb at 150 °C for 24 hours.<sup>48</sup> However, this method suffered from poor yields and intense reaction conditions. In 1967, an improvement to the Rothmund method was introduced by Adler and Longo. The milder reaction conditions required only a 30 minute reflux in propionic acid for 30 minutes, thus allowing for improved yields from a large variety of aldehyde starting materials.<sup>49,50</sup>

In 1960, MacDonald et. al. published their studies on the synthesis of *meso*-substituted *trans*-porphyrins.<sup>51</sup> In their work, they were able to prepare a wide range of *trans*-porphyrins by performing a condensation, followed by oxidation, of a *meso*-substituted dipyrromethane and an aldehyde. However, the major limitation to this method lies in the mixture of porphyrin products formed due to a scrambling process that occurs during the condensation. To improve on this methodology, Lindsey et. al. were able to suppress the scrambling events seen in the MacDonald 2 + 2 condensation by utilizing sterically-hindered dipyrromethanes.<sup>43</sup> Yields were improved by minimizing the amount of scrambling, pushing 48 % for tetratolylporphyrin (TTP).

### 1.5 Porphyrins in Nature

An aromatic analogue to porphyrins that has been used for solar energy conversion for billions of years in plants is the chlorin molecule (Figure 10). Chlorins bear the same skeleton structure as porphyrins, but differ in the number of  $\pi$  electrons present in the macrocycle (20  $\pi$  electrons).

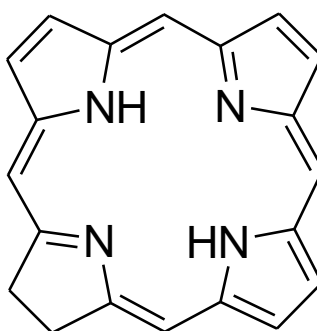


Figure 10: Structure of a chlorin, illustrating the presence of two saturated carbons.

In plants, the chlorins chlorophyll a and chlorophyll b are the principle light absorbers in photosynthesis that aid in the conversion of solar energy into energy usable by the cell, stored in the form of chemical bonds. Figure 11 displays the two main chlorophyll molecules present in plant cells along with their absorption spectra.

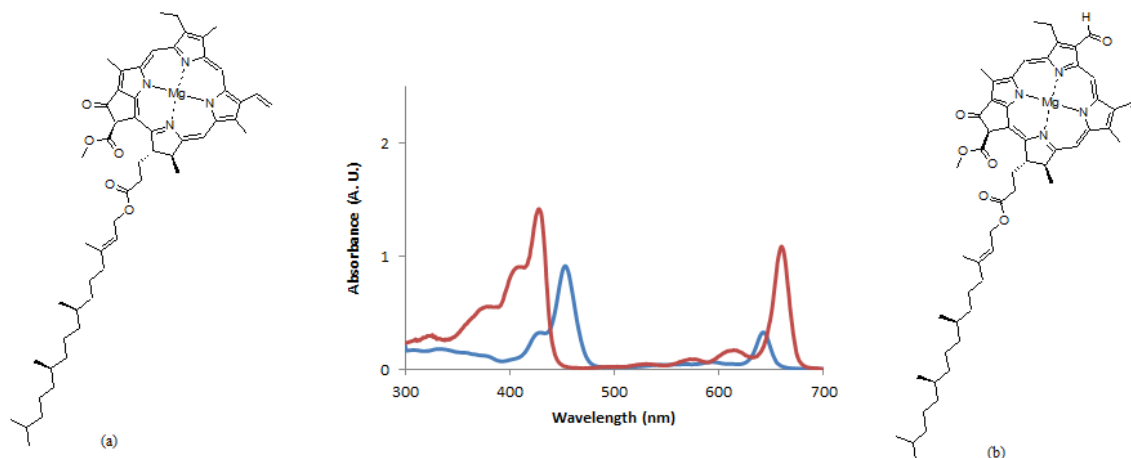


Figure 11: Chemical structures and UV-Vis absorption spectra of (a; red) chlorophyll a and (b; blue) chlorophyll b.

With a similar structure to the chlorophylls seen in plants, along with their similar light absorption characteristics, porphyrins are seen as viable platforms for OSC photoactive materials.

### 1.6 Porphyrins in Organic Photovoltaics

There have been many advances in recent years in OPV research involving porphyrin active layers. Porphyrins are commonly seen in BHJ devices, both in small-molecule<sup>52</sup> and polymer systems<sup>34</sup>, as well as dye-sensitized solar cells (DSSCs).<sup>53</sup>

Figure 12 illustrates the structure of SM315, the porphyrin dye with the highest device efficiency for a porphyrin in a solution processable DSSC, which is also currently the most efficient sensitizer in a DSSC.

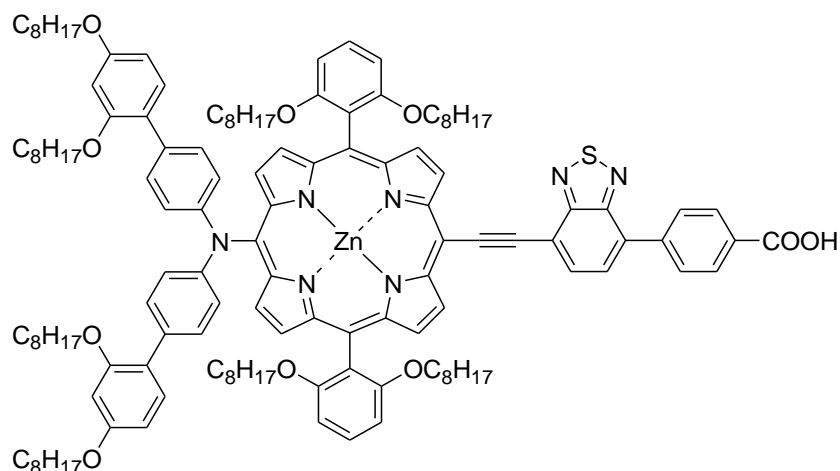


Figure 12: Structure of the porphyrin SM315 found in the active layer of a DSSC that afforded 13 % PCE.

The PCE peaked at 13 %, and is attributed in part to its intramolecular push / pull design: the electron rich amine on the left-hand side of the porphyrin forces the excited state out towards the electron-acceptor benzothiadiazole group.<sup>54</sup> The electron is injected into the TiO<sub>2</sub> nanoparticles on the conductive substrate. A cobalt (II/III) redox shuttle is used as the electrolyte in this system, completing the circuit. Although DSSCs provide the best PCEs for porphyrin systems, issues in manufacturing arise with the electrolyte solution. The device must be hermetically sealed to retain the electrolyte solution, so if the electrolyte is lost due to damage or other external issue, the device is rendered useless.

Porphyrin based polymer systems found in BHJ solar cells have not seen the same acclaim. A recent porphyrin – dithienothiophene copolymer utilized a very interesting donor / acceptor design (Figure 13), but afforded a meager 0.3 % PCE (one of the highest PCEs for porphyrin-based polymer systems).<sup>34</sup>

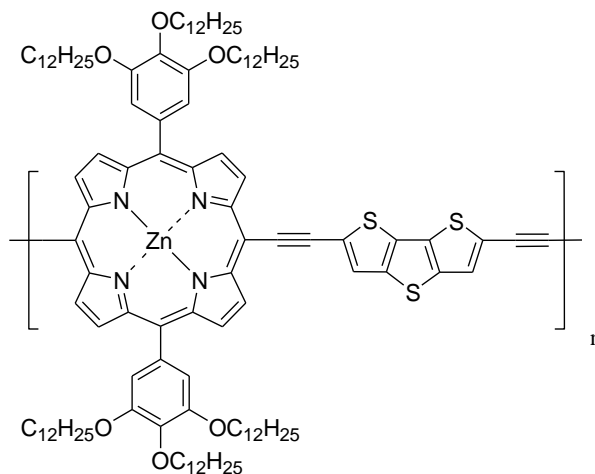


Figure 13: Porphyrin – dithienothiophene copolymer synthesized by Huang et. al.<sup>34</sup>

Due to the extended  $\pi$ -conjugation of this system, an onset of absorbance was seen at over 800 nm in solution, and over 900 nm in thin films. However, the presence of the triple bond spacers limited the molecular weight and thermal stability of the polymer, when compared to the analogous polymer that did not contain the two triple bond spacers.

Porphyrin-containing small molecule systems seen in BHJ solar cells have attracted the interest of many researchers in recent years, largely due to their interesting photophysical properties, but without the reproducibility issues seen in polymer systems. Figure 14 illustrates two porphyrin small molecule systems that have shown to be effective in a BHJ solar cell.

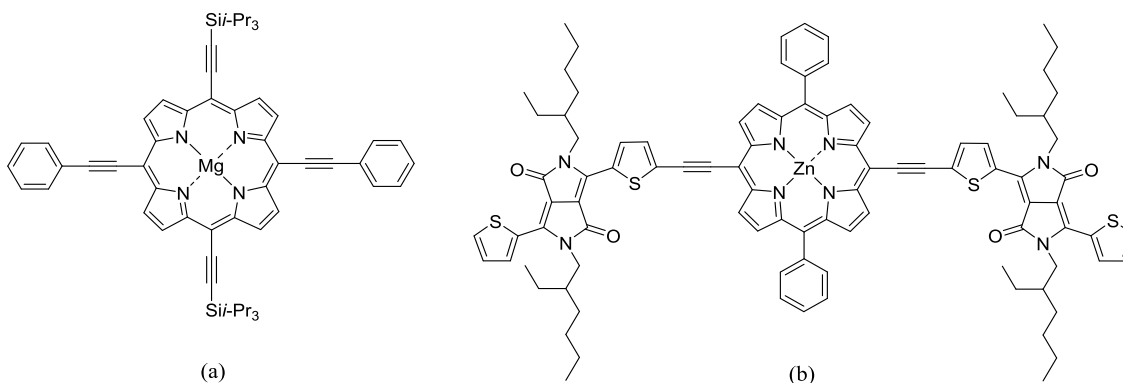


Figure 14: Porphyrin small molecule systems (a) [5,15-bis(phenylethynyl)-10,20-bis[(triisopropylsilyl)ethynyl]porphyrinato]magnesium(II)<sup>20</sup> and (b) DPPEZnP-O.<sup>55</sup>

The *trans*-triisopropylsilyl (Fig. 14 (a)) was designed for extended  $\pi$ -conjugation and solubility; when blended with PCBM (1:4), a modest PCE of 2.5 % was obtained. The porphyrin containing the diketopyrrolopyrrole units (Fig. 14 (b)) displayed an impressive absorption onset over 900 nm in thin film, and an equally impressive PCE of 7.23 % when blended with PCBM.

### 1.7 Thiazolothiazoles

The identity of the aromatic fused, heterocyclic parent thiazolo[5,4,*d*]thiazole (TTz) compound was first determined by Roger Ketcham in 1956 (Fig. 15).<sup>56</sup> The parent heterocycle is most commonly prepared by condensing furfural with dithiooxamide to yield a 2,5-difurfuryl-thiazolo[5,4,*d*]thiazole, which is subsequently oxidized to the diacid and decarboxylated by refluxing in ethanol.<sup>57</sup> The parent compound exhibits absorption maxima at 255 nm and 360 nm.

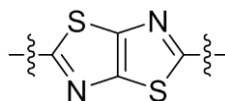


Figure 15: Thiazolo[5,4,*d*]thiazole parent heterocycle.

As shown in Figure 16, research involving TTz compounds remained sporadic for several decades.<sup>24</sup> That is, until researchers were able to tap into its hidden potential as a component of OPV systems.<sup>58-62</sup>

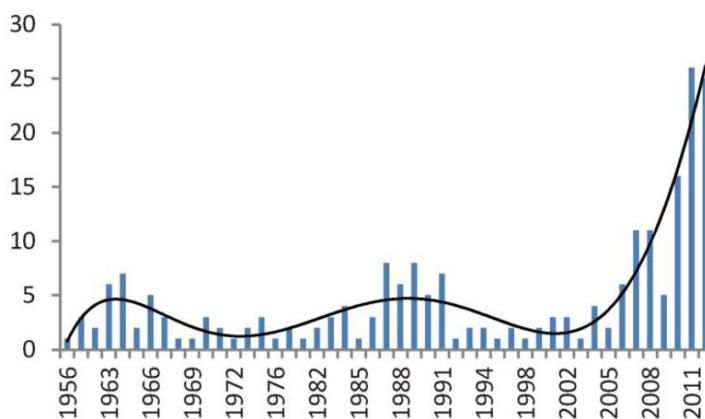


Figure 16: Histogram illustrating the number of TTz research publications as a function of time.<sup>24</sup>

One of the main attractions with TTz compounds is their resistance to degradation from environmental factors like moisture and oxygen, when compared to thiophene systems that are currently flooding OPV research. The electronics vary greatly from electron-rich as seen in thiophene / bithophene systems to electron-deficient. This electron deficiency accounts for the aforementioned environmental stability of the TTz parent heterocycle.

The morphology of the TTz heterocycle also accounts for its interesting electronic behaviors. The parent heterocycle is highly planar and aromatic, allowing for strong  $\pi$ - $\pi$  stacking interactions and orbital overlap to afford high hole and electron mobilities necessary of efficient OPV devices.<sup>24,29</sup> However, poor solubility of the parent heterocycle in organic solvents dictates that solubilizing substituents must be incorporated into the molecule for potential use in solution-processable OPV devices.

## 1.8 Thiazolothiazoles in Organic Photovoltaics

As shown previously, thiazolothiazoles have attracted great attention in recent years: some research has been performed in the small-molecule area of organic electronics;<sup>61,63–65</sup> however, most of the research regarding TTz systems have been polymer based.<sup>14,29,60,66–70</sup>

The typical design of TTz small molecule systems utilizes a donor / acceptor motif, where the TTz acts as the electron-deficient accepting unit to two identical aromatic donor units on either side.<sup>63,65</sup> Figure 17 displays such small molecule systems that exhibit interesting photophysical properties in solution and as cast in thin films.

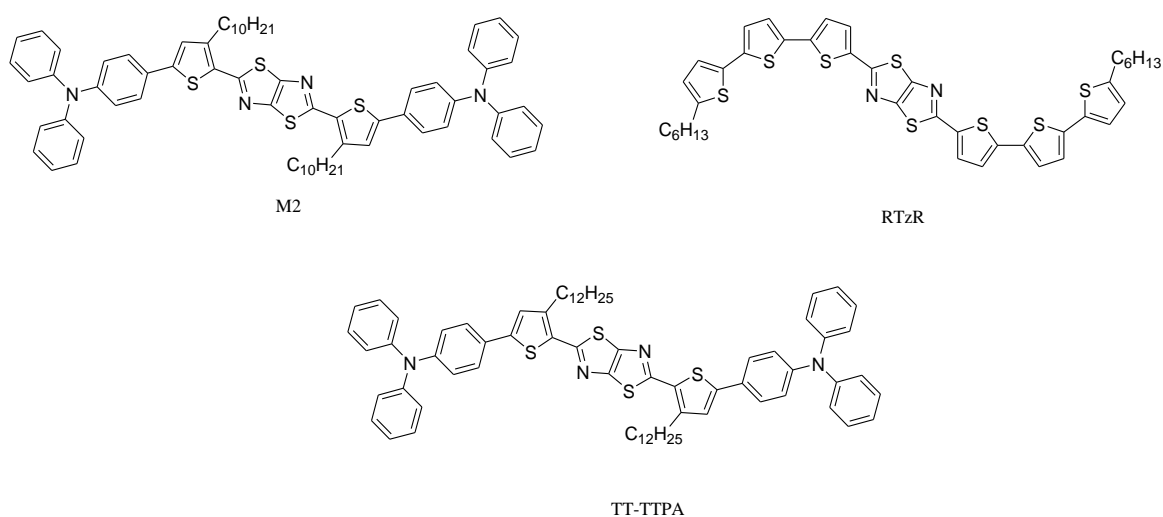


Figure 17: TTz small molecule systems M2 (top left), TT-TTPA (bottom center), and RTzR (top right).

M2 and TT-TTPA are similar in structure, only differing in the number of carbons in the solubilizing chains. Interestingly, they exhibit different absorption maxima of 465 nm and 422 nm for M2 and TT-TTPA, respectively in solution.<sup>61,65</sup> When cast as thin films, M2 and TT-TTPA exhibit slightly red-shifted absorptions (4 nm and 14 nm, respectively) indicating there is some sort of molecular organization in the film, most likely in the form of  $\pi$ - $\pi$ -stacking. RTzR also exhibits small red-shifts in absorption when

cast as a thin film (447 nm to 452 nm). All three compounds produce  $J_{SC}$ 's, but fall short of the high hole mobilities seen in polymer based TTz systems.

Polymer-based TTz systems, like those shown in Figure 18, have only recently emerged as building blocks of OSCs when Choi *et. al.* prepared a low bandgap polymer (Fig. 18 . a) via Stille cross coupling in 2010. Their device afforded a humble PCE of 1.21 %.<sup>69–71</sup>

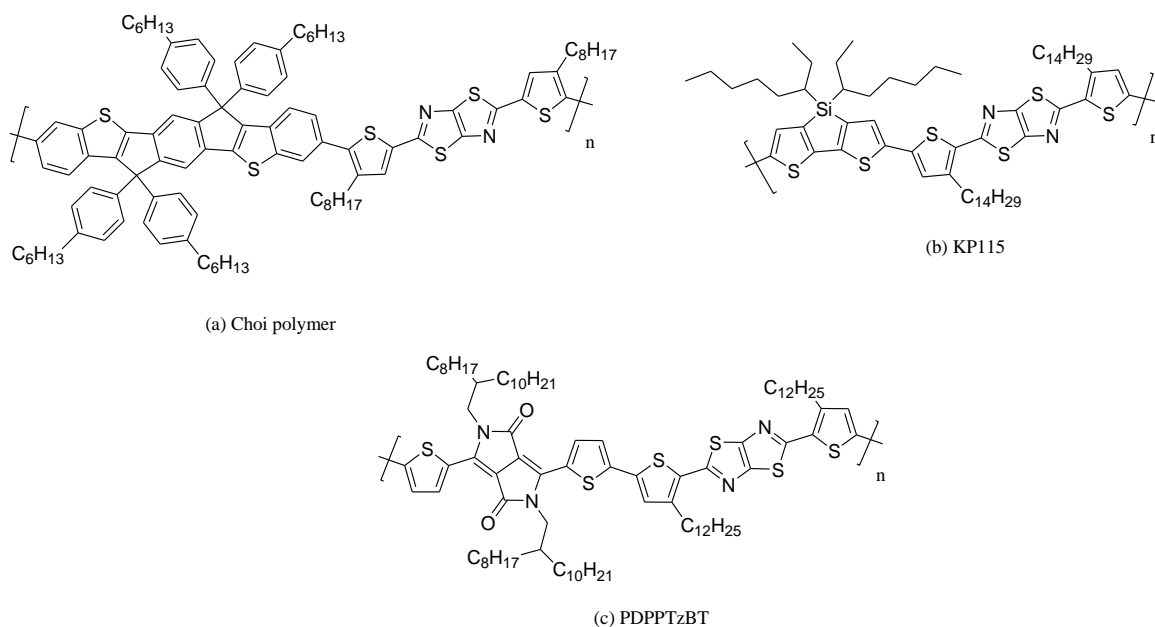


Figure 18: TTz-based polymer systems used in OSCs; (a) Choi polymer, (b) KP115, and (c) PDPPTzBT.

From the structures shown it is apparent that solubilizing substituents are needed in order to prepare solution-processable polymers. The strength of the donor portion of the polymer also appears to correlate with enhanced photophysical properties. PDPPTzBT (Fig. 18(c)) performs the best of the three with respect to hole mobility and absorption in solution and thin films. PDPPTzBT boasts an impressive hole mobility of  $3.43 \text{ cm}^2 \cdot \text{V}^{-1} \cdot \text{s}^{-1}$  and an equally impressive absorption maxima at 772 nm in solution and 806 nm as a thin film.<sup>69</sup>

## 1.9 Design of Thiazolothiazole Functionalized Porphyrin Systems

With porphyrin systems growing in popularity in OPV research, it is of great interest to investigate structure function relationships in these systems. Small molecule systems provide processing advantages over polymer systems due to their relative ease of manipulation. Polymer systems are plagued with issues in charge transfer and electron / hole extraction from devices due to variations in the film processing conditions stemmed from broad molecular weight distributions and poor overall solution processability.<sup>72</sup> As noted previously, extending the conjugation away from the porphyrin macrocycle aids in red-shifted absorbance maxima; adding long-chained substituents to the porphyrin macrocycle aids in solution processability.

Thiazolothiazole systems are of great interest for this research because they have been shown to possess interesting optoelectronic properties i.e. red-shifted absorbances, reduced band gaps, and PCEs approaching 6 %. However, research of TTz-functionalized small molecule systems remains rather scarce;<sup>64,65</sup> to date, there have not been any published investigations of TTz-functionalized porphyrin small molecule systems. It is of great interest to bridge the gap between TTz based conductive polymers and porphyrin based small molecule systems by synthesizing and characterizing a class of TTz-functionalized porphyrins systems. Porphyrins have proven to be dependable light absorbers in nature and recent OPV research indicates that porphyrins are also a fitting platform for light harvesting in OSCs; thiazolothiazoles have also proven promising components of conductive polymers. Taking the factors previously outlined in the introduction into consideration, motivation for pursuing TTz-functionalized small molecule systems for OSC applications has been presented. It is also of great interest to

design these systems for potential applications in polymer systems, as these small molecule systems may hold vital information in the improvement of polymer-based systems (Fig. 19 (b) and (d)).

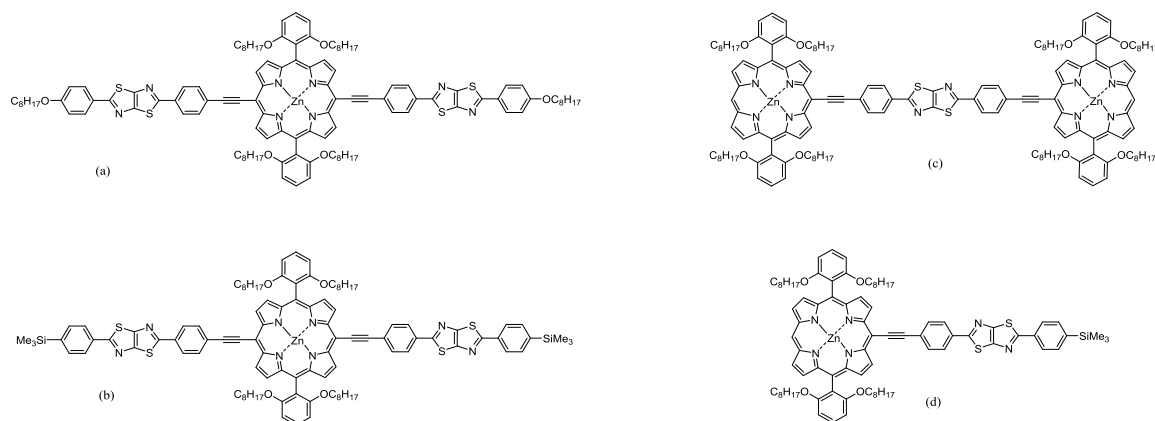


Figure 19: Donor / acceptor porphyrin – thiazolothiazole structures of interest (a) A-D-A TTz-P-TTz, (b) A-D-A (TMSTTz)<sub>2</sub>P (c) D-A-D dyad P-TTz-P and (d) mono-coupled D-A P-TMSTTz.

Synthetic routes in the pursuit of the desired porphyrin molecular systems (Fig. 19) proved demanding in certain aspects, but fruitful in most areas. Several attempts at purifying the TTz components seen in the A-D-A system (Fig. ee (a)) proved unsuccessful. Several synthetic routes were pursued in effort to synthesize the unsubstituted dipyrromethane needed to prepare the *trans*-(dioctoxyphenyl)porphyrin component of all systems,<sup>73–76</sup> but were ultimately abandoned and replaced with a commercially available, albeit expensive, source of the dipyrromethane. The building blocks seen in all the systems were successfully synthesized via Lindsay 2+2 condensation conditions (Figure 22).<sup>77</sup>

The synthesized porphyrin and thiazolothiazole compounds of interest were explored through computational modeling and spectroscopic techniques. The desired small molecule systems were screened through computational modeling to obtain

estimated HOMO / LUMO levels prior to preparation in order to determine potential viability for use in OSC application. This thesis details the synthesis and preliminary characterization of novel thiazolothiazole-functionalized porphyrin components. The work presented provides the framework for future TTz-functionalized porphyrin system studies.

## CHAPTER 2. EXPERIMENTAL

### 2.1 Synthesis of Thiazolothiazole Functionalized Porphyrins

#### 2.1.1 Thiazolothiazole Syntheses

Utilizing the classic Ketcham condensation to produce symmetric TTz derivatives yielded easily purified reaction mixtures.<sup>56</sup> However, using the same process to synthesize asymmetric TTz derivatives yielded reaction mixtures containing multiple condensation products, as shown in Figure 20.

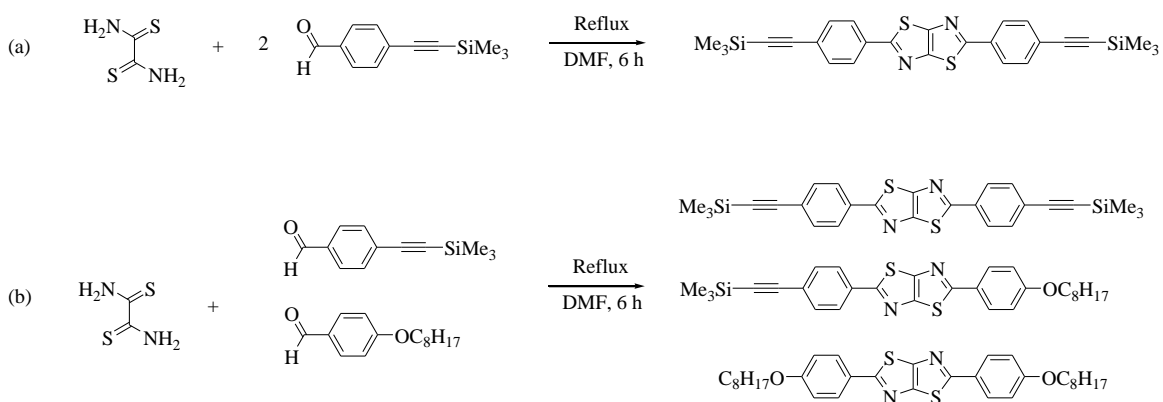


Figure 20: Synthetic route to prepare (a) the symmetric di-TMS TTz and (b) asymmetric TTz.

The purification procedures to isolate the asymmetric TTz were quite cumbersome. Early attempts at purifying the asymmetric TTz from the product mixture yielded small amounts of the desired asymmetric TTz along with starting aldehyde impurities. Several routes were explored for the purification of the desired asymmetric TTz, but were

unsuccessful due to similar retention factors ( $R_f$ ) by the three TTz compounds on TLC, as shown in Figure 21.

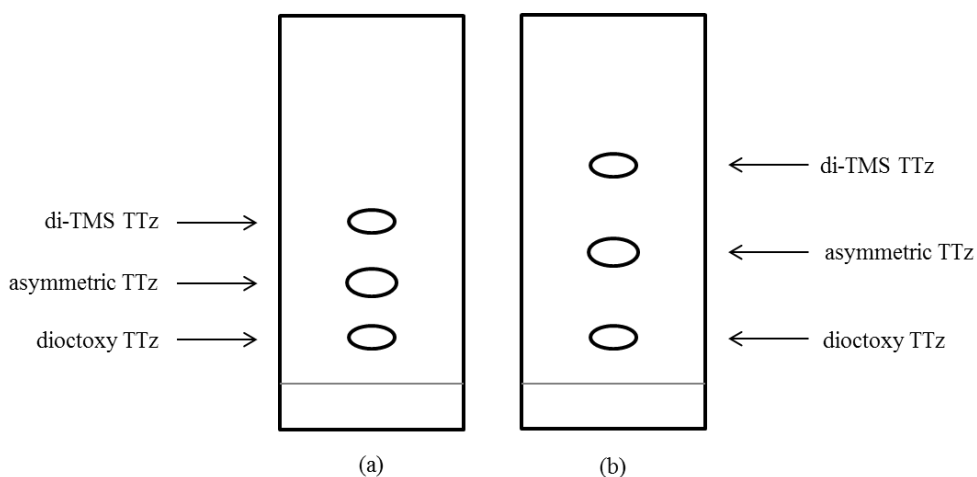


Figure 21: (a) Silica and (b) basic alumina TLC plates indicating the relative  $R_f$  values of the three TTz condensation products.

Purification techniques involving various solvents included: silica column

chromatography, HPFC, centrifugal chromatography, sublimation, and selective

recrystallization. TLC analysis of the reaction mixture on basic alumina plates afforded

spots that were spaced apart enough to warrant column chromatography with basic

alumina. However, several attempts to purify the reaction mixture on basic alumina were

unsuccessful. The tendency of the bands to streak and overlap, even with careful

monitoring of column flow rates, afforded very small amounts of the desired asymmetric

TTz product (< 2 mg) per run, along with the precursor TMS-benzaldehyde. The copious

amounts of alumina and solvents needed to afford these small amounts of desired product

ultimately led to its withdrawal from consideration in preparation of thiazolothiazole

functionalized porphyrins. It is of great interest to either identify an appropriate isolation

technique or another synthetic pathway to prepare the asymmetric TTz directly without

the need for a mixed-pot condensation.

### 2.1.1.a Synthesis of Di-TMS TTz

2,5-Bis-(4-trimethylsilylethynyl-phenyl)-thiazolo[5,4-*d*]thiazole: A stirred solution of 4-[(trimethylsilyl)ethynyl]benzaldehyde (0.77 g, 3.81 mmol) and dithiooxamide (0.22 g, 1.83 mmol) dissolved in DMF (20 mL) was refluxed for 4 h. After cooling to room temperature, the reaction mixture was filtered and washed with cold hexanes yielding a brown solid. The brown solid was subjected to silica column chromatography, eluting with DCM/hexanes (1/1) to afford a yellow solid (0.358 g, 41%).  $^1\text{H NMR}$  (500 MHz,  $\text{TFA}_d$ ,  $\delta$ ): 7.92 (d,  $J=8.6$  Hz, 4H), 7.69 (d,  $J=8.5$  Hz, 4H), 0.38 (s, 18H) UV-Vis  $\lambda_{\text{max}}$ (EtOAc,  $\epsilon=\text{M}^{-1}\text{cm}^{-1}$ ): 283 nm (33,000) melting point: 297 - 300 °C (subl.).

### 2.1.1.b Synthesis of Di-Ethynyl TTz

2,5-bis-(4-ethynylphenyl)-thiazolo[5,4,*d*]thiazole: One equivalent of the di-TMS TTz (50.0 mg, 0.103 mmol) was dissolved in dry THF (20 mL) and cooled to 0 °C in an ice water bath. 2.2 equivalents (66  $\mu\text{L}$ , 0.209 mmol) of TBAF in THF (1M solution with 5 %  $\text{H}_2\text{O}$  content) was then added in one portion and the reaction mixture was allowed to stir for 10 min. Then hexanes (22 mL) was added and allowed to stir an additional 15 min. The solvent was removed under reduced pressure and washed with copious amounts of cold water to remove the excess TBAF and *t*-butyl ammonium hydroxide, to afford a yellow solid. The yellow solid was then treated with warm benzene and centrifuged. The supernatant was decanted and the pellet placed in a vacuum oven to dry, to give the final product as a yellow solid (26.5 mg, 75.1 %).  $^1\text{H NMR}$  (500 MHz,  $\text{TFA}_d$ ,  $\delta$ ): 7.90 (d,  $J=8.4$  Hz, 4H), 7.66 (d,  $J=8.5$  Hz, 4H), 3.25 (s, 2H) UV-Vis  $\lambda_{\text{max}}$ (EtOAc,  $\epsilon=\text{M}^{-1}\text{cm}^{-1}$ ): 277 nm (42,000) melting point: 260 - 265 °C (dec.).

### 2.1.1.c Synthesis of Asymmetric TTz

2-(4-octoxyphenyl)-5-(4-trimethylsilylethynyl-phenyl)-thiazolo[5,4-*d*]thiazole: A stirred solution of 4-[(trimethylsilyl)ethynyl]benzaldehyde (2.54 g, 12.5 mmol), 4-octoxybenzaldehyde (2.94 g, 12.5 mmol), and dithiooxamide (1.01 g, 8.40 mmol) dissolved in dry DMSO (10 mL) was refluxed for 45 min. After cooling to room temperature, the reaction mixture was placed in the refrigerator overnight. The reaction mixture was filtered and washed with cold hexanes yielding a brown solid. The brown solid was dry-loaded onto alumina and subjected to column chromatography, utilizing a gradient elution of DCM/hexanes (3/1) to afford an oily yellow solid. As shown in the <sup>1</sup>H NMR (Appendix B.3), the structure can be suggested, but the remaining presence of a starting aldehyde prevents an accurate integration of the spectrum and accurate determination of overall product yield.

### 2.1.2 Synthesis of Porphyrin Precursors

The synthetic route for preparing the two porphyrin derivatives needed for the palladium cross-coupling reactions are outlined in Figures 22 and 23. Several synthetic pathways were pursued to obtain the unsubstituted dipyrromethane needed for the *trans*-bis(2,6-dioctoxyphenyl)porphyrin synthesis.<sup>73-76,78,79</sup> However, all pathways yielded minute (if any) amounts of the desired dipyrromethane, due largely to the low solubility and reactivity of the paraformaldehyde needed for the reactions. A commercially available source of the unsubstituted dipyrromethane was eventually obtained.

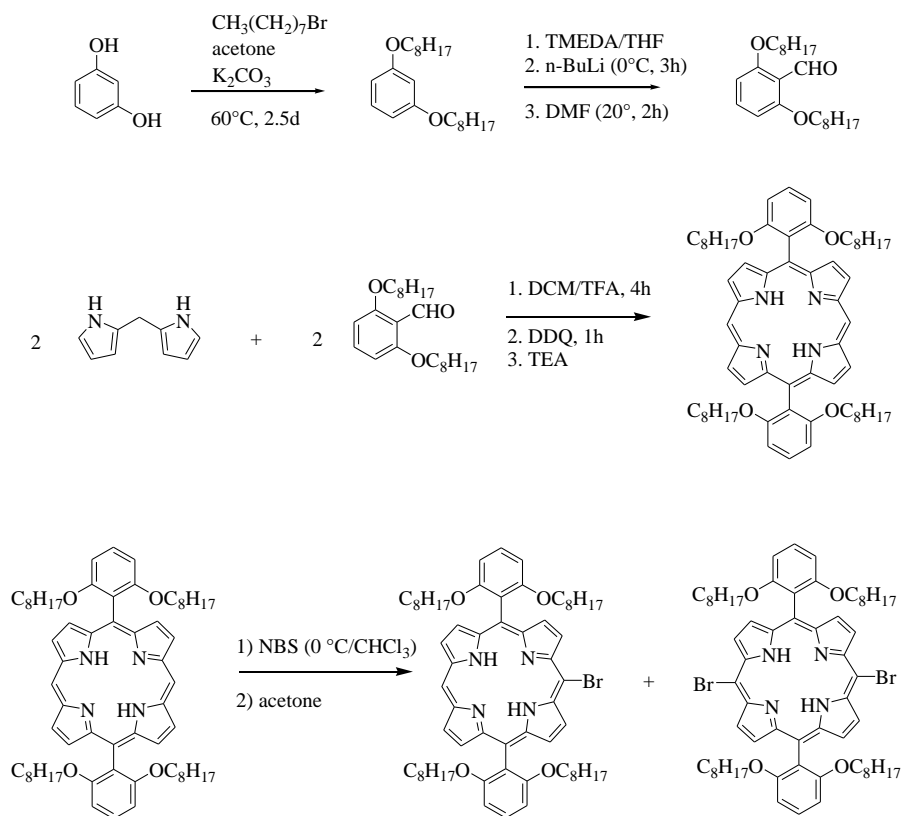


Figure 22: Synthetic route for preparing the free-base brominated porphyrin derivatives for palladium cross-coupling

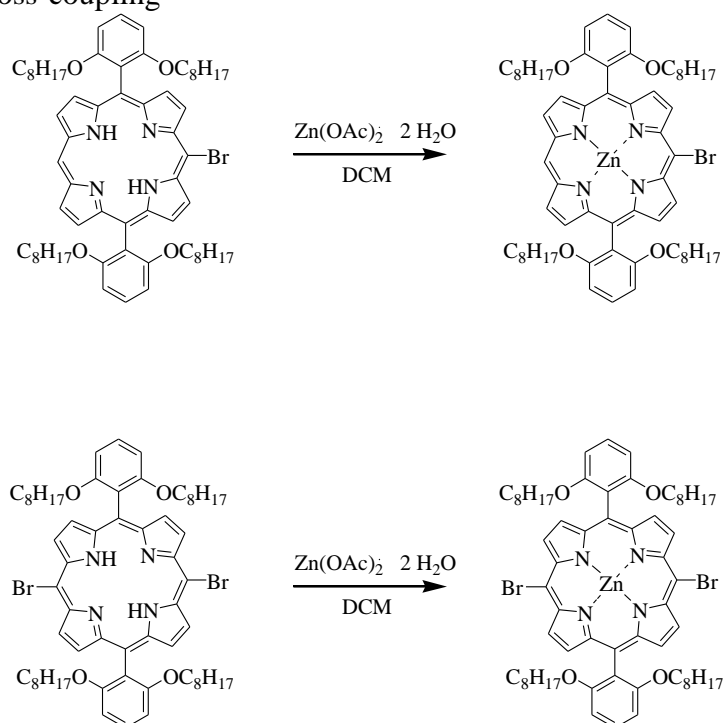


Figure 23. Reaction conditions necessary for zinc-metallation of the brominated porphyrin derivatives.

### 2.1.2.a Synthesis of 1,3-Dioctoxybenzene

1,3-dioctoxybenzene: To a stirred suspension of KOH (40.0 g, 0.713 mol) in DMSO (160 mL), resorcinol was added (10.0 g, 0.0908 mol) followed by a dropwise addition of 1-bromooctane (35.9 mL, 0.208 mol) over 60 min. The reaction mixture was left overnight at room temperature. The reaction was quenched with 150 mL H<sub>2</sub>O and hexanes (75 mL) was added. The organic layer was separated and washed with water (3 x 100 mL) and the solvent removed under reduced pressure to yield a tan solid. The final product was recrystallized from hexanes to afford a white solid (18.6 g, 61 %). <sup>1</sup>H NMR was consistent with literature values<sup>80</sup> (300 MHz, CDCl<sub>3</sub>, δ): 7.13 (t, *J*=8.3 Hz, 1H), 6.45 (m, 3H), 3.91 (t, *J*=6.4 Hz, 4H), 1.78-1.71 (m, 4H), 1.46-1.38 (m, 4H), 1.38-1.20 (m, 16H), 0.87 (t, *J*=7.1 Hz, 6H) GC-MS *m/z* calcd for C<sub>22</sub>H<sub>38</sub>O<sub>2</sub>: 334.29 (Found: 334.3).

### 2.1.2.b Synthesis of 2,6-Dioctoxybenzaldehyde

2,6-dioctoxybenzaldehyde: To a stirred solution containing 1,3-dioctoxybenzene (10.0 g, 30.0 mmol) in 85 mL of tetrahydrofuran (THF), *N,N,N',N'*-tetramethylethylenediamine (TMEDA) (1.15 mL, 7.67 mmol) was added. This mixture was degassed with a stream of argon for 20 min and cooled to 0°C, then *n*-butyllithium (3.59 mL, 10.0 M solution in hexanes, 11.5 mmol) was added dropwise over 15 min. After allowing the reaction to stir for 3 h, the reaction flask was lifted out of the ice bath and allowed to warm to room temperature. Once at room temperature, dimethylformamide (DMF) (4.38 mL, 60.0 mmol) was added dropwise over 15 min, and the reaction stirred for 2 h. The reaction was quenched with 50 mL of water and the organic product extracted with ether (4 x 50 mL), dried over anhydrous magnesium sulfate (MgSO<sub>4</sub>), and filtered. The solvent was removed using a rotary evaporator, producing a light yellow oil. The product was

recrystallized in hexanes to yield the final product as an off-white solid (3.78 g, 34.9 %).

$^1\text{H}$  NMR was consistent with literature values<sup>80</sup> (300 MHz,  $\text{CDCl}_3$ ,  $\delta$ ): 10.51 (s, 1H), 7.35 (t,  $J=8.5$  Hz, 1H), 6.50 (d,  $J=8.8$  Hz, 2H), 4.00 (t,  $J=6.6$  Hz, 4H), 1.80 (m, 4H), 1.54-1.37 (m, 3H), 1.37-1.18 (m, 17H), 0.86 (t,  $J=7.0$  Hz, 6H) GC-MS  $m/z$  calcd for  $\text{C}_{23}\text{H}_{38}\text{O}_3$ : 362.2 (Found: 362.2).

### 2.1.2.c Synthesis of *trans*-(Dioctoxyphenyl)porphyrin

5,15-bis(2,6-dioctoxyphenyl)porphyrin: A solution of dipyrromethane (1.00 g, 6.86 mmol) and 2,6-dioctoxybenzaldehyde (2.48 g, 6.86 mmol) in DCM (900 mL) was degassed with a stream of argon for 30 min, then TFA (456  $\mu\text{L}$ , 6.18 mmol) was added dropwise. The solution was stirred at room temperature for 4 h., then DDQ (2.33 g, 10.3 mmol) was added; the solution was left to stir for an additional hour. The TFA was neutralized with triethylamine (10 mL), then the mixture was filtered through a plug of silica to remove the oxidant, and the solvent was removed using a rotary evaporator, producing a dark purple solid. The solid was purified via silica column chromatography, using hexanes / DCM (2/1) as the eluent to give the product (1.04 g, 31.2 %) as a purple solid.  $^1\text{H}$  NMR was consistent with literature values<sup>80</sup> (500 MHz,  $\text{CDCl}_3$ ,  $\delta$ ): 10.11 (s, 2H), 9.23 (d,  $J=4.7$  Hz, 4H), 8.45 (d,  $J=4.7$  Hz, 4H), 7.68 (t,  $J=8.4$  Hz, 2H), 7.00 (d,  $J=8.5$  Hz, 4H), 3.81 (t,  $J=6.2$  Hz, 8H), 0.93 – 0.78 (m, 16H), 0.67 – 0.58 (m, 8H), 0.58 – 0.46 (m, 28H), 0.46 – 0.37 (m, 8H), -3.00 (s, 2H) MALDI-TOF  $m/z$  calcd for  $\text{C}_{64}\text{H}_{86}\text{N}_4\text{O}_4$ : 974.66 (Found: 973.92) UV-Vis  $\lambda_{\text{max}}$ (chlorobenzene,  $\epsilon=\text{M}^{-1}\text{cm}^{-1}$ ): 410 nm (321,000), 503 nm (17,800), 535 nm (5,200), 577 nm (4,900), 633 nm (1,100).

#### 2.1.2.d Synthesis of Bromo-(Dioctoxyphenyl)porphyrin

5-bromo-10,20-bis(dioctoxyphenyl)porphyrin: A mixture of 5,15-bis(2,6-dioctoxyphenyl)porphyrin (63.7 mg, 0.069 mmol) in chloroform (50 mL) was cooled to 0 °C. Then a solution of NBS (11.6 mg, 0.65 mmol) in chloroform (15 mL) was added dropwise over 4 h. Once the addition was complete, the reaction was quenched with acetone (15 mL). The solvent was removed under reduced pressure and the crude product was purified by silica column chromatography using hexanes / DCM (2/1) as the eluent to afford the product (40 mg, 58 %) as a dark purple solid. <sup>1</sup>H NMR was consistent with literature values<sup>80</sup> (500 MHz, CDCl<sub>3</sub>, TMS, δ): 10.00 (s, 1H), 9.61 (d, J=4.7 Hz, 2H), 9.15 (d, J=4.2 Hz, 2H), 8.87 (t, J=4.6 Hz, 4H), 7.70 (t, J=7.8 Hz, 2H), 6.99 (d, J=8.3 Hz, 4H), 3.82 (t, J=6.4 Hz, 8H), 0.97 – 0.70 (m, 24H), 0.70-0.36 (m, 36H), -2.90 (s, 2H) MALDI-TOF *m/z* calcd for C<sub>64</sub>H<sub>85</sub>BrN<sub>4</sub>O<sub>4</sub>: 1054.57 (Found: 1054.61) UV-Vis λ<sub>max</sub>(THF, ε=M<sup>-1</sup>cm<sup>-1</sup>): 415 nm (234,000), 510 nm (13,500), 542 nm (3,400), 588 nm (3,900), 645 nm (930).

#### 2.1.2.e Synthesis of Bromo-(Dioctoxyphenyl)porphyrin [Zn]

[5-bromo-10,20-bis(2,6-dioctoxyphenyl)porphinato] zinc (II): A suspension of 5-bromo-10,20-bis(dioctoxyphenyl)porphyrin (50 mg, 0.047 mmol) in DCM (100 mL), ethanol (50 mL), and zinc acetate (0.25 g, 1.14 mmol) was gently refluxed for 5 h. After allowing the mixture to cool to room temperature the suspension was washed with water and separated. The solvent was evaporated with a rotary evaporator to afford a pink/red solid (49 mg, 92 %). <sup>1</sup>H NMR was consistent with literature values<sup>80</sup> (500 MHz, CDCl<sub>3</sub>, TMS, δ): 10.05 (s, 1H), 9.68 (d, J=4.6 Hz, 2H), 9.23 (d, J=4.6 Hz, 2H), 8.95 (t, J=5.4 Hz, 4H), 7.68 (t, J=8.3 Hz), 6.98 (d, J=8.7 Hz, 4H), 3.81 (t, J=6.3 Hz, 8H), 0.92-0.82 (m, 16H),

0.73-0.62 (m, 9H), 0.62-0.55 (t,  $J=7.7$  Hz, 11H), 0.54-0.26 (m, 24H) MALDI-TOF  $m/z$  calcd for  $C_{64}H_{83}BrN_4O_4Zn$ : 1116.49 (Found: 1116.01) UV-Vis  $\lambda_{max}$ (THF,  $\epsilon=M^{-1}cm^{-1}$ ): 422 nm (510,000), 554 nm (25,600), 592 nm (3,700).

#### 2.1.2.f Synthesis of Dibromo-(Dioctoxyphenyl)porphyrin

5,15-dibromo-10,20-bis(dioctoxyphenyl)porphyrin: A mixture of 5,15-bis(2,6-dioctoxyphenyl)porphyrin (74.7 mg, 0.0766 mmol) in chloroform (50 mL) and pyridine (500  $\mu$ L) was cooled to 0 °C, then NBS (0.0285 g, 0.161 mmol) was added in one solid portion and allowed to stir for 30 min. The reaction was quenched with acetone (15 mL), washed with water, dried over  $Na_2SO_4$ , and filtered. The solvent was removed with a rotary evaporator and the crude product was purified by silica column chromatography using hexanes / DCM (2/1) as the eluent to afford the product as a brownish-purple solid (58.7 mg, 67.7 %).  $^1H$  NMR was consistent with literature values<sup>81</sup> (500 MHz,  $CDCl_3$ , TMS  $\delta$ ): 9.48 (d,  $J= 4.9$  Hz, 4H), 8.76 (d,  $J= 5.4$  Hz, 4H), 7.68 (t,  $J= 8.5$  Hz, 2H), 6.96 (d,  $J= 8.9$  Hz, 4H), 3.82 (t,  $J= 6.5$  Hz, 8H), 1.00-0.70 (m, 16H), 0.65-0.30 (m, 44H), -2.62 (s, 2H) MALDI-TOF:  $m/z$  calcd for  $C_{64}H_{84}Br_2N_4O_4$  1132.48 (Found 1134.41) UV-Vis  $\lambda_{max}$ (THF,  $\epsilon=M^{-1}cm^{-1}$ ): 421 nm (335,000), 519 nm (19,500), 552 nm (10,300), 600 nm (5,600), 659 nm (4,400).

#### 2.1.2.g Synthesis of Dibromo-(Dioctoxyphenyl)porphyrin [Zn]

[5,15-dibromo-10,20-bis(2,6-dioctoxyphenyl)porphyrinato] zinc (II): A suspension of 5,15-dibromo-10,20-bis(dioctoxyphenyl)porphyrin (68 mg, 0.057 mmol) and zinc acetate (200 mg, 0.911 mmol) in DCM (75 mL) and ethanol (40 mL) was gently refluxed for 4 h. After cooling to room temperature, water was added and the organic layer separated. The organic layer was washed with water and dried over sodium sulfate. The solvent was

removed under reduced pressure to afford the product (66.7 mg, 95.0 %) as a pink/red solid.  $^1\text{H}$  NMR was consistent with literature values<sup>81</sup> (500 MHz,  $\text{CD}_2\text{Cl}_2$ ,  $\delta$ ): 9.65 (d,  $J=$  5.0 Hz, 4H), 8.88 (d,  $J=$  4.8 Hz, 4H), 7.73 (t,  $J=$  8.2 Hz, 2H), 7.03 (d,  $J=$  9.2 Hz, 4H), 3.87 (t,  $J=$  6.1 Hz, 8H), 0.99-0.81 (m, 28H), 0.68-0.59 (m, 10H), 0.58-0.42 (m, 30H) UV-Vis  $\lambda_{\text{max}}$ (THF,  $\epsilon=\text{M}^{-1}\text{cm}^{-1}$ ): 429 nm (251,000), 564 nm (11,000), 607 nm (4,700).

### 2.1.3 Sonogashira Coupling of Thiazolothiazoles and Porphyrins

The synthetic pathways for obtaining the desired thiazolothiazole functionalized porphyrins are outlined in Figure 24. The palladium cross-coupling reactions took place in degassed solvents within a glove box to ensure an inert atmosphere.

On thin-layer chromatography plates, aliquots of the reaction mixtures were spotted and developed to indicate partial consumption of the porphyrin material and the apparent complete consumption of the thiazolothiazole material. As the porphyrin starting material started to decrease in size, a small green band appeared just below the starting material. However, once the reaction is stopped and purified, the green band is no longer evident. This suggests that the oxidative addition of palladium to the brominated porphyrin is occurring and is stable in air-free conditions. Likewise, the consumption of the thiazolothiazole linker leads to speculation of its role in the reaction. The blue fluorescent spot on TLC appeared closer to the baseline once the reaction was stopped, suggesting that the terminal alkynes on the thiazolothiazole linkers dimerized.

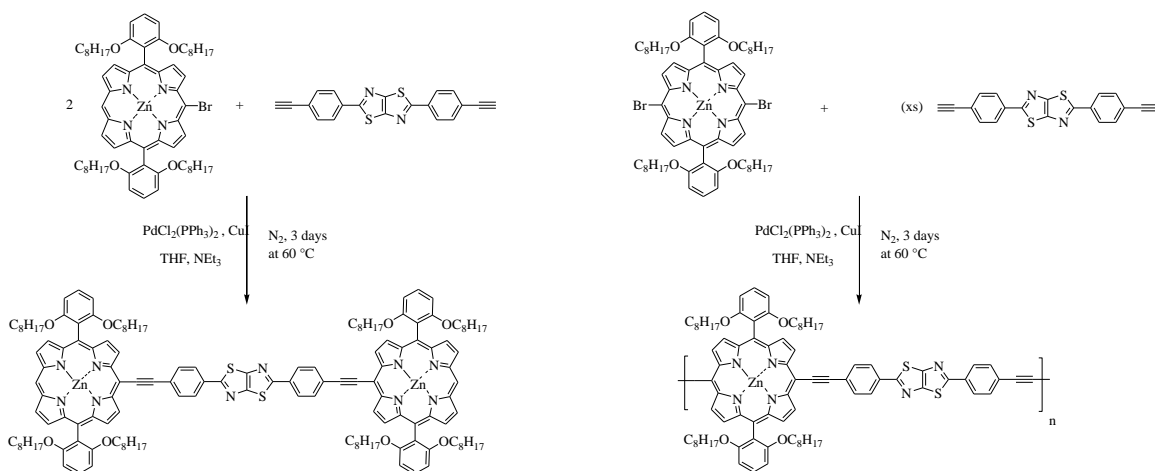


Figure 24: Synthetic routes for obtaining (a) the P-TTz-P dyad and (b) P-TTz polymer.

### 2.1.3.a D – A – D P-TTz-P Dyad Synthesis

The zinc-metallated mono-bromo porphyrin (65.1 mg, 0.058 mmol),  $\text{CuI}$  (0.83 mg,  $4.4 \times 10^{-3}$  mmol),  $(\text{PPh}_3)_2\text{PdCl}_2$  (10.2 mg, 0.015 mmol), and di-ethynyl TTz (10.0 mg, 0.029 mmol) was dissolved in dry THF (5 mL) and triethylamine (1 mL) and heated at  $60^\circ\text{C}$  for 3 d under  $\text{N}_2$ . After the heating period, the solvent was removed under reduced pressure and the crude product purified by silica column chromatography using DCM as the eluent. The product remained at the top of the silica, so the silica was recovered from the column and the product removed by adding methanol to the silica gel. Removal of the methanol under reduced pressure afforded an orange-brown solid of negligible mass. This solid was dissolved in ethyl acetate and subjected to UV-Vis spectroscopy to determine if the coupling took place, as seen in Section 3.2.3.b.

### 2.1.3.b D – A P-TTz Polymer Synthesis

The zinc-metallated di-bromo porphyrin (67.0 mg, 0.056 mmol),  $\text{CuI}$  (2.1 mg, 0.011 mmol),  $(\text{PPh}_3)_2\text{PdCl}_2$  (11.7 mg, 0.017 mmol), and di-ethynyl TTz (57.2 mg, 0.17 mmol) was dissolved in dry THF (5 mL) and triethylamine (1 mL) and heated at  $60^\circ\text{C}$  for 3 d under  $\text{N}_2$ . The solvent was then removed under reduced pressure to afford a black,

spongy material which was then subjected to silica column chromatography using DCM as the eluent. The product remained embedded at the top of the column, so the silica was recovered from the column and the product removed by adding methanol to the silica gel. Removal of the methanol under reduced pressure afforded a brown solid of negligible mass. This solid was dissolved in ethyl acetate and subjected to UV-Vis spectroscopy to determine if the coupling took place, as seen in Section 3.2.3.a.

## 2.2 Molecular Modeling

Spartan 10 was used for all molecular modeling simulations. Equilibrium geometry was calculated at the ground state, using Density Functional Theory (DFT) with B3LYP theory and 6-31G\* basis in vacuum. These calculations produced estimated HOMO / LUMO levels for all compounds listed in Section 3.1.

DFT calculations for the porphyrins and TTz-functionalized porphyrin systems were performed by using methoxy groups in lieu of octoxy groups, as those functional groups do not significantly affect HOMO / LUMO levels. Also, increasing the number of atoms can cause Spartan to time out (max out calculation iterations without solving the energy levels) due to the increasing number of atoms the program needs to process.

## 2.3 Dibromo-(Dioctoxyphenyl)porphyrin Crystal Structure

After purifying the reaction mixture containing the di-bromo porphyrin, a crystallization attempt was made in efforts to produce a crystal suitable for x-ray diffraction studies. 10 mg of the di-bromo porphyrin was dissolved in a minimum of chloroform, and heated. Then, absolute ethanol was added dropwise until cloudiness in the flask persisted. The flask was removed from heat and allowed to cool, undisturbed over the weekend. No crystal formation was evident at this point, so a syringe needle (21

gauge) was inserted into the septum sealing the flask and the solvent was allowed to slowly evaporate, undisturbed for several more days. Several small crystals formed upon the slow solvent evaporation, which were collected and washed with cold methanol and then prepared for X-Ray diffraction analysis.

## 2.4 UV-Vis Spectroscopy

UV-Vis absorption spectra were collected for all porphyrin and thiazolothiazole components on a Cary 300 UV-Vis spectrophotometer, using THF and ethyl acetate as the solvent for porphyrins and thiazolothiazoles, respectively, unless otherwise noted. For TTz molecules, the Cary 300 was set to scan from 450 nm to 250 nm; for porphyrin molecules, the Cary 300 was set to scan from 700 nm to 350 nm. To ensure there were no omitted absorbance peaks produced by the coupled systems, the Cary 300 was set to scan from 900 nm to 290 nm.

For each compound, a stock solution was prepared and several dilutions were made to afford solutions of varying concentrations, as noted in Section 3.2. For TTz compounds, more dilute solutions were necessary. Calibration curves (Appendix A) were prepared after performing absorbance measurements of the dilution standards in a 1 cm quartz cuvette. Taking the slope of the line of best fit for a calibration curve, the extinction coefficient ( $\epsilon$ ) was determined for each absorbance peak for their respective compound, using the Beer – Lambert law for absorbance shown in Equation 2 below.

$$A = \epsilon \cdot b \cdot c \quad (2)$$

In Eq. 2, the absorbance of a compound ( $A$ ) is equal to the product of the extinction coefficient ( $\epsilon$ ;  $\text{M}^{-1} \cdot \text{cm}^{-1}$ ), path length ( $b$ ), and concentration ( $c$ ).

## CHAPTER 3: RESULTS AND DISCUSSION

### 3.1 Computational Models for Porphyrin Dyes

#### 3.1.1 *trans*-(Dioctoxyphenyl)porphyrin [Zn]

The zinc-metallated *trans* porphyrin served as the fundamental porphyrin building block in the synthetic efforts to prepare a thiazolothiazole functionalized porphyrin.

Figure 25 shows the DFT calculated HOMO and LUMO levels for this porphyrin. The HOMO level (-4.8 eV) resides on the methine carbons and pyrrolic nitrogens, while the LUMO level (-1.8 eV) is distributed throughout the macrocycle. This calculation provides a band gap of -3.0 eV for this porphyrin.

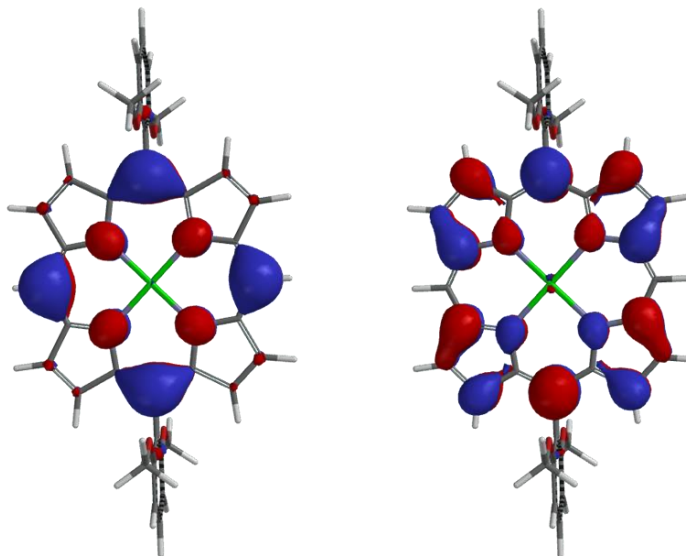


Figure 25: DFT calculated HOMO (left) and LUMO (right) levels of the zinc-metallated *trans* porphyrin.

### 3.1.2 D-A P-TTz

The mono-coupled porphyrin – TTz compound served as the “model compound” in these synthetic efforts. This compound is expected to provide the fundamental photophysical properties seen in an intramolecular system when a porphyrin’s  $\pi$ -conjugation is extended towards an electron accepting TTz periphery. This compound can also serve as a component in polymer systems, once the terminal alkyne is made available by removing the TMS protecting group. The HOMO and LUMO levels are seen in Figure 26. The HOMO level (-4.8 eV) resides mostly on the methine carbons and the ethynyl carbon bridge. The LUMO level (-2.4 eV) resides mainly on the TTz acceptor, indicating that there is the potential for an intramolecular donor / acceptor system for electron transfer in an OPV device. This system displays a band gap of – 2.4 eV. When compared to the LUMO level of the porphyrin in Section 3.1.1, it is apparent that functionalizing the porphyrin with the thiazolothiazole functional group results in a lower LUMO (0.6 eV difference), thus suggesting that light absorption at longer wavelengths is possible.

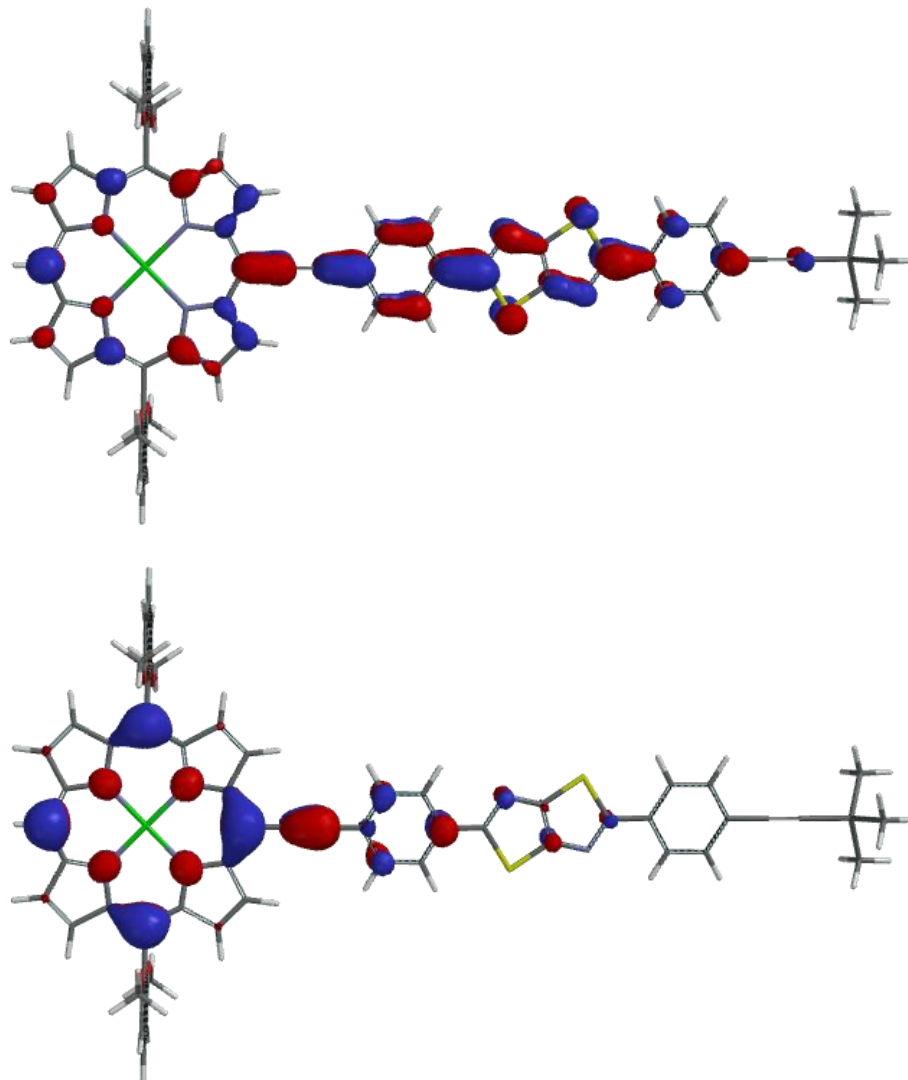


Figure 26: Calculated HOMO (bottom) and LUMO (top) levels of the model donor – acceptor thiazolothiazole functionalized porphyrin system.

### 3.1.3 A-D-A TTz-P-TTz

#### 3.1.3.a Alkoxy TTz functional groups

This A-D-A system was pursued to aid in the overall solution processability of the system in device manufacturing. The DFT calculations are illustrated in Figure 27; the HOMO level (bottom) has an energy of  $-4.7$  eV, while the LUMO level (top) has an energy of  $-2.5$  eV, for an overall energy gap of  $-2.2$  eV.

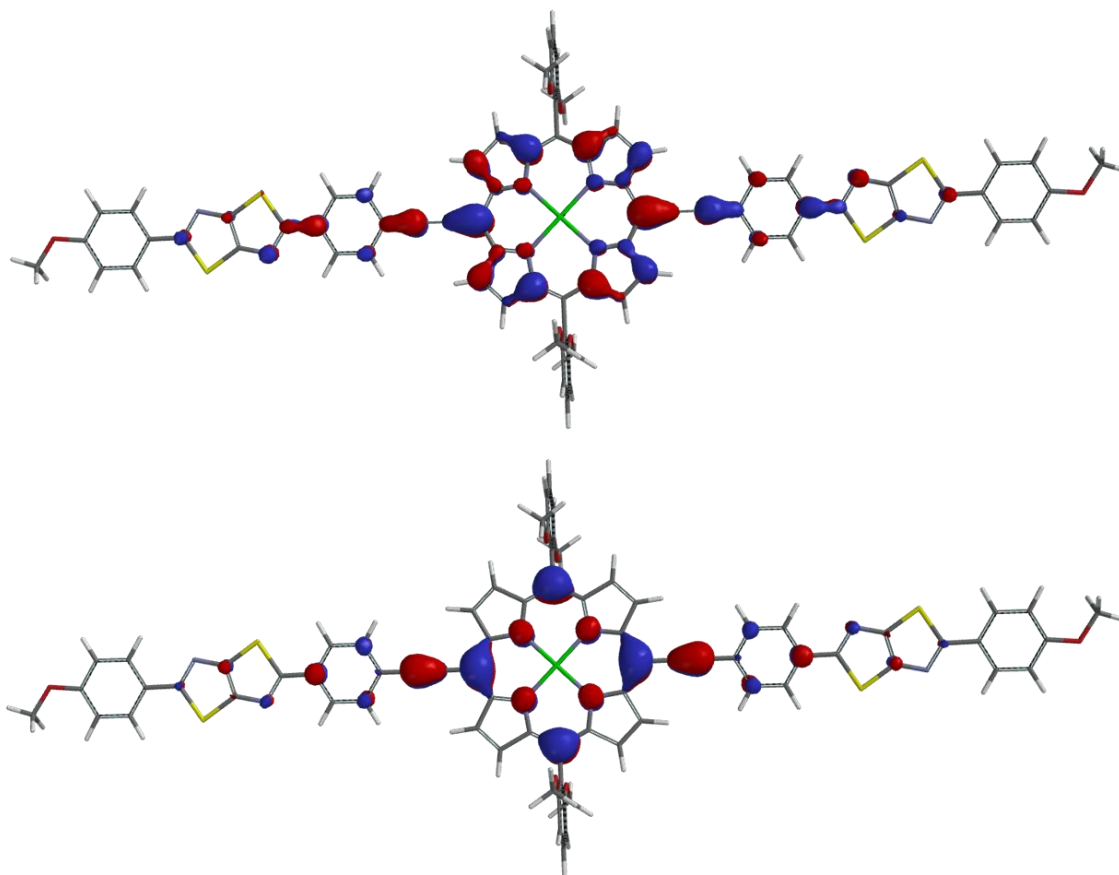


Figure 27: DFT calculations of TTz-P-TTz, showing the locations of the HOMO level (bottom) and LUMO level (top).

### 3.1.3.b Ethynyl TTz functional groups

This small molecule system is similar to the TTz-P-TTz system seen in 3.1.3.a but contains ethynyl terminal ends. This system contains some advantages over the alkoxy system in that the free ethynyl groups allow for coupling of other functional groups or systems allowing for increased tenability of the overall system. Also, as seen in Figure 28, the LUMO level extends ever so slightly to the edge of the phenyl ring on the terminal end of the TTz functional group, suggesting that charge separation may be more likely and favorable compared to the system in 3.1.3.a above.

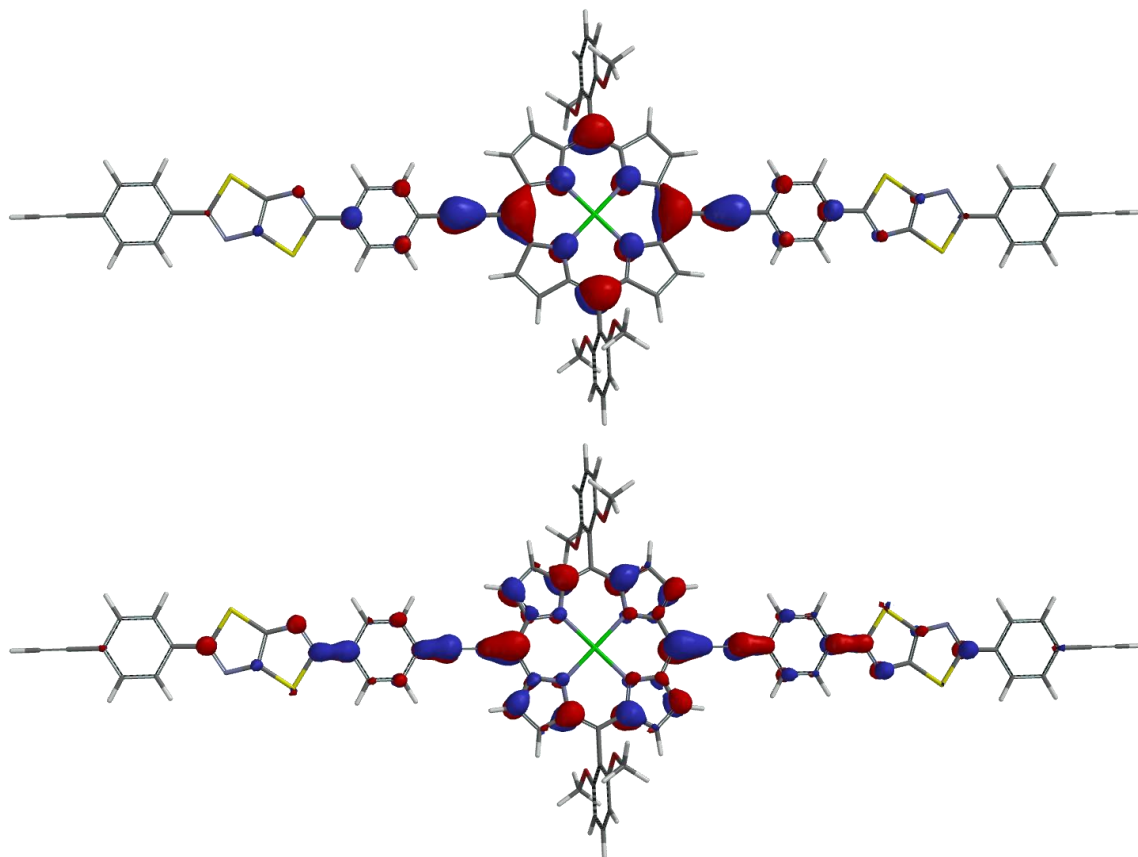


Figure 28: DFT calculations showing the HOMO (bottom) and LUMO (top) levels of the ethynyl TTz-P-TTz small molecule system.

#### 3.1.4 D-A-D P-TTz-P

Figure 29 shows the HOMO / LUMO DFT calculations for the dyad system. The HOMO (bottom) has an energy level of  $-4.7$  eV, while the LUMO (top) has an energy level of  $-2.4$  eV, for an energy gap of 2.3 eV.

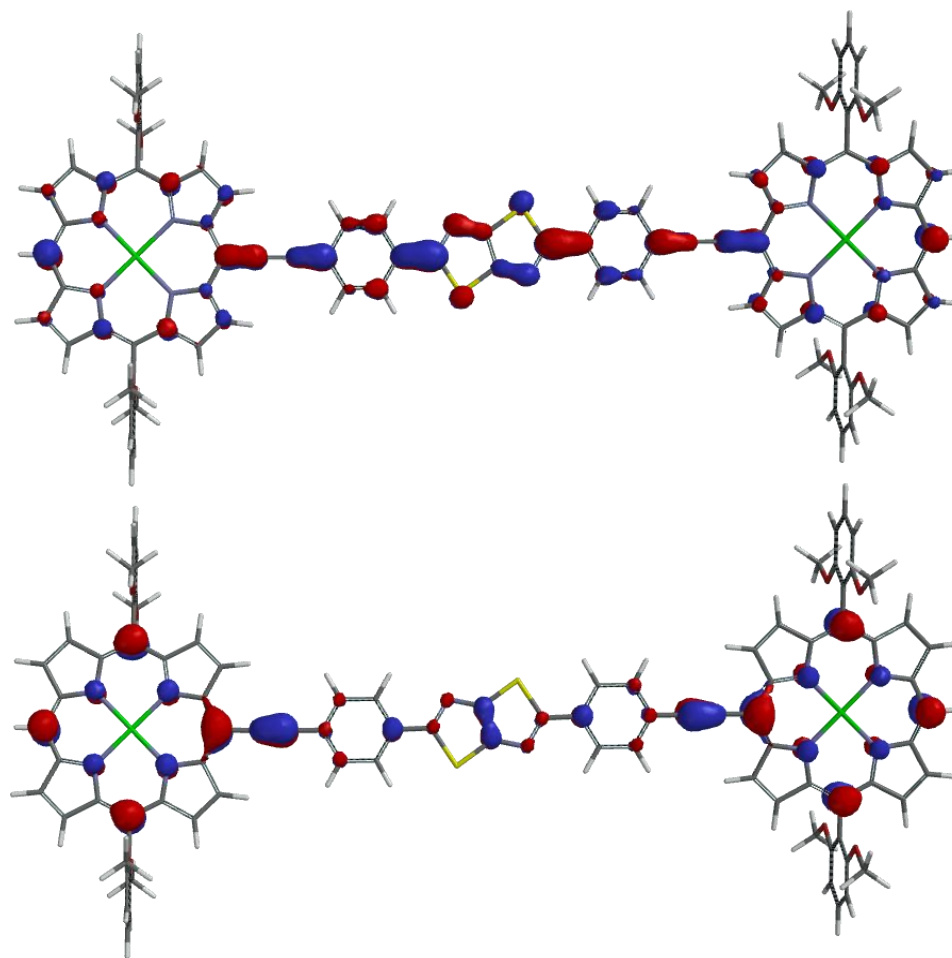


Figure 29: DFT calculations for the P-TTz-P dyad system, showing the locations of the HOMO (bottom) and LUMO (top) levels of the system.

### 3.2 UV-Vis Spectroscopy

#### 3.2.1 Porphyrin Compounds

##### 3.2.1.a *trans*-(Dioctoxyphenyl)porphyrin

Figure 30 shows the normalized UV-Vis absorption spectrum of the free-base *trans*-porphyrin in chlorobenzene, scanning from 700 – 350 nm. A stock solution of 60  $\mu\text{M}$  was prepared and dilutions of 40, 20, 10, and 1.25  $\mu\text{M}$  were made from the stock solution and measured. The calibration curve for this porphyrin is provided in Appendix A. The *trans*-porphyrin has a strong Soret peak at 410 nm ( $\epsilon = 321,000 \text{ M}^{-1} \cdot \text{cm}^{-1}$ ) and

four Q bands at 503 nm ( $\epsilon = 17,800 \text{ M}^{-1} \cdot \text{cm}^{-1}$ ), 535 nm ( $\epsilon = 5,200 \text{ M}^{-1} \cdot \text{cm}^{-1}$ ), 577 nm ( $\epsilon = 4,900 \text{ M}^{-1} \cdot \text{cm}^{-1}$ ), and 633 nm ( $\epsilon = 1,100 \text{ M}^{-1} \cdot \text{cm}^{-1}$ ).

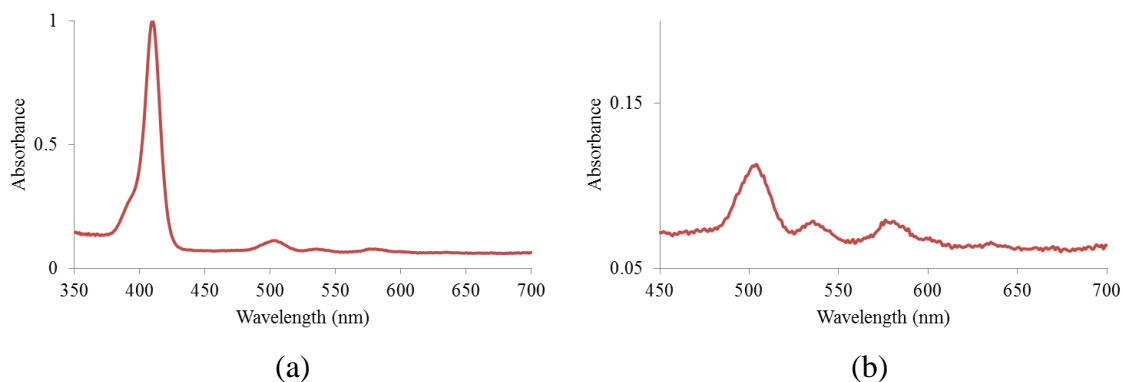


Figure 30: (a) Normalized UV-Vis spectrum for the *trans*-porphyrin in chlorobenzene, scanning from 700 to 350 nm (b) enhanced Q band region.

### 3.2.1.b Bromo-(Diocetoxyphenyl)porphyrin

Figure 31 illustrates the normalized UV-Vis absorption spectrum of the free-base mono-bromo porphyrin in chlorobenzene, scanning from 700 – 350 nm. A stock solution of 118.56  $\mu\text{M}$  was prepared in a UV-Vis cuvette and two-fold dilutions were prepared to afford dilutions of 59.28, 29.64, 14.82, 7.41, 3.71, and 1.86  $\mu\text{M}$ . Once a bromine is substituted onto the porphyrin, a slight absorption shift to longer wavelength is apparent, relative to the free-base *trans*-porphyrin. This porphyrin has a Soret peak at 415 nm ( $\epsilon = 234,000 \text{ M}^{-1} \cdot \text{cm}^{-1}$ ), with four Q bands at 510 nm ( $\epsilon = 13,500 \text{ M}^{-1} \cdot \text{cm}^{-1}$ ), 542 nm ( $\epsilon = 3,400 \text{ M}^{-1} \cdot \text{cm}^{-1}$ ), 588 nm ( $\epsilon = 3,900 \text{ M}^{-1} \cdot \text{cm}^{-1}$ ), and 645 nm ( $\epsilon = 930 \text{ M}^{-1} \cdot \text{cm}^{-1}$ ). It is important to note that the molar absorptivity of the Soret peak and the Q1 peak are much lower than typical free-base porphyrins, due to the presence of a bromine atom on the macrocycle.

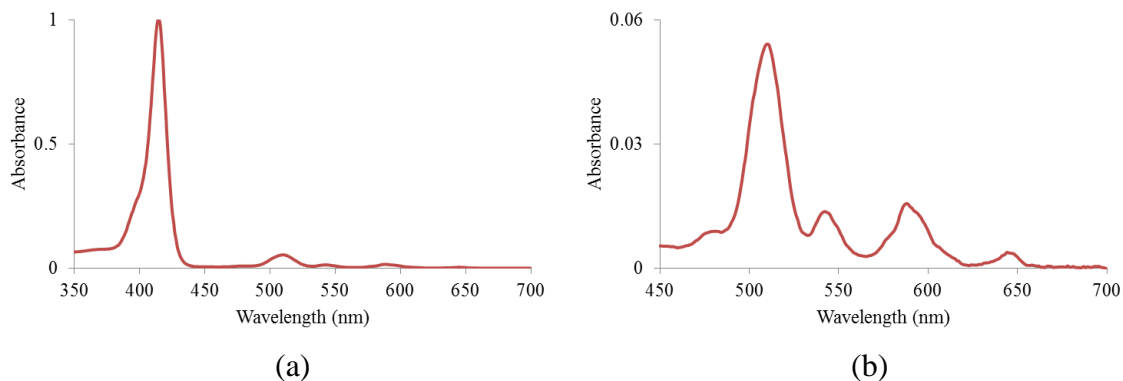


Figure 31: (a) Normalized UV-Vis absorption spectrum of the free-base mono-bromo porphyrin in THF, scanning from 700 to 350 nm; (b) enhanced Q band region.

### 3.2.1.c Bromo-(Diocetoxyphenyl)porphyrin [Zn]

As seen with the zinc-metallated porphyrin in Section 3.2.2, a red-shift in absorbance ( $\sim 7$  nm) is observed with the zinc-metallated di-bromo porphyrin relative to its free-base precursor. A stock solution of  $89.5 \mu\text{M}$  was prepared in a UV-Vis cuvette and subsequent two-fold dilutions afforded solutions of  $44.7$ ,  $22.4$ ,  $11.2$ ,  $5.6$ ,  $2.8$ ,  $1.4$ , and  $0.7 \mu\text{M}$ . This porphyrin (Figure 32) has a Soret peak at  $422$  nm ( $\epsilon = 510,000 \text{ M}^{-1}\cdot\text{cm}^{-1}$ ) and a two Q bands at  $554$  nm ( $\epsilon = 25,600 \text{ M}^{-1}\cdot\text{cm}^{-1}$ ) and  $592$  nm ( $\epsilon = 3,680 \text{ M}^{-1}\cdot\text{cm}^{-1}$ ).

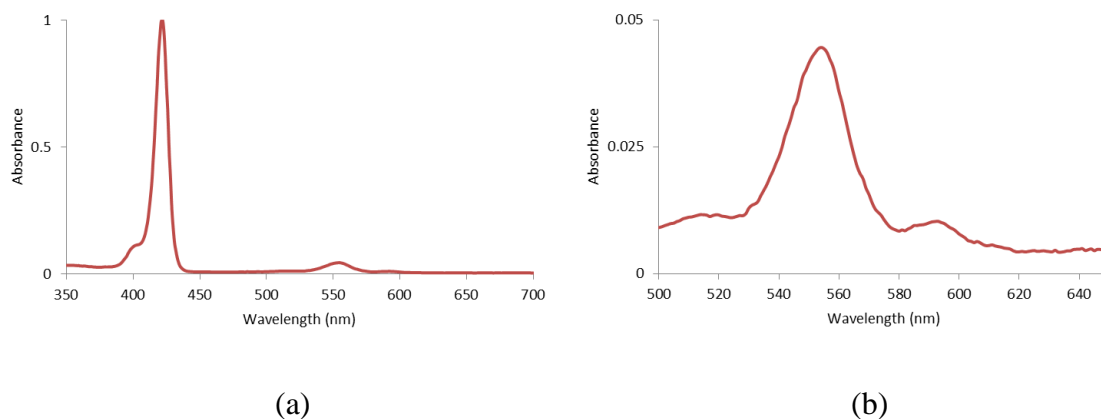


Figure 32: (a) Normalized absorption spectrum of the zinc-metallated mono-bromo porphyrin in THF, scanning from 700 to 350 nm; (b) enhanced view of the Q band region.

### 3.2.1.d Dibromo-(Diocetoxyphenyl)porphyrin

Figure 33 illustrates a normalized spectrum of the di-bromo porphyrin in THF, scanning from 700 to 350 nm. A stock solution of 132.4  $\mu\text{M}$  was prepared in a UV-Vis cuvette and subsequent two-fold dilutions afforded concentrations of 66.2, 33.1, 16.55, 8.28, 4.14, 2.07, 1.04, and 0.52  $\mu\text{M}$ . The di-bromo porphyrin exhibits a Soret peak at 421 nm ( $\epsilon = 335,000 \text{ M}^{-1} \cdot \text{cm}^{-1}$ ), and four Q bands at 519 nm ( $\epsilon = 19,500 \text{ M}^{-1} \cdot \text{cm}^{-1}$ ), 552 nm ( $\epsilon = 10,300 \text{ M}^{-1} \cdot \text{cm}^{-1}$ ), 600 nm ( $\epsilon = 5,600 \text{ M}^{-1} \cdot \text{cm}^{-1}$ ), and 659 nm ( $\epsilon = 4,400 \text{ M}^{-1} \cdot \text{cm}^{-1}$ ). The Soret peak exhibits a higher molar absorptivity than the mono-bromo porphyrin, due to the increase in symmetry of two bromine atoms present on the macrocycle.

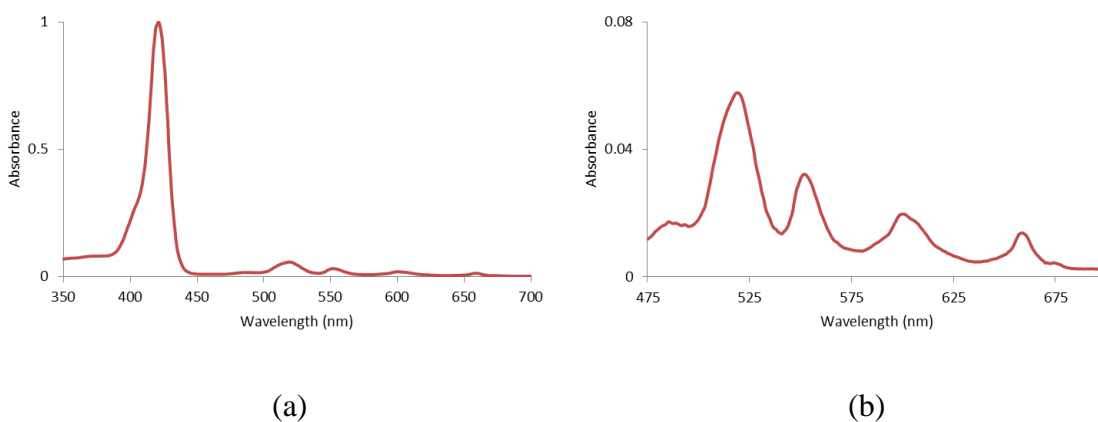


Figure 33: (a) Normalized absorption spectrum of the di-bromo porphyrin in THF; (b) enhanced view of the Q band region.

### 3.2.1.e Dibromo-(Diocetoxyphenyl)porphyrin [Zn]

As seen in the zinc-metallated mon-bromo porphyrin, the Soret peak in the zinc-metallated di-bromo porphyrin (Figure 34) is red shifted slightly relative to its free-base analog. A stock solution of 104.5  $\mu\text{M}$  was prepared in a UV-Vis cuvette and dilutions performed to acquire concentrations of 13.08, 6.54, 3.26, 1.64, and 0.82  $\mu\text{M}$ .

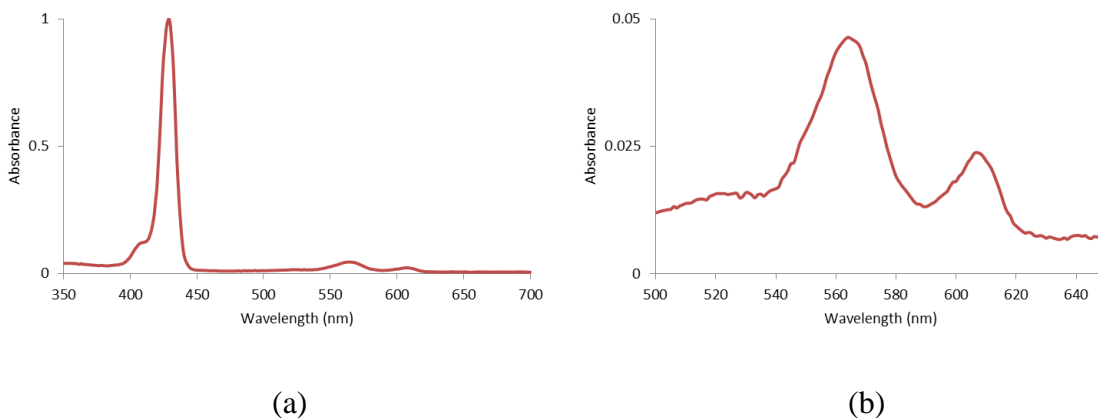


Figure 34: (a) Normalized UV-Vis absorption spectrum of the zinc-metallated di-bromo porphyrin in THF, scanning from 700 to 350 nm; (b) enhanced view of the Q band region.

This porphyrin has a Soret peak at 429 nm ( $\epsilon = 251,000 \text{ M}^{-1}\cdot\text{cm}^{-1}$ ) and a two Q bands at 564 nm ( $\epsilon = 11,000 \text{ M}^{-1}\cdot\text{cm}^{-1}$ ) and 607 nm ( $\epsilon = 4,700 \text{ M}^{-1}\cdot\text{cm}^{-1}$ ).

### 3.2.2 Thiazolothiazole Compounds

#### 3.2.2.a Di-TMS TTz

Figure 35 displays the normalized absorption spectrum of the di-TMS TTz in ethyl acetate. A stock solution of 32  $\mu\text{M}$  was prepared in a UV-Vis cuvette and serial dilutions from the cuvette afforded dilutions of 16, 8, 4, 2, and 1  $\mu\text{M}$ . There is an absorption maximum at 283 nm ( $\epsilon = 33,000 \text{ M}^{-1}\cdot\text{cm}^{-1}$ ), with a shoulder on either side of the peak, at 368 and 400 nm.

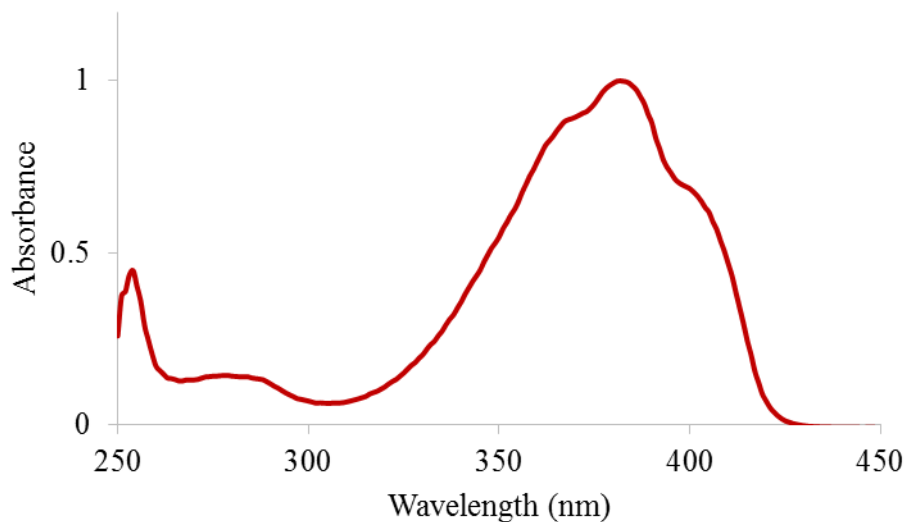


Figure 35: Normalized absorption spectrum of di-TMS TTz in ethyl acetate, scanning from 450 to 250 nm.

### 3.2.2.b Di-Ethynyl TTz

A stock solution of 146  $\mu\text{M}$  was prepared in a UV-Vis cuvette and serial dilutions in the cuvette afforded dilutions of 36.5, 18.3, 9.13, 4.6, and 2.3  $\mu\text{M}$ . Figure 36 displays the normalized absorption spectrum of the di-TMS TTz compound in ethyl acetate. There is an absorption maximum at 377 nm ( $\epsilon = 42,000 \text{ M}^{-1}\cdot\text{cm}^{-1}$ ) with a shoulder on both side of the maximum peak, at 363 and 394 nm.

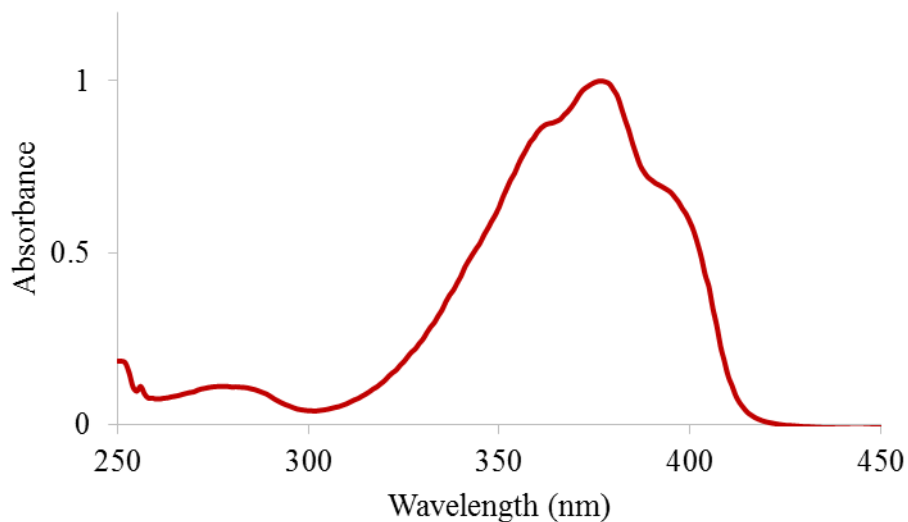


Figure 36: Normalized absorption spectrum of di-ethynyl TTz in ethyl acetate, scanning from 450 to 250 nm.

### 3.2.3 Palladium Coupling

#### 3.2.3.a P-TTz Polymer

Figure 37 illustrates the absorption spectrum obtained of the crude product obtained from the coupling of the zinc-metallated di-bromo porphyrin with an excess of the di-ethynyl TTz. There is an absorption maximum at 382 nm, consistent with excess di-ethynyl TTz remaining in the product mixture.

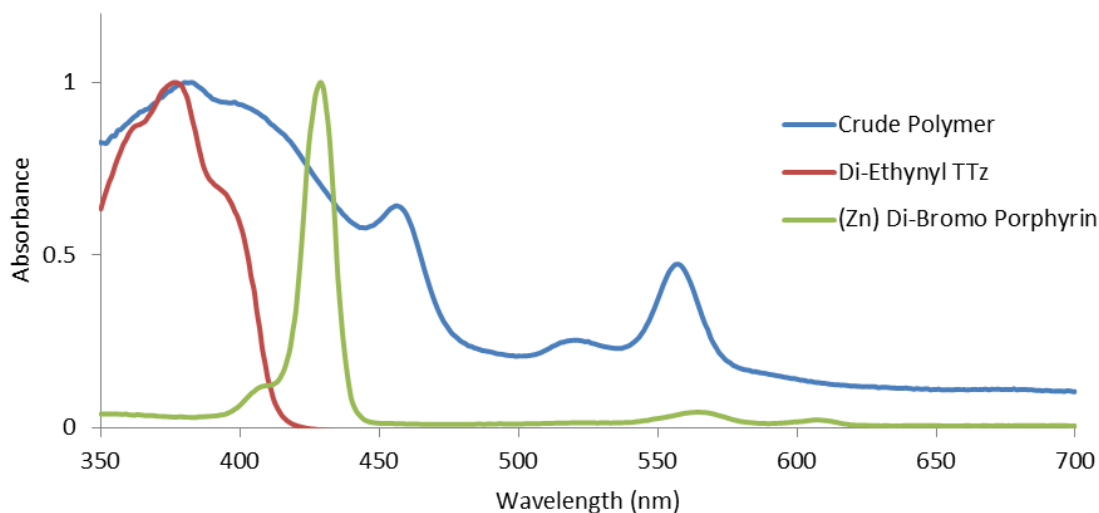


Figure 37: Normalized absorption spectrum of the crude product (blue) in methanol, obtained from the Sonogashira coupling of the zinc-metallated di-bromo porphyrin (green) with an excess of the di-ethynyl TTz (red), scanning from 700 to 300 nm.

There are several peaks present at 458, 518, and 560 nm that do not coincide with any of the absorption peaks from the other porphyrins, suggesting that coupling of the porphyrin and thiazolothiazole was successful to some extent. The broadened and enhanced absorption across the visible spectrum is also consistent with other known porphyrin-containing D-A polymer systems.<sup>34,82</sup>

### 3.2.3.b P-TTz-P Dyad

Figure 38 displays the absorption spectrum obtained from the crude PTTzP dyad reaction mixture. There is no peak evident for the remaining di-ethynyl thiazolothiazole. The peaks present are consistent with the starting (Zn) mono-bromo porphyrin; however, the pure (Zn) mono-bromo porphyrin displays a 20:1 ratio of peak heights between the Soret band and the Q band, while the crude dyad mixture displays a ~2:1 ratio between the Soret band and the Q band region along with significant broadening across the visible spectrum. This enhancement in the Q band region, and broadening of the absorption

spectrum through the visible region, is consistent with other known porphyrin dyad systems.<sup>83,84</sup>

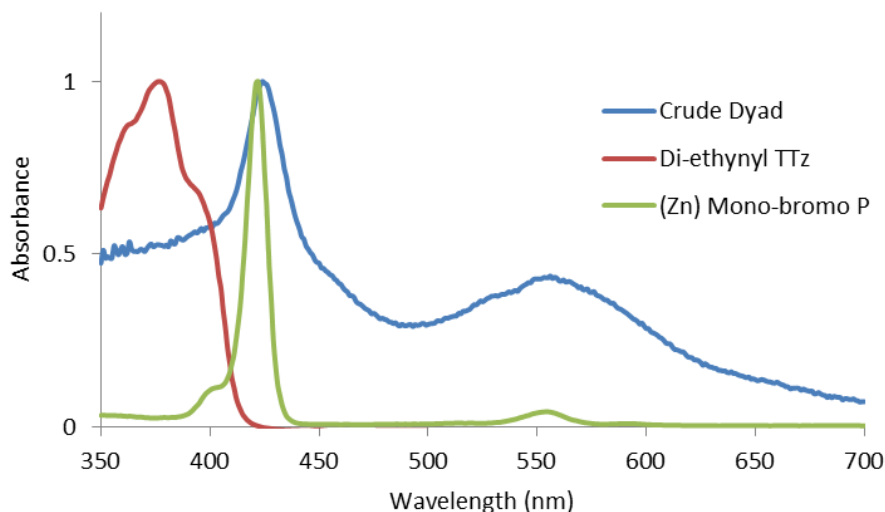


Figure 38: Absorption spectrum of the crude PTTzP dyad (blue) in ethyl acetate, obtained from the coupling of the zinc-metallated mono-bromo porphyrin (green) and di-ethynyl TTz (red).

### 3.3 Dibromo-(Dioctoxyphenyl)porphyrin Crystal Structure

Figure 39 shows the preliminary crystal structure for the dibromo-

(dioctoxyphenyl)porphyrin. It is important to note that this particular porphyrin's crystal structure has not been previously reported in the literature. In fact, only a limited number of alkylated porphyrin small molecule systems have had successful crystal structure determinations,<sup>85</sup> so further refinement in the crystal structure is currently underway. This crystal structure can provide insight into the morphology of similar porphyrins in the photoactive layers of OSCs, and ultimately provide clues into the photophysical properties of these OSCs.

The crystal displays porphyrin “steps,” where an adjacent porphyrin is slightly offset by a distance roughly to that of the height of the octoxy chains; the octoxy chains

are aligned parallel to each other, covering the periphery of the macrocycle while leaving the center exposed.

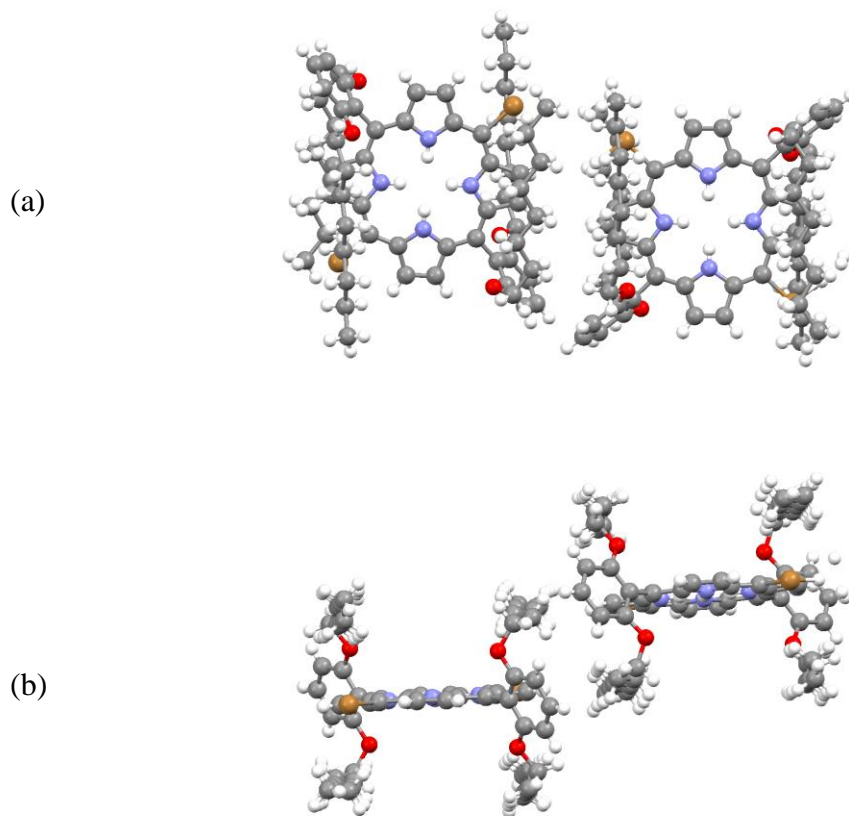


Figure 39: Unrefined crystal structure of the dibromo-(dioctoxyphenyl)porphyrin, viewed from (a) above and (b) from the side

## CHAPTER 4. CONCLUSION

Porphyrin and thiazolothiazole materials were synthesized via multi-step synthetic pathways, resulting in mono-brominated and di-brominated porphyrins and novel symmetric thiazolothiazoles for future use in donor – acceptor (D – A) porphyrin materials. Each porphyrin and symmetric thiazolothiazole was successfully characterized by  $^1\text{H}$  NMR, UV-Vis spectroscopy, and MALDI-TOF mass spectrometry.

A novel porphyrin crystal structure of dibromo-(dioctoxyphenyl)porphyrin has been preliminarily solved, but is awaiting further refinement. The crystal structure displays parallel arrangement of octoxy chains within the staggered porphyrin macrocycles. The asymmetric thiazolothiazole desired for the A – D – A system was synthesized via mixed pot condensation of two aromatic aldehydes with dithiooxamide. However, purification and isolation of significant quantities of the desired asymmetric TTz material was inefficient for future synthetic pathways.

Initial attempts at synthesizing the P-TTz-P dyad provided promising insight into the palladium cross-coupling reaction in general. Reaction progress was monitored by TLC and the fluorescent spot on the baseline isolated. UV-Vis absorption spectroscopy of fluorescent material that remained on the baseline of the TLC plate only shows a very slight red-shifted Soret peak, but displayed enhanced absorption across the visible spectrum, consistent with literature findings on porphyrin dyad systems.

A Sonogashira coupling reaction to afford a porphyrin / thiazolothiazole polymer indicates successful coupling. The material that remained on the baseline of the TLC plate was analyzed by UV-Vis spectroscopy. The absorption spectrum displayed a red-shifted peak relative to the starting porphyrin's Soret peak, along with an enhanced Q band region. This characteristic change in absorption is consistent with previously reported porphyrin polymers with extended conjugation.

Further optimization of both Sonogashira coupling conditions are necessary in future studies. Decreasing the amount of copper iodide as well as increasing the amount of palladium present can lead to more favorable reaction conditions. Preliminary spectroscopic characterization of the coupled porphyrin and thiazolothiazole suggests extended  $\pi$ -conjugation and enhanced absorption characteristics across the visible spectrum. The calculated HOMO / LUMO energy gaps and distribution of orbitals are in agreement with these initial spectroscopic studies of thiazolothiazole functionalized porphyrin materials.

## REFERENCES

- (1) Finley, J. W.; Seiber, J. N. *J. Agric. Food Chem.* **2014**, *62*, 6255–6262.
- (2) Shafiee, S.; Topal, E. *Energy Policy.* **2009**, *37*, 181–189.
- (3) Jacoby, M. *Chem. Eng. News* **2013**, *91*, 28–30.
- (4) Hermann, W. *Energy.* **2006**, *31*, 1685–1702.
- (5) Xu, Y.; He, Y.; Cao, X.; Zhong, D.; Jia, J. *Environ. Sci. Technol.* **2008**, *42*, 2612–2617.
- (6) Kargar, A.; Sun, K.; Jing, Y.; Choi, C.; Jeong, H.; Jung, G. Y.; Jin, S. *ACS Nano.* **2013**, *7*, 9407–9415.
- (7) Huang, S.; Zhang, H.; Wu, Z.; Kong, D.; Lin, D.; Fan, Y.; Yang, X.; Zhong, Z.; Huang, S.; Jiang, Z.; Cheng, C. *ACS Appl. Mater. Interfaces.* **2014**, *6*, 12111–12118.
- (8) Lee, Y.-H.; Kim, J.-S.; Noh, J.; Lee, I.; Kim, H. J.; Choi, S.; Seo, J.; Jeon, S.; Kim, T.-S.; Lee, J.-Y.; Choi, J. W. *Nano Lett.* **2013**, *13*, 5753–5761.
- (9) Walter, M. G.; Rudine, A. B.; Wamser, C. C. *J. Porphyrins Phthalocyanines.* **2010**, *14*, 759–792.
- (10) Garnett, E.; Yang, P. *Nano Lett.* **2010**, *10*, 1082–1087.
- (11) Barber, G. D.; Hoertz, P. G.; Lee, S. A.; Abrams, N. M.; Mikulca, J.; Mallouk, E.; Liska, P.; Zakeeruddin, S. M.; Gr, M.; Ho-baillie, A.; Green, M. A.; Polytechnique, F. *J. Phys. Chem. Lett.* **2011**, *2*, 581–585.
- (12) Buonassisi, T.; Istratov, A. a; Marcus, M. a; Lai, B.; Cai, Z.; Heald, S. M.; Weber, E. R. *Nat. Mater.* **2005**, *4*, 676–679.
- (13) Cheng, Y.-J.; Yang, S.-H.; Hsu, C.-S. *Chem. Rev.* **2009**, *109*, 5868–5923.
- (14) Lin, Y.; Fan, H.; Li, Y.; Zhan, X. *Adv. Mater.* **2012**, *24*, 30873106.
- (15) Kallmann, H. P.; Pope, M. *J. Chem. Phys.* **1959**, *30*, 585–586.
- (16) Geacintov, N.; Pope, M.; Kallman, H. *J. Chem. Phys.* **1966**, *45*, 2639–2649.
- (17) Tang, C. W. *Appl. Phys. Lett.* **1986**, *48*, 183–185.

- (18) Li, Y. *Acc. Chem. Res.* **2012**, *45*, 723–733.
- (19) Huang, Y.; Li, L.; Peng, X.; Peng, J.; Cao, Y. *J. Mater. Chem.* **2012**, *22*, 21841–21844.
- (20) Hatano, J.; Obata, N.; Yamaguchi, S.; Matsuo, Y. *J. Mater. Chem.* **2012**, 19258–19263.
- (21) Seiffter, J.; Sun, Y.; Heeger, A. J. *Adv. Mater.* **2014**, *26*, 2486–2493.
- (22) Mori, D.; Benten, H.; Okada, I.; Ohkita, H.; Ito, S. *Energy Environ. Sci.* **2014**, *7*, 2939–2943.
- (23) National Renewable Energy Laboratory. Research Cell Efficiency Records. <http://www.nrel.gov/ncpv/> (accessed November 10, 2014).
- (24) Bevk, D.; Marin, L.; Lutsen, L.; Vanderzande, D.; Maes, W. *RSC Adv.* **2013**, *3*, 11418–11431.
- (25) Johnson, J. R.; Rotenberg, D. H.; Ketcham, R. *J. Am. Chem. Soc.* **1970**, *92*, 4046–4050.
- (26) Nakano, A.; Yasuda, Y.; Yamazaki, T.; Akimoto, S.; Yamazaki, I.; Miyasaka, H.; Itaya, A.; Murakami, M.; Osuka, A. *J. Phys. Chem. A.* **2001**, *105*, 4822–4833.
- (27) Moore, G. F.; Konezny, S. J.; Song, H.; Milot, R. L.; Blakemore, J. D.; Lee, M. L.; Batista, V. S.; Schmittenmaer, C. a.; Crabtree, R. H.; Brudvig, G. W. *J. Phys. Chem. C.* **2012**, *116*, 4892–4902.
- (28) Imahori, H.; Kang, S.; Hayashi, H.; Haruta, M.; Kurata, H.; Isoda, S.; Canton, S. E.; Infahsaeng, Y.; Kathiravan, A.; Pascher, T.; Chábera, P.; Yartsev, A. P.; Sundström, V. *J. Phys. Chem. A.* **2011**, *115*, 3679–3690.
- (29) Wudl, F.; Naraso. *Macromolecules.* **2008**, *41*, 3169–3174.
- (30) Clarke, T. M.; Durrant, J. R. *Chem. Rev.* **2010**, *110*, 6736–6767.
- (31) Halls, J. J. J. M.; Pichler, K.; Friend, R. H.; Moratti, S. C.; Holmes, A. B. *Synth. Met.* **1996**, *77*, 277–280.
- (32) Stübinger, T.; Brütting, W. *J. Appl. Phys.* **2001**, *90*, 3632.
- (33) Mihailetchi, V. D.; Blom, P. W. M.; Hummelen, J. C.; Rispen, M. T. *J. Appl. Phys.* **2003**, *94*, 6849–6854.

- (34) Huang, X.; Zhu, C.; Zhang, S.; Li, W.; Guo, Y.; Zhan, X.; Liu, Y.; Bo, Z. *Macromolecules* **2008**, *41*, 6895–6902.
- (35) Sun, Y.; Welch, G. C.; Leong, W. L.; Takacs, C. J.; Bazan, G. C.; Heeger, A. J. *Nat. Mater.* **2011**, *11*, 44–48.
- (36) Katono, M.; Wielopolski, M.; Marszalek, M.; Bessho, T.; Moser, J.-E.; Humphry-Baker, R.; Zakeeruddin, S. M.; Grätzel, M. *J. Phys. Chem. C* **2014**.
- (37) Lan, C.-M.; Wu, H.-P.; Pan, T.-Y.; Chen, C.-T.; Chang, C.-W.; Chao, W.-S.; Wang, C.-L.; Lin, C.-Y.; Diau, E. W.-G. *Energy Environ. Sci.* **2012**, *5*, 6460–6464.
- (38) Zhou, H.; Yang, L.; You, W. *Macromolecules* **2012**, *45*, 607–632.
- (39) Aihara, J.; Nakagami, Y.; Sekine, R.; Makino, M. *J. Phys. Chem. A* **2012**, *116*, 11718–11730.
- (40) Vogel, E. *Pure Appl. Chem.* **1993**, *65*, 143–152.
- (41) Stępień, M.; Sprutta, N.; Latos-Grażyński, L. *Angew. Chem. Int. Ed. Engl.* **2011**, *50*, 4288–4340.
- (42) Milgrom, L. R. *The Colours of Life: An Introduction to the Chemistry of Porphyrins and Related Compounds*; Oxford University Press: New York, 1997.
- (43) Littler, J.; Ciringh, Y.; Lindsey, J. S. *J. Org. Chem.* **1999**, *64*, 2864–2872.
- (44) Martínez-Díaz, M. V.; de la Torre, G.; Torres, T. *Chem. Commun.* **2010**, *46*, 7090–7108.
- (45) Choi, S.; Chae, S. H.; Shin, J.; Kim, Y.; Kim, S.; Choi, D. H.; Lee, S. J. *Chem. Commun.* **2013**, *49*, 3994–3996.
- (46) Detty, M. R.; Gibson, S. L.; Wagner, S. J. *J. Med. Chem.* **2004**, *47*, 3897–3915.
- (47) Hirakawa, K.; Nishimura, Y.; Arai, T.; Okazaki, S. *J. Phys. Chem. B* **2013**, *117*, 13490–13496.
- (48) Rothmund, P. *J. Am. Chem. Soc.* **1936**, *58*, 625–627.
- (49) Adler, A. D.; Longo, F. R.; Finarelli, J. D. *J. Org. Chem.* **1967**, *32*, 476.
- (50) Dolphin, D. *J. Heterocycl. Chem.* **1970**, *7*, 275–283.
- (51) Arsenault, G. P.; Bullock, E.; MacDonald, S. F. *J. Am. Chem. Soc.* **1960**, *82*, 4384–4389.

- (52) Walker, B.; Kim, C.; Nguyen, T.-Q. *Chem. Mater.* **2011**, *23*, 470–482.
- (53) Lee, C.-W.; Lu, H.-P.; Lan, C.-M.; Huang, Y.-L.; Liang, Y.-R.; Yen, W.-N.; Liu, Y.-C.; Lin, Y.-S.; Diau, E. W.-G.; Yeh, C.-Y. *Chem. Eur. J.* **2009**, *15*, 1403–1412.
- (54) Mathew, S.; Yella, A.; Gao, P.; Humphry-Baker, R.; Curchod, B. F. E.; Ashari-Astani, N.; Tavernelli, I.; Rothlisberger, U.; Nazeeruddin, M. K.; Grätzel, M. *Nat. Chem.* **2014**, *6*, 242–247.
- (55) Qin, H.; Li, L.; Guo, F.; Su, S.; Peng, J.; Cao, Y.; Peng, X. *Energy Environ. Sci.* **2014**, *7*, 1397–1401.
- (56) Johnson, J. R.; Ketcham, R. *J. Am. Chem. Soc.* **1960**, *82*, 2719–2724.
- (57) Benin, V.; Yeates, A. T.; Dudis, D. *Chem. Inform.* **2008**, *39*, 811–819.
- (58) Ando, S.; Nishida, J.; Inoue, Y.; Tokito, S.; Yamashita, Y. *J. Mater. Chem.* **2004**, *14*, 1787–1790.
- (59) Zampese, J. A.; Keene, F. R.; Steel, P. J. *Dalt. Trans.* **2004**, *9*, 4124–4129.
- (60) Shi, Q.; Fan, H.; Liu, Y.; Hu, W.; Li, Y.; Zhan, X. *J. Phys. Chem. C.* **2010**, *114*, 16843–16848.
- (61) Shi, Q.; Cheng, P.; Li, Y.; Zhan, X. *Adv. Energy Mater.* **2012**, *2*, 63–67.
- (62) Tao, T.; Geng, J.; Hong, L.; Huang, W.; Tanaka, H.; Tanaka, D.; Ogawa, T. *J. Phys. Chem. C.* **2013**, *117*, 25325–25333.
- (63) Nazim, M.; Ameen, S.; Akhtar, M. S.; Lee, Y.-S.; Shin, H.-S. *Chem. Phys. Lett.* **2013**, *574*, 89–93.
- (64) Cheng, P.; Shi, Q.; Lin, Y.; Li, Y.; Zhan, X. *Org. Electron.* **2013**, *14*, 599–606.
- (65) Dutta, P.; Yang, W.; Eom, S. H.; Lee, S.-H. *Org. Electron.* **2012**, *13*, 273–282.
- (66) Subramaniyan, S.; Xin, H.; Kim, F. S.; Jenekhe, S. a. *Macromolecules.* **2011**, *44*, 6245–6248.
- (67) Zhang, M.; Guo, X.; Wang, X.; Wang, H.; Li, Y. *Chem. Mater.* **2011**, *23*, 4264–4270.
- (68) Liu, Y.; Dong, H.; Jiang, S.; Zhao, G.; Shi, Q.; Tan, J.; Jiang, L.; Hu, W.; Zhan, X. *Chem. Mater.* **2013**, *25*, 2649–2655.

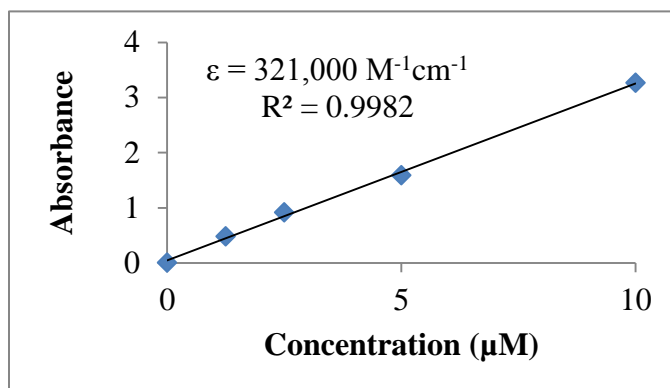
- (69) Cheng, C.; Yu, C.; Guo, Y.; Chen, H.; Fang, Y.; Yu, G.; Liu, Y. *Chem. Commun.* **2013**, *49*, 1998–2000.
- (70) Peet, J.; Wen, L.; Byrne, P.; Rodman, S.; Forberich, K.; Shao, Y.; Drolet, N.; Gaudiana, R.; Dennler, G.; Waller, D. *Appl. Phys. Lett.* **2011**, *98*, 043301–043303.
- (71) Lee, T. ae W.; Kang, N. S.; Yu, J. ae W.; Hoang, M. H.; Kim, K. H.; Jin, J.; Choi, D. H. *J. Polym. Sci., Part A Polym. Chem.* **2010**, *48*, 5921–5929.
- (72) Villers, B. T. De; Tassone, C. J.; Tolbert, S. H.; Schwartz, B. J. *J. Phys. Chem. C.* **2009**, *113*, 18978–18982.
- (73) Laha, J. K.; Dhanalekshmi, S.; Taniguchi, M.; Ambroise, A.; Lindsey, J. S. *Org. Process Res. Dev.* **2003**, *7*, 799–812.
- (74) Littler, J.; Miller, M. A.; Hung, C.-H.; Wagner, R. W.; O’Shea, D. F.; Boyle, P. D.; Lindsey, J. S. *J. Org.* **1999**, *64*, 1391–1396.
- (75) Amarnath, V.; Anthony, D. C.; Amarnath, K.; Valentine, W. M.; Wetterau, L. a.; Graham, D. G. *J. Org. Chem.* **1991**, *56*, 6924–6931.
- (76) Sobral, A. J. F. N.; Rebanda, N. G. C. L.; de Silva, M.; Lampreia, S. H.; Silva, M. R.; Beja, A. M.; Paixao, J. A.; d’A. Rocha Gonsalves, A. M. *Tetrahedron Lett.* **2003**, *44*, 3971–3973.
- (77) Zaidi, S. H. H.; Loewe, R. S.; Clark, B. A.; Jacob, M. J.; Lindsey, J. S.; Carolina, N. *Org. Process Res. Dev.* **2006**, *10*, 304–314.
- (78) Lee, C.-H.; S. Lindsey, J. One-flask synthesis of meso-substituted dipyrromethanes and their application in the synthesis of trans-substituted porphyrin building blocks. *Tetrahedron*, 1994, *50*, 11427–11440.
- (79) Ka, J.; Lee, C. *Tetrahedron Lett.* **2000**, *41*, 4609–4613.
- (80) Yella, A.; Lee, H.-W.; Tsao, H. N.; Yi, C.; Chandiran, A. K.; Nazeeruddin, M. K.; Diau, E. W.-G.; Yeh, C.-Y.; Zakeeruddin, S. M.; Grätzel, M. *Science* **2011**, *334*, 629–634.
- (81) Lee, S.; Sarker, A. K.; Hong, J.-D. *Bull. Korean Chem. Soc.* **2014**, *35*, 3052–3058.
- (82) Shi, S.; Wang, X.; Sun, Y.; Chen, S.; Li, X.; Li, Y.; Wang, H. *J. Mater. Chem.* **2012**, *22*, 11006–11008.
- (83) Gust, D.; Moore, T. A.; Moore, A. L.; Leggett, L.; Lin, S.; Degraziano, J. M.; Hermant, R. M.; Nicodem, D.; Craig, P.; Seely, G. R.; Nieman, R. A. *J. Phys. Chem.* **1993**, *97*, 7926–7931.

- (84) Sun, X.; Li, D.; Chen, G.; Zhang, J. *Dye. Pigment.* **2006**, *71*, 118–122.
- (85) Wagner, W.; Lindsey, S.; Turowska-tyrk, I.; Robert, W. *Tetrahedron* **1994**, *50*, 11097–11112.

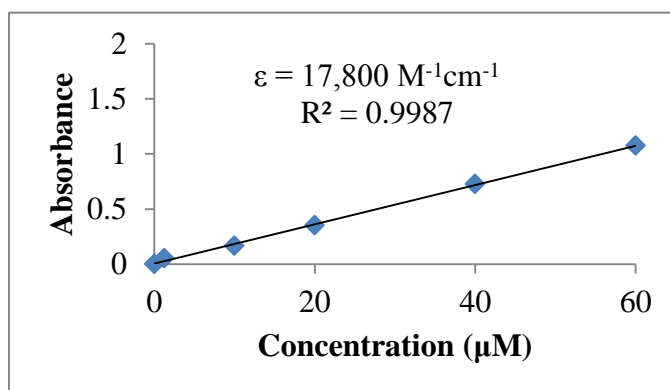
## APPENDIX A: UV-VIS CALIBRATION CURVES

A.1 *trans*-(Diocetoxyphenyl)porphyrin

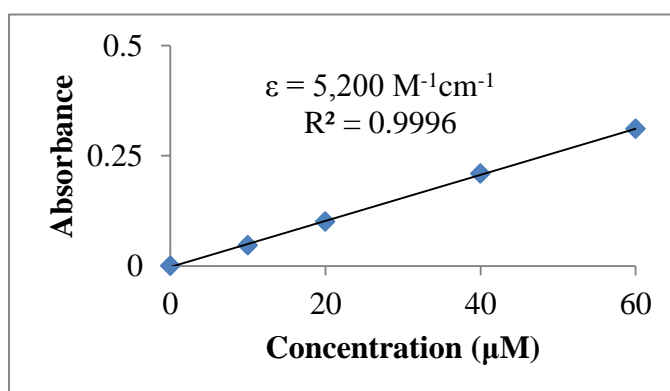
Concentration ( $\mu\text{M}$ )	Absorbance ( $\lambda=410$ )
0	0
1.25	0.47749
2.5	0.91388
5	1.5859
10	3.2663



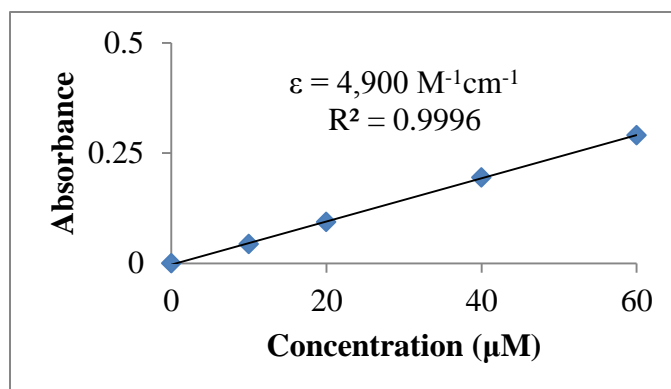
Concentration ( $\mu\text{M}$ )	Absorbance ( $\lambda=503$ )
0	0
1.25	0.05399
10	0.16667
20	0.35071
40	0.7252
60	1.0761



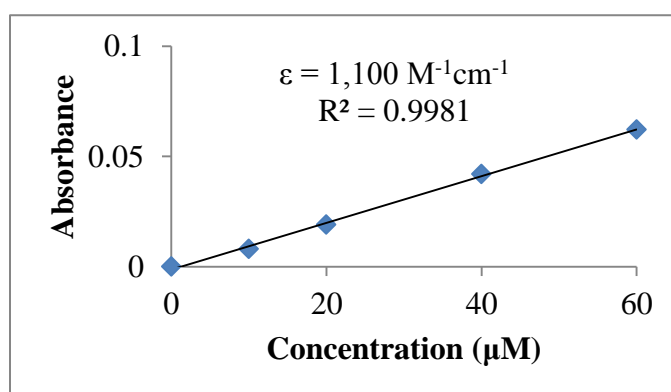
Concentration ( $\mu\text{M}$ )	Absorbance ( $\lambda=535$ )
0	0
10	0.04679
20	0.10016
40	0.20907
60	0.31087



Concentration ( $\mu\text{M}$ )	Absorbance ( $\lambda=577$ )
0	0
10	0.043366
20	0.09354
40	0.1948
60	0.29078

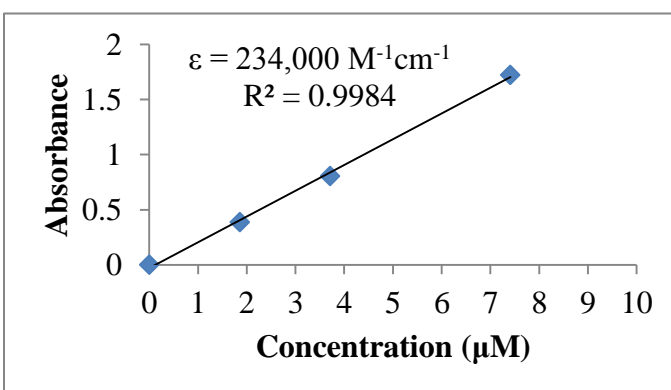


Concentration ( $\mu\text{M}$ )	Absorbance ( $\lambda=633$ )
0	0
10	0.008035
20	0.018987
40	0.042016
60	0.062205

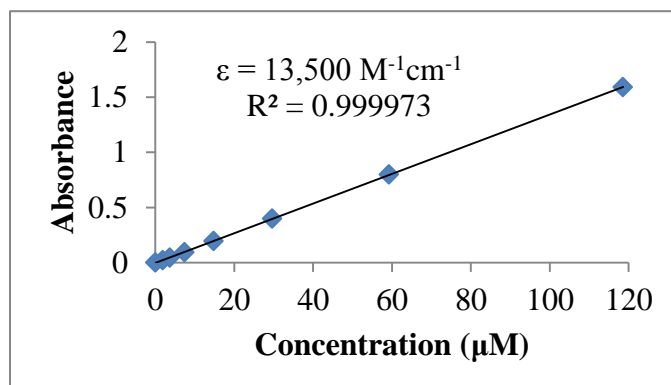


## A.2 Bromo-(Di-octoxyphenyl)porphyrin

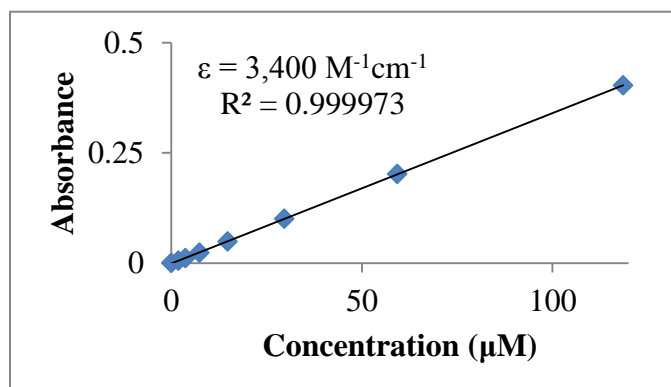
Concentration ( $\mu\text{M}$ )	Absorbance ( $\lambda=415$ )
0	0
1.86	0.38713
3.71	0.8064
7.41	1.7233



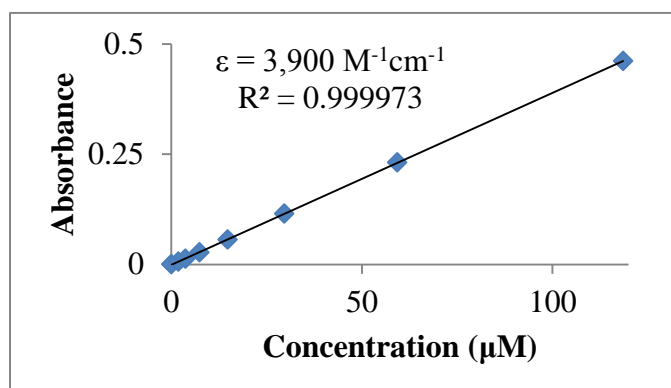
Concentration ( $\mu\text{M}$ )	Absorbance ( $\lambda=510$ )
0	0
1.86	0.020804
3.71	0.043649
7.41	0.093325
14.8	0.193709
29.6	0.397130
59.3	0.799817
118.6	1.592970



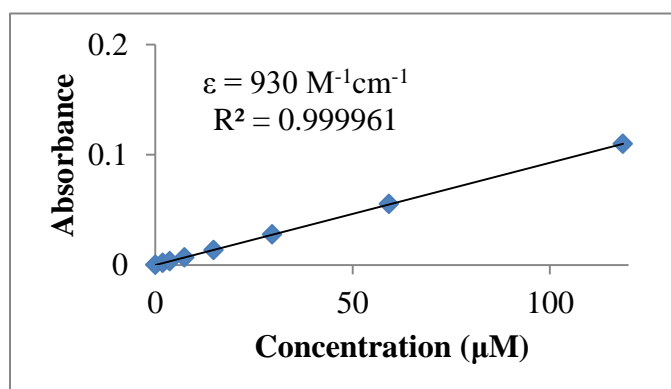
Concentration ( $\mu\text{M}$ )	Absorbance ( $\lambda=542$ )
0	0
1.86	0.00518
3.71	0.010925
7.41	0.023531
14.8	0.048801
29.6	0.100621
59.3	0.202115
118.6	0.403159



Concentration ( $\mu\text{M}$ )	Absorbance ( $\lambda=588$ )
0	0
1.86	0.0060843
3.71	0.0123319
7.41	0.0269511
14.8	0.055742
29.6	0.114624
59.3	0.321025
118.6	0.460223

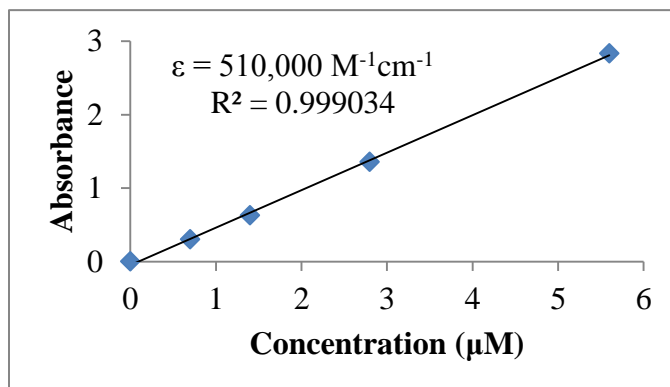


Concentration ( $\mu\text{M}$ )	Absorbance ( $\lambda=645$ )
0	0
1.86	0.001828
3.71	0.003108
7.41	0.006609
14.8	0.0134541
29.6	0.0277089
59.3	0.0552951
118.6	0.1098445

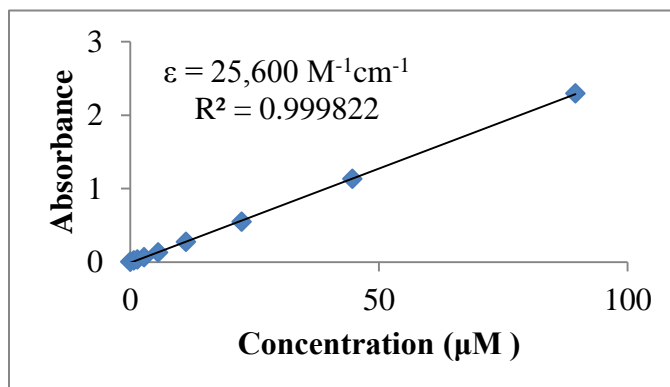


## A.3 Bromo-(Di-octoxyphenyl)porphyrin [Zn]

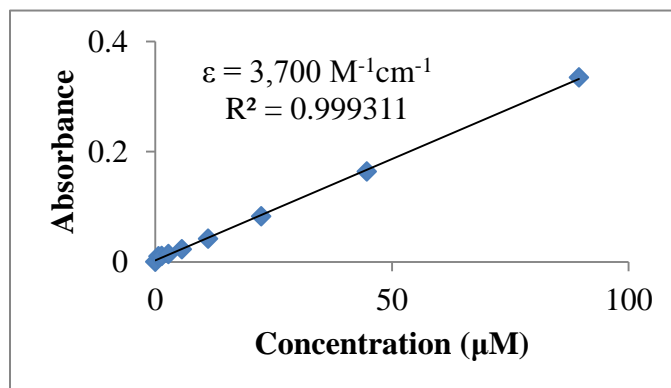
Concentration ( $\mu\text{M}$ )	Absorbance ( $\lambda=422$ )
0	0
0.7	0.299178
1.4	0.629309
2.8	1.354158
5.6	2.830726



Concentration ( $\mu\text{M}$ )	Absorbance ( $\lambda=554$ )
0	0
0.7	0.019758
1.4	0.032575
2.8	0.060382
5.6	0.125628
11.2	0.270279
22.4	0.546777
44.7	1.127661
89.5	2.292841

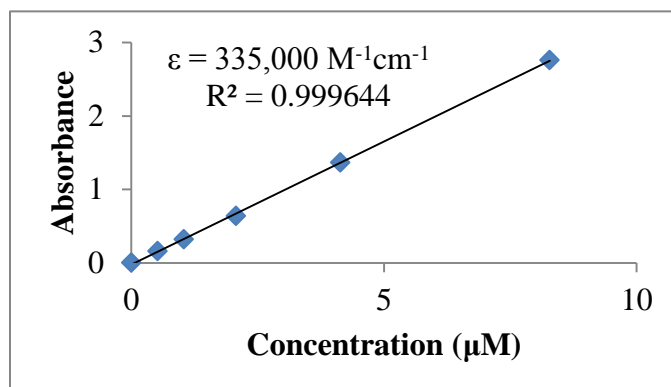


Concentration ( $\mu\text{M}$ )	Absorbance ( $\lambda=592$ )
0	0
0.7	0.009839
1.4	0.010546
2.8	0.013991
5.6	0.022869
11.2	0.042142
22.4	0.082376
44.7	0.163781
89.5	0.334880

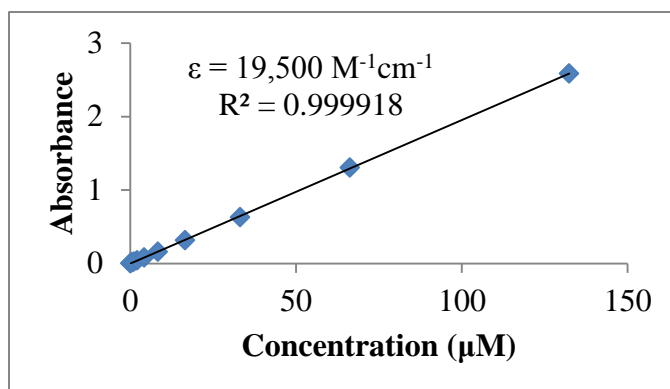


#### A.4 Dibromo-(Diocetoxyphenyl)porphyrin

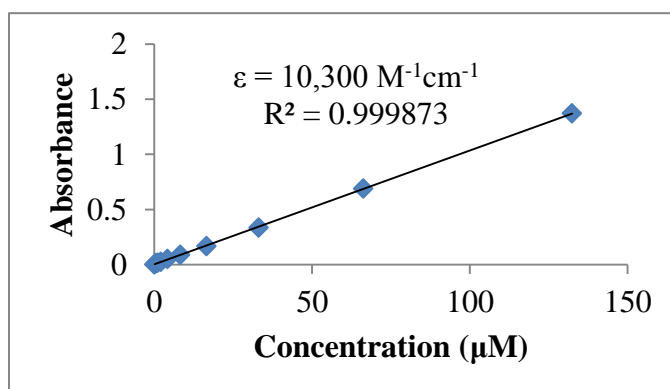
Concentration ( $\mu\text{M}$ )	Absorbance ( $\lambda=421$ )
0	0
0.52	0.158445
1.04	0.319929
2.07	0.634853
4.14	1.363879
8.28	2.758507



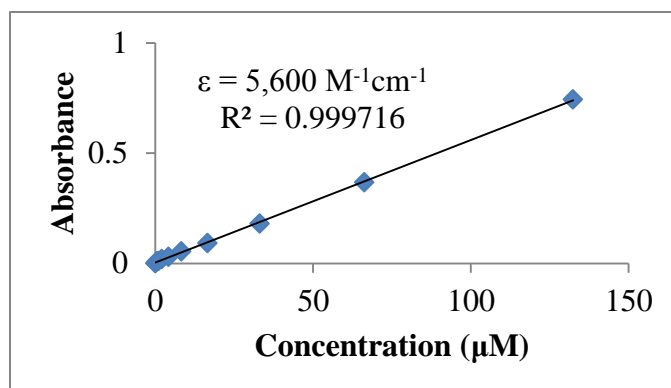
Concentration ( $\mu\text{M}$ )	Absorbance ( $\lambda=519$ )
0	0
0.52	0.01487
1.04	0.02348
2.07	0.04069
4.14	0.07907
8.28	0.15937
16.55	0.31479
33.1	0.62985
66.2	1.30449
132.4	2.58366



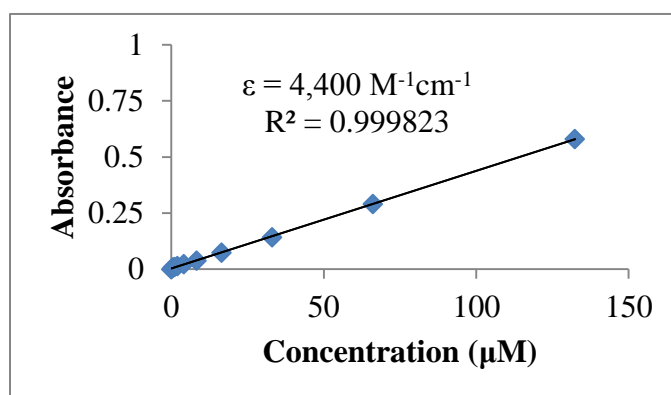
Concentration ( $\mu\text{M}$ )	Absorbance ( $\lambda=552$ )
0	0
0.52	0.01099
1.04	0.015335
2.07	0.02439
4.14	0.04931
8.28	0.08885
16.55	0.16601
33.1	0.33339
66.2	0.68916
132.4	1.37191



Concentration ( $\mu\text{M}$ )	Absorbance ( $\lambda=600$ )
0	0
0.52	0.00876
1.04	0.01085
2.07	0.01851
4.14	0.02879
8.28	0.05429
16.55	0.09237
33.1	0.18096
66.2	0.36806
132.4	0.74401

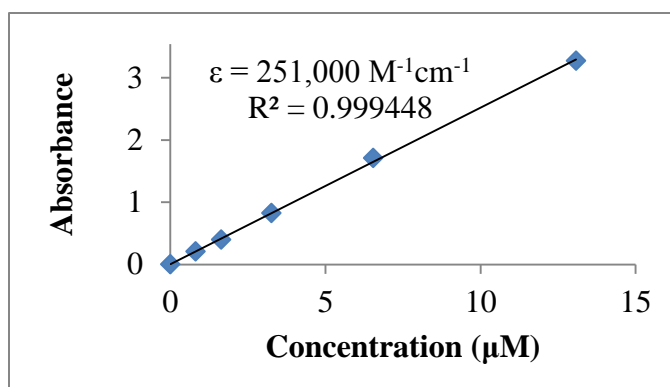


Concentration ( $\mu\text{M}$ )	Absorbance ( $\lambda=659$ )
0	0
0.52	0.0085
1.04	0.0099
2.07	0.0133
4.14	0.0218
8.28	0.0379
16.55	0.07311
33.1	0.14247
66.2	0.29093
132.4	0.58070

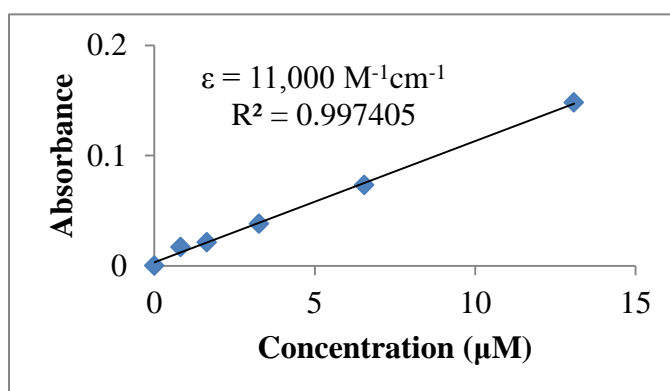


## A.5 Dibromo-(Diocetoxyphenyl)porphyrin [Zn]

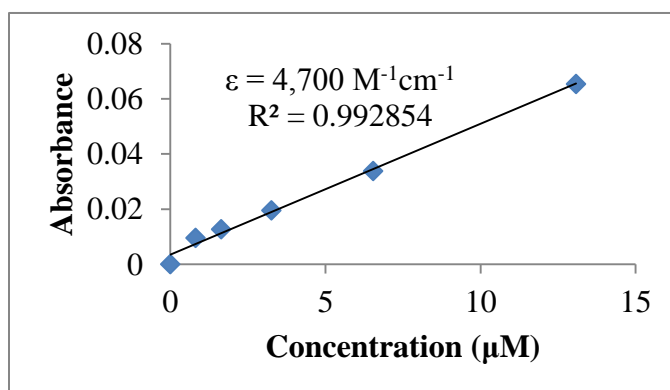
Concentration ( $\mu\text{M}$ )	Absorbance ( $\lambda=429$ )
0	0
0.82	0.20789
1.64	0.39717
3.26	0.82265
6.54	1.70651
13.08	3.27094



Concentration ( $\mu\text{M}$ )	Absorbance ( $\lambda=564$ )
0	0
0.82	0.01695
1.64	0.02137
3.26	0.038158
6.54	0.07323
13.08	0.14816

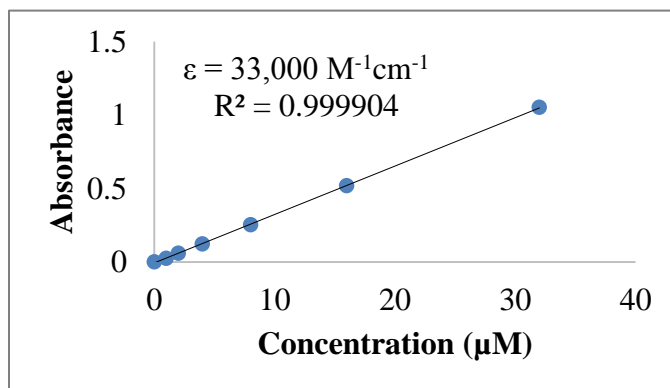


Concentration ( $\mu\text{M}$ )	Absorbance ( $\lambda=607$ )
0	0
0.82	0.00952
1.64	0.01268
3.26	0.01956
6.54	0.03381
13.08	0.06543



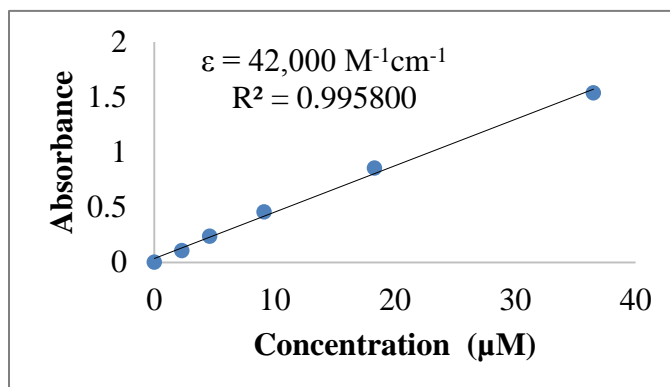
## A.6 Di-TMS TTz

Concentration ( $\mu\text{M}$ )	Absorbance ( $\lambda=607$ )
0	0
1	0.025095
2	0.058463
4	0.121986
8	0.253811
16	0.518223
32	1.051589



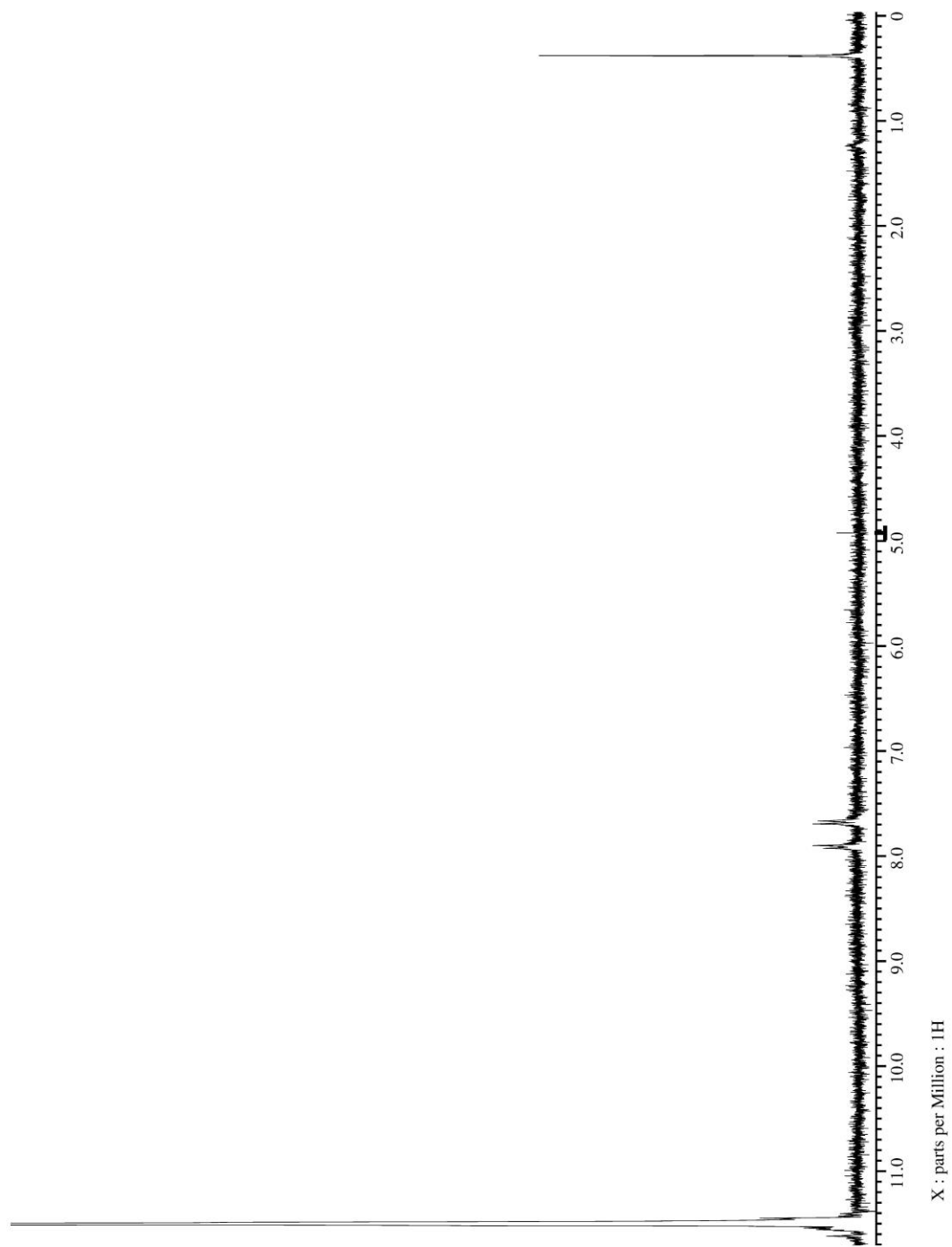
## A.7 Di-Ethynyl TTz

Concentration ( $\mu\text{M}$ )	Absorbance ( $\lambda=607$ )
0	0
2.3	0.105466
4.6	0.237071
9.13	0.455818
18.3	0.855216
36.5	1.536658

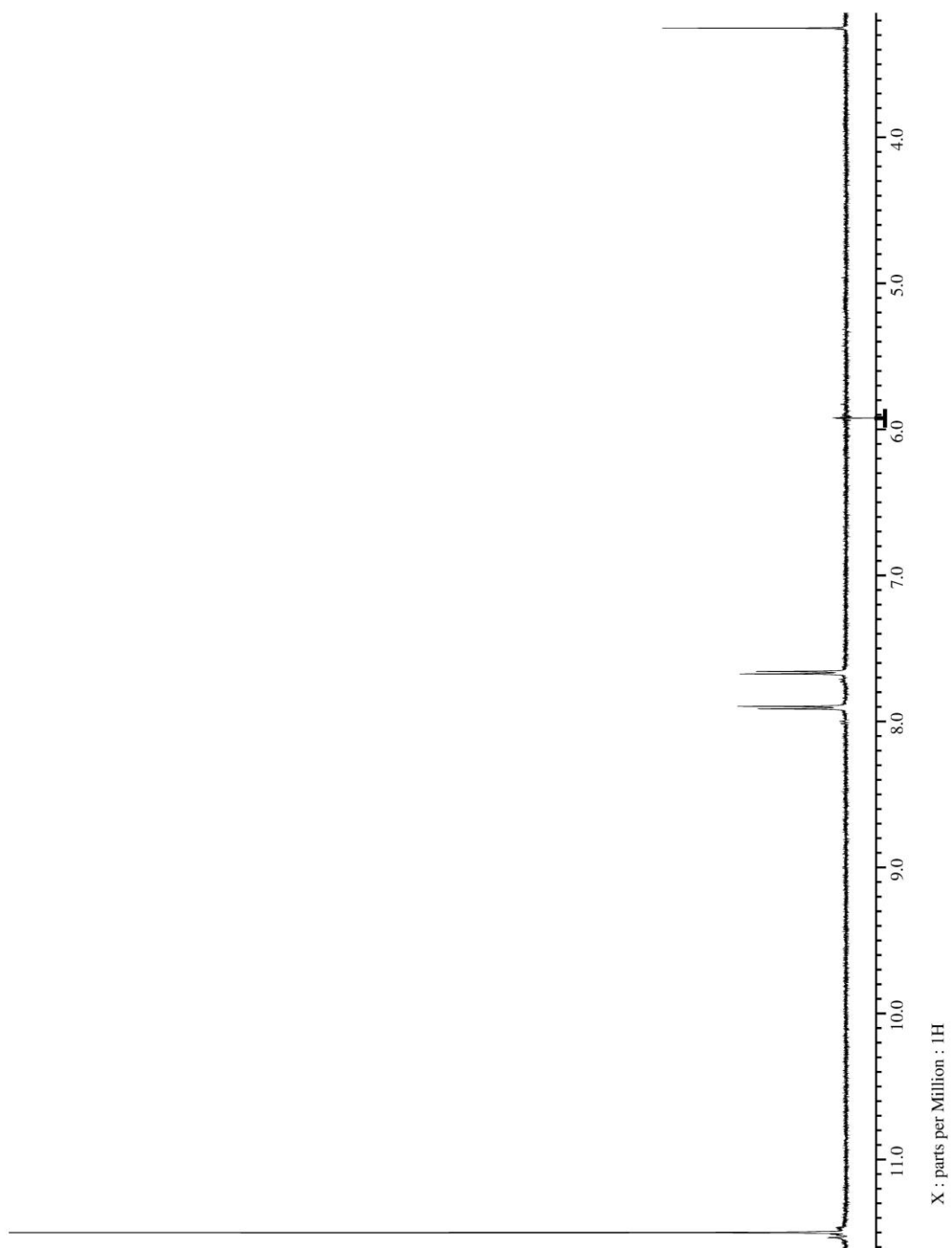


APPENDIX B:  $^1\text{H}$  NMR SPECTRA

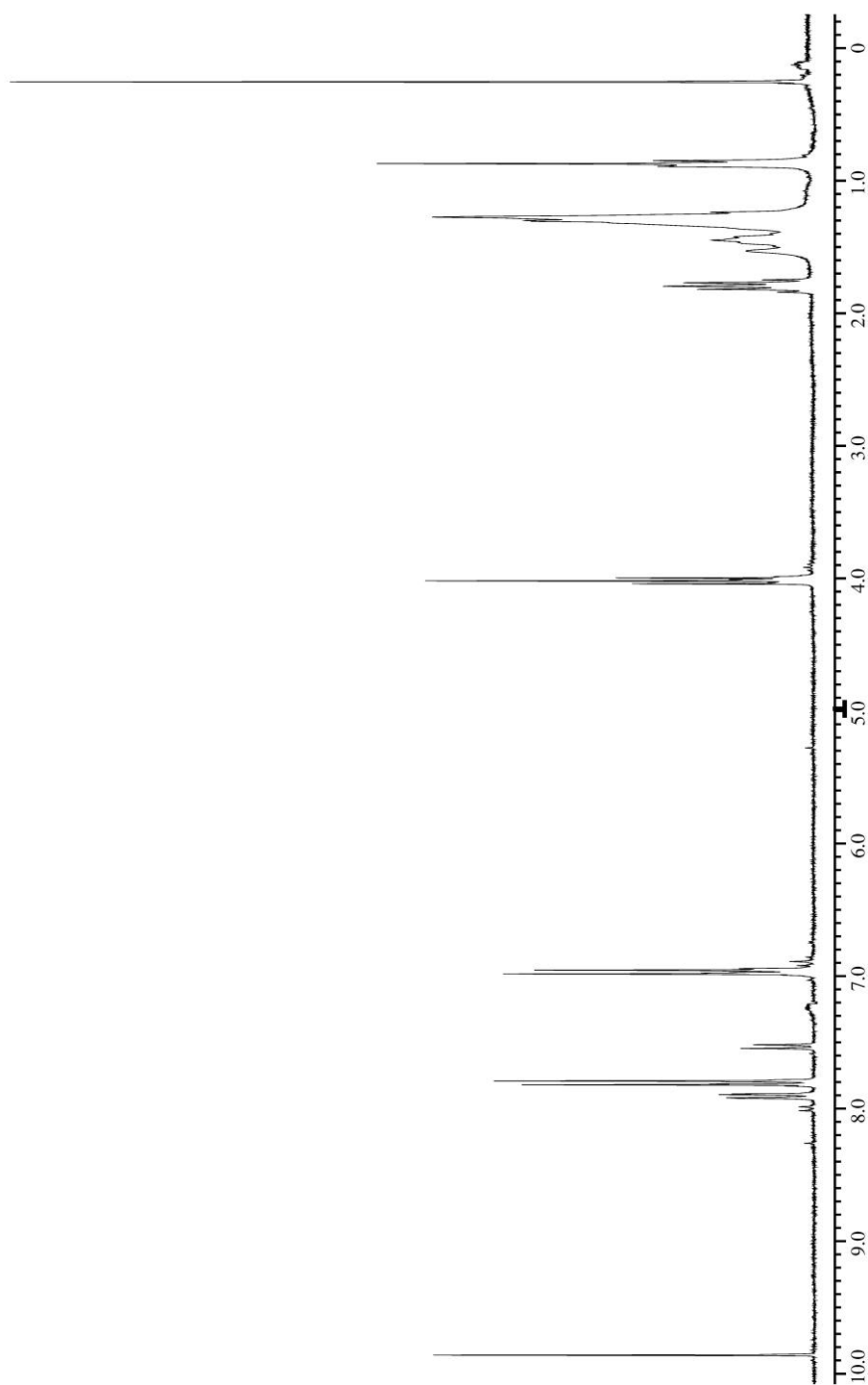
## B.1 Di-TMS TTz



## B.2 Di-Ethynyl TTz

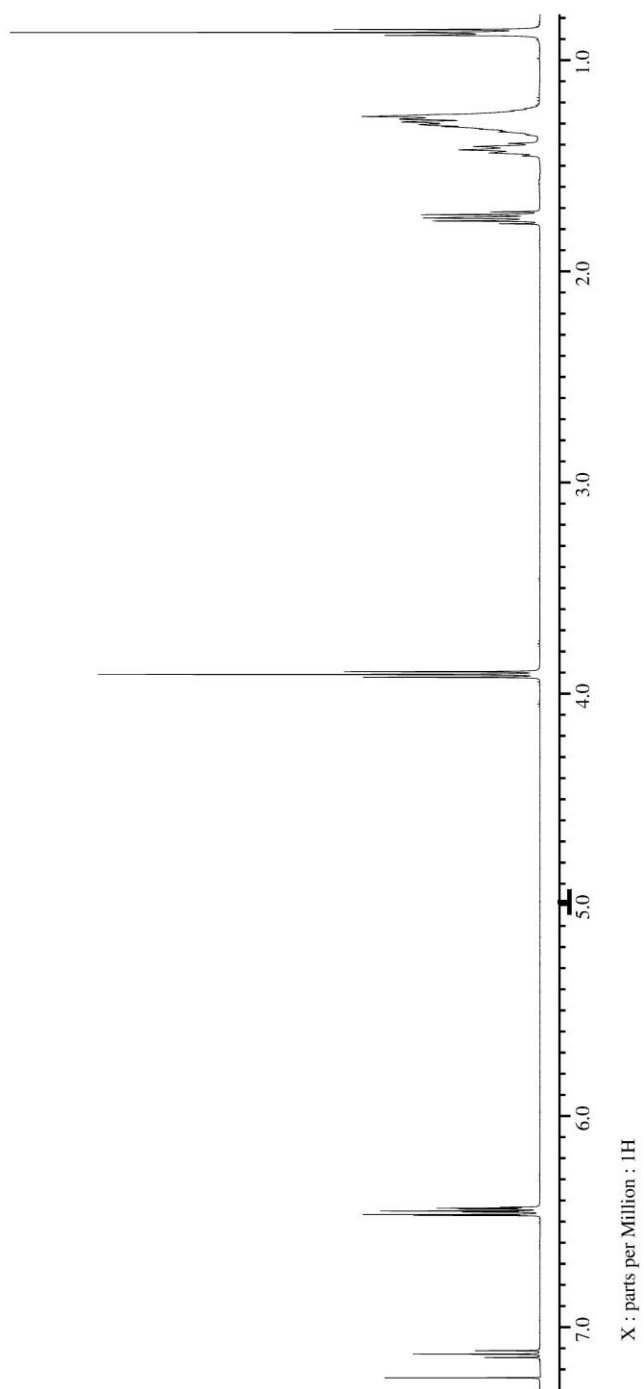


## B.3 Asymmetric TTz



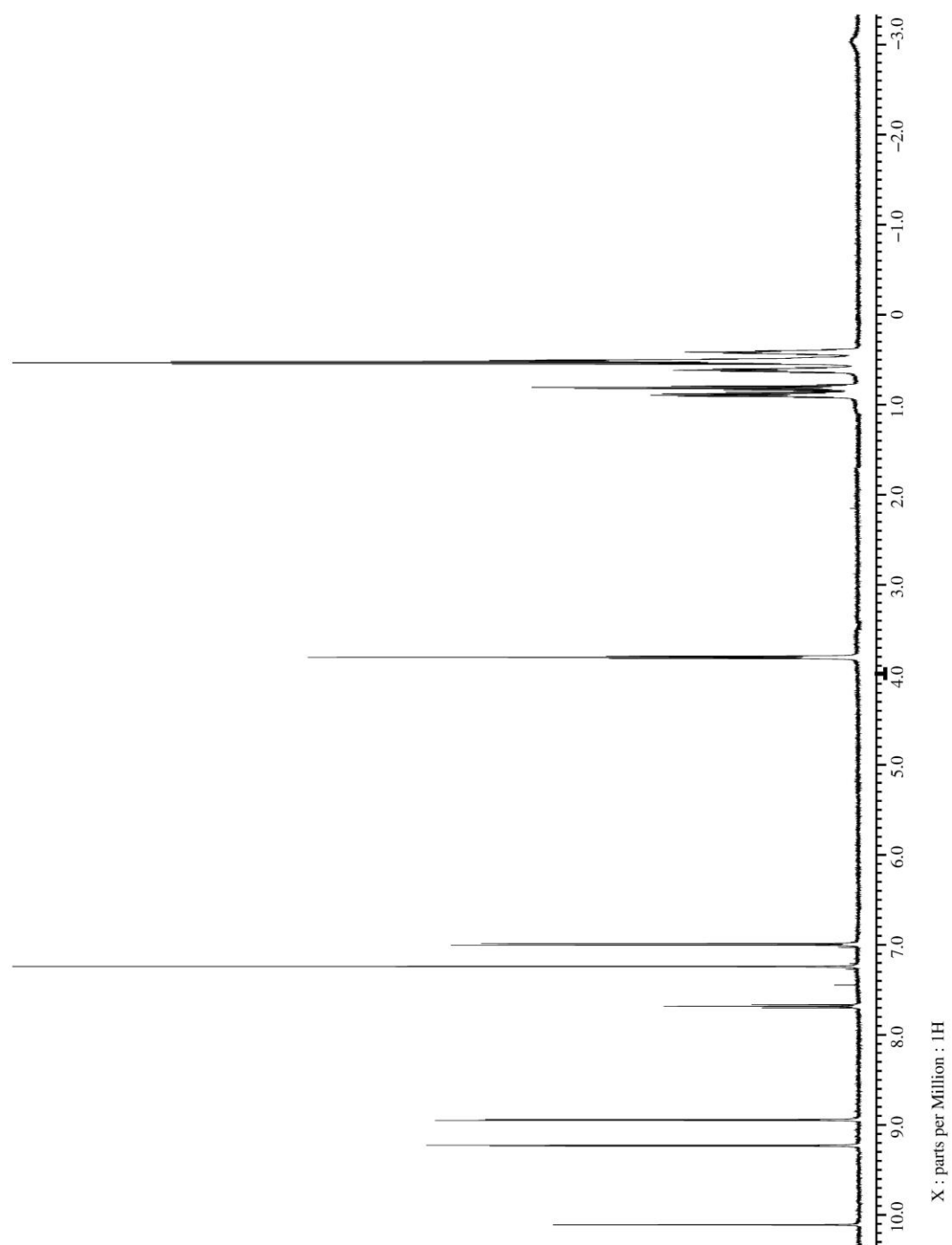
X : parts per Million : 1H

## B.4 1,3-Dioctoxybenzene

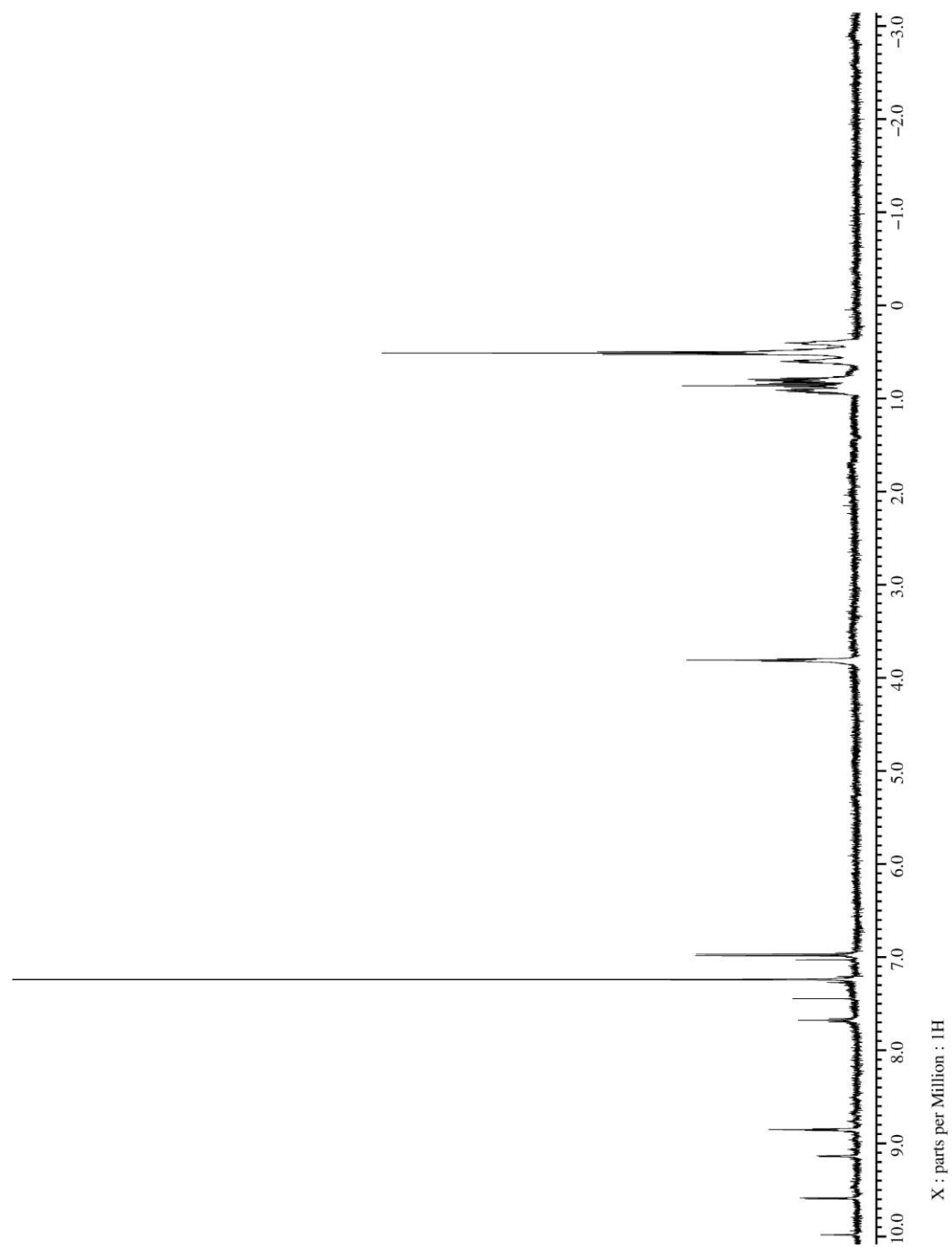


## B.5 2,6-Dioctoxybenzaldehyde

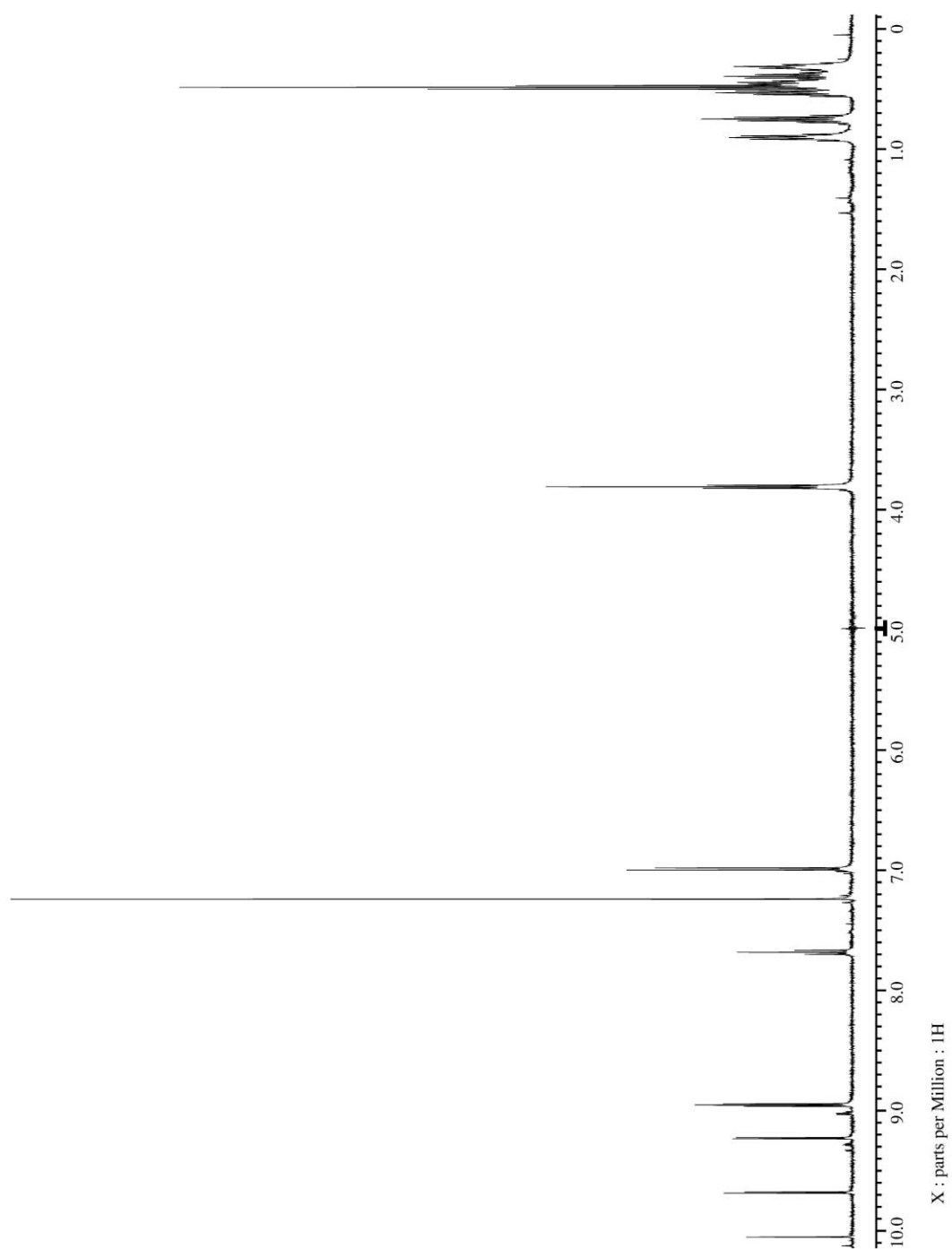


B.6 *trans*-(Dioctoxyphenyl)porphyrin

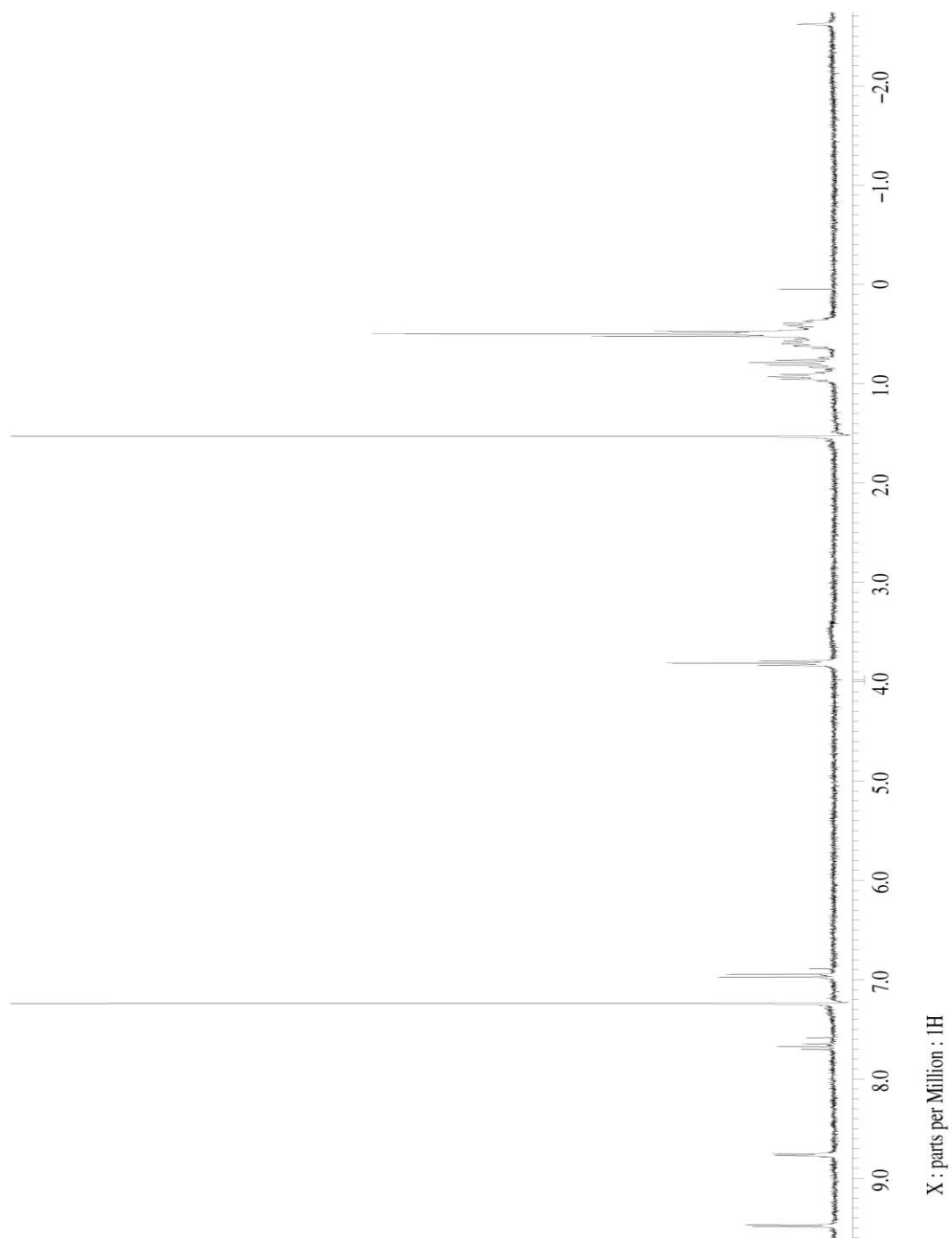
## B.7 Bromo-(Diocetoxyphenyl)porphyrin



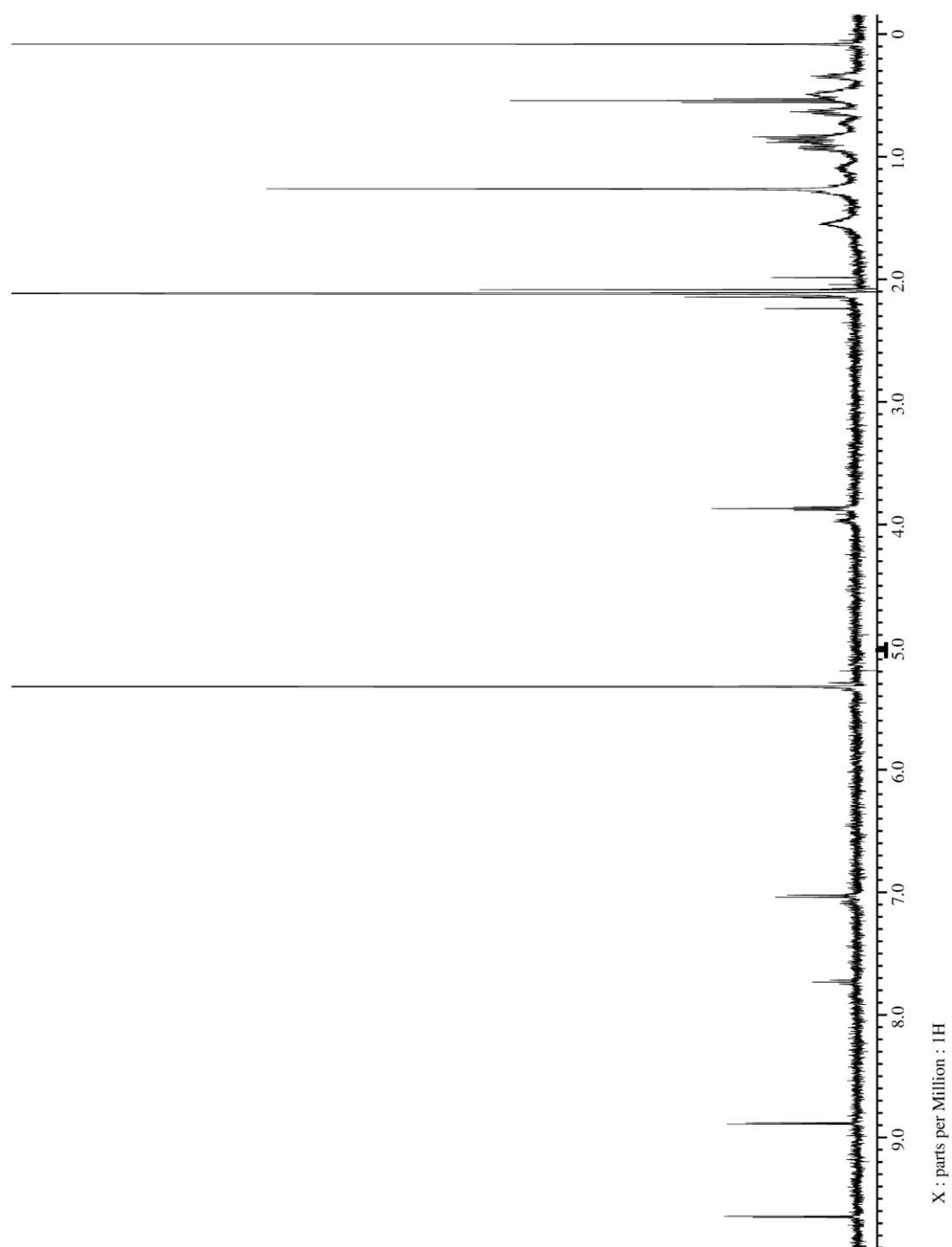
## B.8 Bromo-(Diethoxyphenyl)porphyrin [Zn]



## B.9 Dibromo-(Diocetoxyphenyl)porphyrin

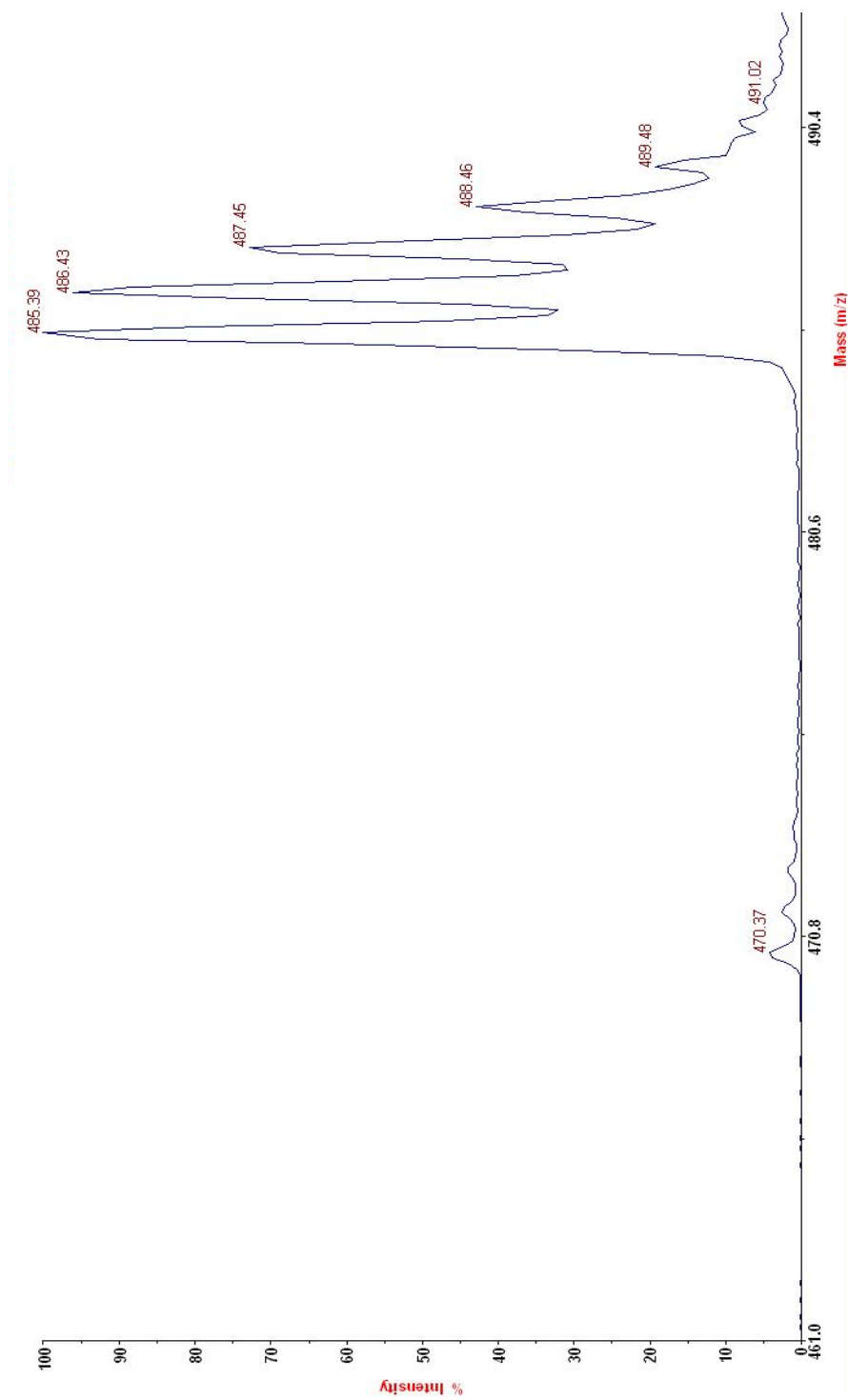


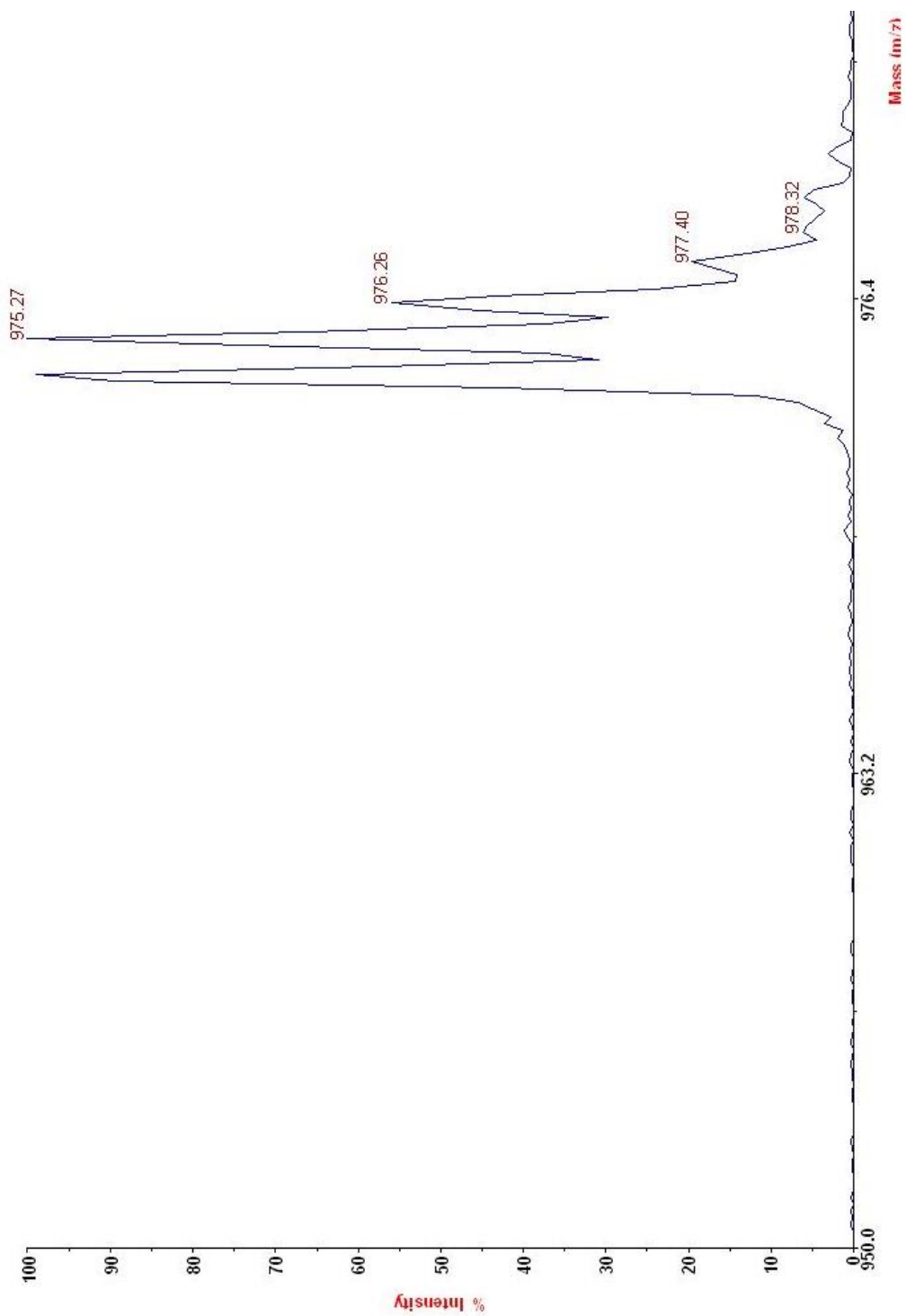
## B.10 Dibromo-(Dioctoxyphenyl)porphyrin [Zn]



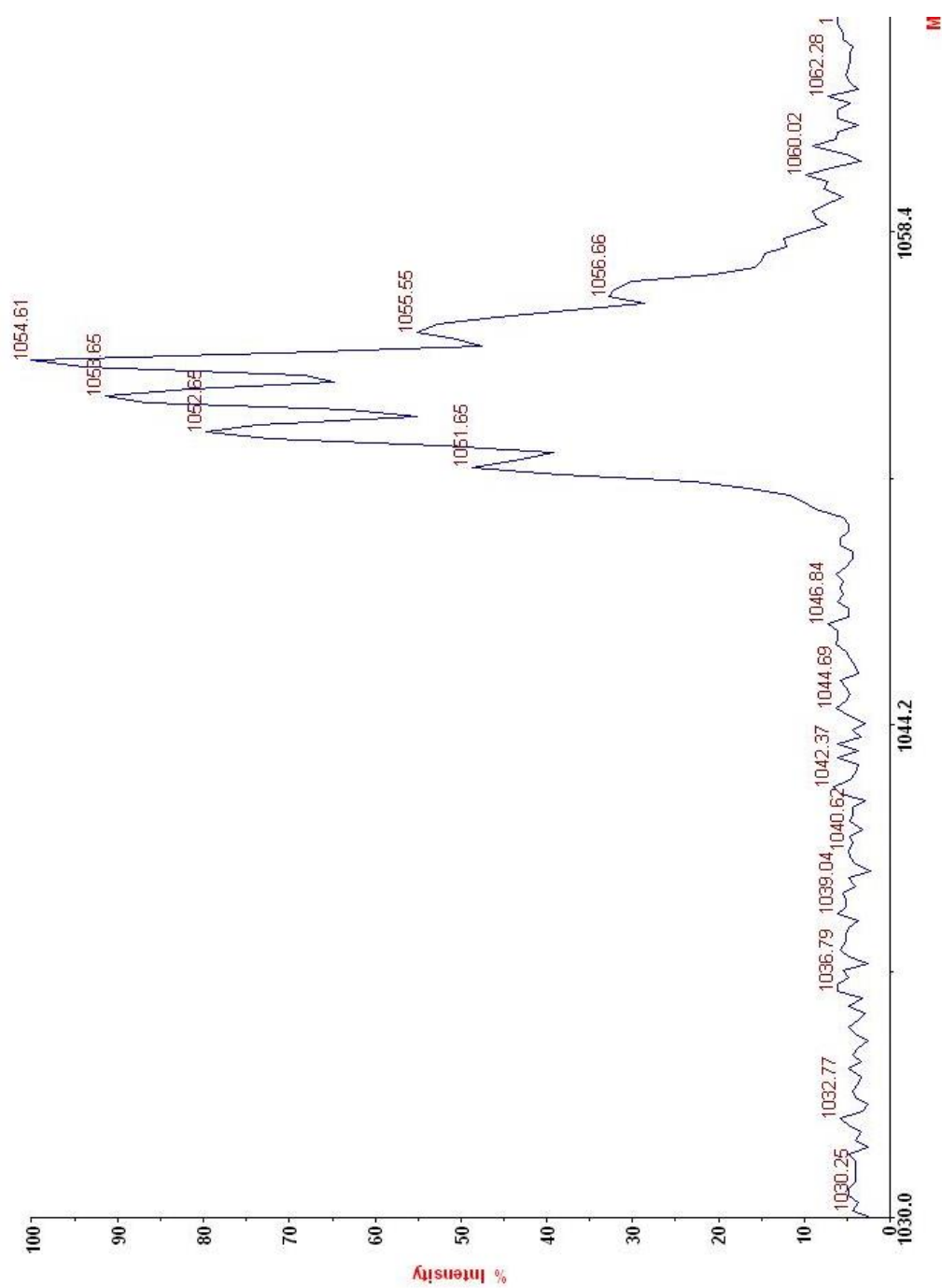
## APPENDIX C: MALDI – TOF SPECTRA

## C.1 Di-TMS TTz

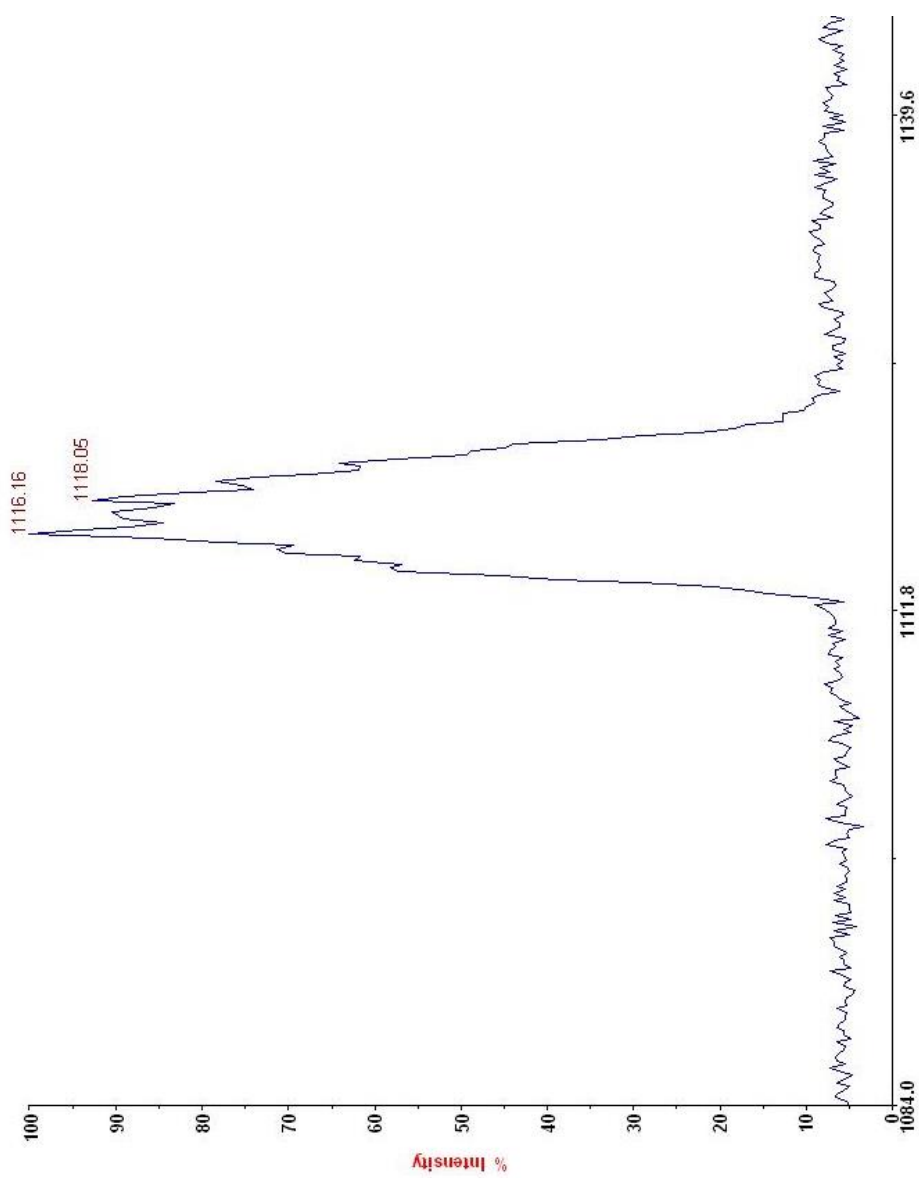


C.2 *trans*-(Diocetoxyphenyl)porphyrin

## C.3 Bromo-(Di-octoxyphenyl)porphyrin



## C.4 Bromo-(Di-octoxyphenyl)porphyrin [Zn]



## C.5 Dibromo-(Di-octoxyphenyl)porphyrin

